Transforming growth factor β signaling – a regulator of photoreceptor degeneration in Retinitis Pigmentosa

Dissertation

zur Erlangung des Doktorgrades der Naturwissenschaften (Dr. rer. nat.) der
Fakultät der Biologie und Vorklinischen Medizin
der Universität Regensburg

durchgeführt am
Lehrstuhl für Embryologie und Humananatomie der Universität Regensburg

vorgelegt von
Christina Bielmeier, geb. Ecker
aus Kollnburg

Im Jahr 2023

Transforming growth factor β signaling – a regulator of photoreceptor degeneration in Retinitis Pigmentosa

Dissertation

zur Erlangung des Doktorgrades der Naturwissenschaften (Dr. rer. nat.) der
Fakultät der Biologie und Vorklinischen Medizin
der Universität Regensburg

durchgeführt am
Lehrstuhl für Embryologie und Humananatomie der Universität Regensburg

vorgelegt von
Christina Bielmeier, geb. Ecker
aus Kollnburg

Im Jahr 2023

Das Promotionsgesuch wurde eingereicht am:

12.01.2023.

Die Arbeit wurde angeleitet von:

Prof. Dr. Dr. Barbara Braunger

Unterschrift:

…….

Christina Bielmeier

Manuscripts included in this thesis:

Bielmeier CB, Schmitt SI, Braunger BM. (2019). „**Light Intensity-Dependent Dysregulation of Retinal Reference Genes"** *Advances in experimental medicine and biology*, *1185*, 295–299. https://doi.org/10.1007/978-3-030-27378-1_48

Bielmeier CB, Roth S, Schmitt SI, Boneva SK, Schlecht A, Vallon M, Tamm ER, Ergün S, Neueder A, & Braunger BM. (2021). **„Transcriptional Profiling Identifies Upregulation of Neuroprotective Pathways in Retinitis Pigmentosa"** *International journal of molecular sciences*, *22*(12), 6307. https://doi.org/10.3390/ijms22126307

Bielmeier CB, Schmitt SI, Kleefeldt N, Boneva SK, Schlecht A, Vallon M, Tamm ER, Hillenkamp J, Ergün S, Neueder A, Braunger BM. (2022). **"Deficiency in Retinal TGFβ Signaling Aggravates Neurodegeneration by Modulating Pro-Apoptotic and MAP Kinase Pathways"** *International Journal of Molecular Sciences* 23, no. 5: 2626. https://doi.org/10.3390/ijms23052626

Author contributions are noted at the end of each manuscript.

…….

Christina Bielmeier

Table of content

Chapter 1

1 General Introduction

1.1 A progressive way to blindness: Retinitis Pigmentosa

Retinitis pigmentosa (RP) has a prevalence of about 0.3‰ (Bird, 1995; Kellner et al., 2004) and is one of the major causes of blindness in younger patients (Buch et al., 2004; Farrar et al., 2002). RP includes a large group of inherited retinal diseases leading to loss of vision up to blindness. It is characterized by a progressive degeneration of rods and cones, respectively (Hartong et al., 2006). The disease starts with night blindness in adolescence and progresses to partial visual field loss, tunnel vision, higher sensitivity to brightness and may result in complete blindness.

The course of the disease can strongly vary between patients depending on the mutated genes. Recently published studies identified mutations in more than 70 genes to cause RP (Hartong et al., 2006; Ruzickova & Stanek, 2017). Moreover, even within families with similar gene pools, the outcome of the disease can vary. It has been shown, that apoptosis is the cell death pathway occurring in RP (Chang et al., 1993; Portera-Cailliau et al., 1994), but the underlying molecular mechanisms leading to the loss of photoreceptor cells are still not fully understood. Hence, to mitigate the disease-induced degeneration of photoreceptors, it is crucial to better understand the molecular mechanisms leading to RP in order to one day be able to better help participants suffering from RP.

1.2 Photoreceptors

This thesis focuses on the light sensitive cells of the retina, the photoreceptors, as they are the main target of RP. Photoreceptor cell perikarya are located in the outer nuclear layer (ONL) and their synapses form together with horizontal and bipolar cells the outer plexiform layer (OPL). Connected through a cilium, the outer and inner segments are the outermost part of the neuroretina and are embedded in microvilli of the retinal pigment epithelium (RPE). Two types of photoreceptors are found in the mammalian retina: rods and cones. The majority consists of rod photoreceptor cells (in total 91 million in human retina) and are located mainly in the periphery of the retina (Purves et al., 2001), important for the dim and night vision as they react to very low-level light (Bowmaker & Hunt, 2006). Cone

photoreceptors (in total 4.5 million in human retina) are found predominantly in the central part of the retina, in the foveola even exclusively (Purves et al., 2001). Cones enable colour vision as they inherit different photopigments and need high light intensities (Bowmaker & Hunt, 2006; Kolb, 1995).

The perception of light is enabled by a process called phototransduction in the photoreceptor cells. Thereby, a photon is turned into an electrochemical signal that can be transmitted to the downstream neurons in the central nervous system (CNS). In cones the opsin and the chromophore 11-cis retinal build up the photopigment Iodopsin, in rods the photopigment Rhodopsin. Iodopsin and Rhodopsin are G-protein coupled receptors and located in the outer segments of photoreceptors. In most mammals, photons reaching the inverse neuroretina must permeate through all retinal layers and hit the photopigment in the photoreceptor discs (shown as filled circles in Figure 1A). Only one type of overall five known opsins is expressed per photoreceptor cell and named on the light wavelength, which kind responses to the stimulus. Four types of these opsins are found in cones: the Long-wave sensitive (LWS), Short-wave sensitive 1 and 2 (SWS1 and SWS2) and the Rhodopsin-like (Rh2), enabling the colour vision. The 5^{th} opsin type is the Rhodopsin-like 1 (Rh1) and located in the rods and essential for dim and night vision (Bowmaker & Hunt, 2006)

Under dark conditions, high level of cyclic guanosine monophosphate (cGMP) is found in the discs of the outer segments keeping sodium channels open. Thus, there is a steady inward flow which depolarizes the cells at -40 mV. Thereby, glutamate is continuously released, inhibiting neuronal signaling (Crooks & Kolb, 1992).

After a photon hits the Iodo-/Rhodopsin, 11-cis retinal transforms into its all-trans retinal (called photoisomerization) and changes the conformation of the opsin protein. The activated G-coupled receptor can activate the GTP-binding Protein Transducin (T). Phosphodiesterase (PDE) responds to activated Transducin by hydrolysing (cGMP) to 5`GMP. This results in closure of the cGMP gated sodium/calcium channels leading to a hyperpolarization of the cell membrane (Figure 1B). The continuous release of glutamate is inhibited in the synapses of the photoreceptor cells (Baylor, 1996).

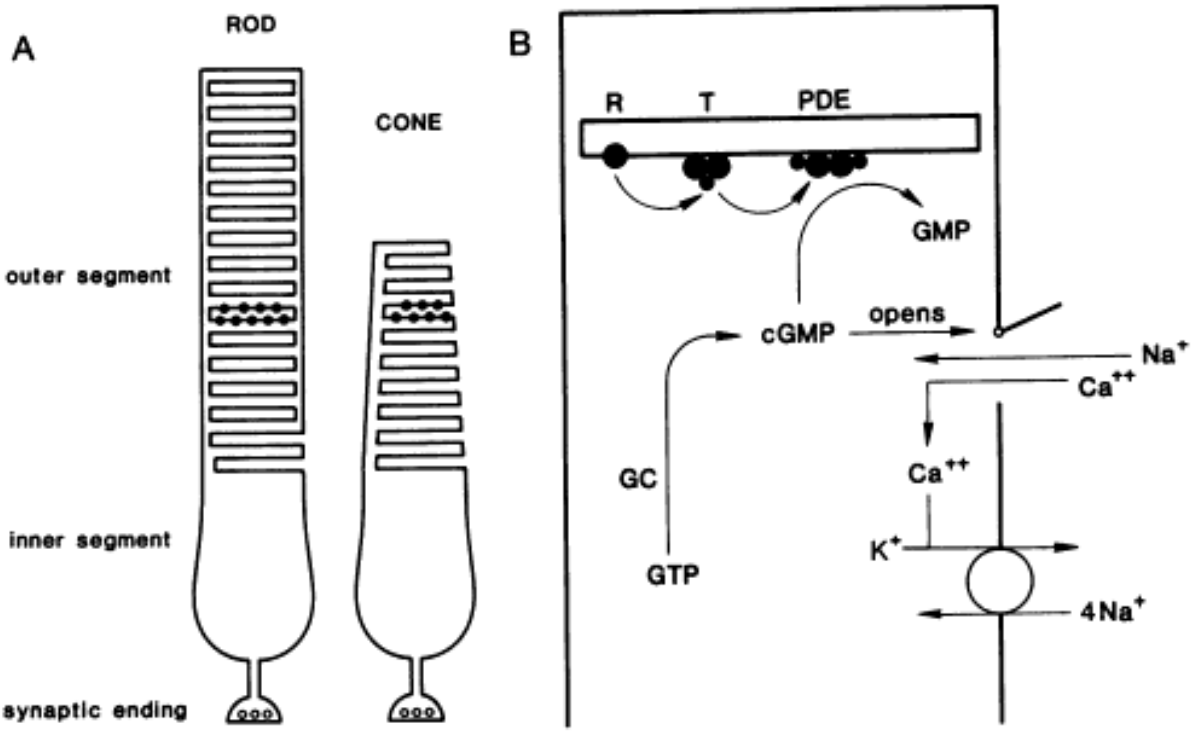

Figure 1: Schematic model of rod and cone cell and overview of the phototransduction

(A) *Schematic structure of a rod and cone cell. The synaptic endings build up the OPL with the dendrites of the horizontal and bipolar cells (not shown). Light sensitive photopigments (Rhodopsin/Iodopsin filled circles) are located in the discs of the outer segments of the photoreceptors. (**B**) Under dark conditions cGMP is built by Guanylate cyclase (GC) and binds to the sodium/calcium channels (trap door) to hold them open. A steady inward flow of sodium and calcium depolarizes the cell membrane. After a photon hits Rhodopsin (R) the GTP-binding protein Transducin (T) gets activated, which in turn can activate the phosphodiesterase (PDE). cGMP gets hydrolysed to 5`GMP leading to a closure of the sodium/calcium channels and hyperpolarization of the cell membrane. OPL = Outer plexiform layer, cGMP = Cyclic guanosine monophosphate, GC = Guanylate cyclase, R =Rhodopsin, GTP = Guanosine triphosphate, T = Transducin, PDE = phosphodiesterase. Figure from (Baylor, 1996) © (1996) National Academy of Sciences, U.S.A.*

1.3 Mouse models to investigate Retinitis Pigmentosa

To investigate RP and potential underlying mechanisms, different experimental settings can be used.

1.3.1 Light damage

The light damage paradigm is a well-established damage model to investigate photoreceptor degeneration and its molecular mechanisms (Grimm & Remé, 2013; Organisciak & Vaughan, 2010). Before the actual experiment, the mice are dark-adapted, followed by exposure to a defined light intensity for a certain time. This leads to a high number of apoptotic photoreceptors in the central part of the retina and just few in the periphery, a very characteristic degeneration pattern of the light damage paradigm (Rapp & Williams, 1980).

Advantage of this model is the high number of photoreceptor cells undergoing apoptosis at the same time. Hence, the molecular mechanism underlying photoreceptor degeneration can be studied in a more controlled fashion. Moreover, this damage model can be adapted easily for the specific research aim e.g. age of experimental mice or the degree of retinal damage (Grimm & Remé, 2013).

However, this damage paradigm does not result in a progressive degeneration of photoreceptors as it can be seen in the RP. Moreover, if very high light intensities are used, the massive damage to the photoreceptor cells could lead to unwanted side effects, e.g. oxidative stress or dysregulation of retinal reference genes (Benedetto & Contin, 2019; Bielmeier et al., 2019; Nakamura et al., 2017; Yusifov et al., 2000). This can result in an enhanced apoptosis rate in the retina that is not an exclusive outcome of the light damage and thus distort the experimental output (Jacob et al., 2013).

1.3.2 Vpp Model

In 1993, Naash and her team generated a transgene mouse model that mimic autosomal dominant RP (Naash et al., 1993). These mice express the wildtype rhodopsin and a mutated rhodopsin with three amino acid substitutions: **V**al-20 → Gly (V20G), **P**ro-23 → His (P23H), **P**ro-27 → Leu (P27L) and are named VPP mice. Of note, the P23H mutation is the most prevalent mutation in U.S patients with RP (Berson et al., 1991; Sung et al., 1991). Mice expressing the VPP transgene develop a progressive retinal degeneration beginning at postnatal day 21 (Figure 2B). The VPP transgene has become a common mouse model to study the effects of autosomal dominant RP. It results in a comparable progressive degeneration of the photoreceptors mimicking the disease in a natural way. However, this progressive event entails also a problem in using this model as only few photoreceptor cells are undergoing apoptosis at the same time resulting in a steady but weak response of the underlying molecular mechanism. Thereby, the identification of any involved factors and signaling pathways gets impeded.

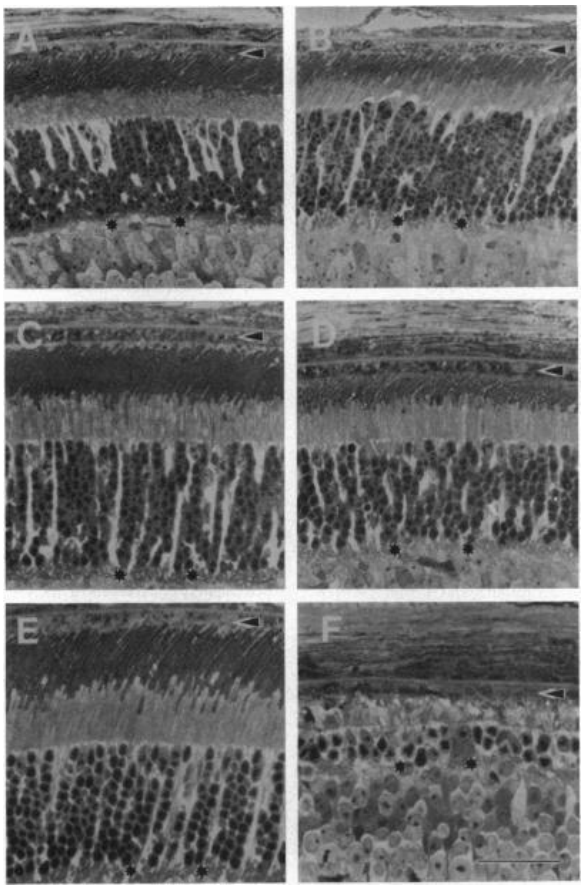

Figure 2: Morphology of control and VPP retinae at different ages

*Sagittal sections of 20 days old VPP transgenic mice (**B**) show a normal retina pattern, but already shortened outer segments of the photoreceptors can be detected compared to controls (**A**). At the age of 32 days, additionally to the shortened outer segments the ONL is thinned in VPP mice (**D**) compared to control littermates (**C**). In seven-month-old VPP mice (**F**) the ONL consists just of a row of two to three photoreceptor nuclei and the outer segments have nearly vanished while seven-month-old controls (**E**) show a healthy retinal structure. ONL =Outer nuclear layer. Figure from (Naash et al., 1993) © (1996) National Academy of Sciences, U.S.A.*

1.3.3 Cre/loxP System

The Cre/*loxP* system has become a widely used method to conditionally delete, insert or inverse a DNA sequence of the target gene in experimental animal models (Kühn & Torres, 2002). Whereas the constitutive modulation/deletion of genes could lead to embryonic lethality or other developmental disabilities, the conditional deletion using the Cre/*loxP* system circumvents such negative effects.

The *loxP* sequence consists of an asymmetric 8 bp sequence between two symmetric 13 bp sequences. The gene of interest or a part of it is flanked by the *loxP* sites and is targeted by the Cre recombinase. The Cre recombinase is a nuclease which is encoded by the *Cre* gene of the bacteriophage P1 (Sternberg & Hamilton, 1981). Different Cre mouse strains have been established by using promoters under cell- or tissue-specific control or promotors administrated by certain drugs (Nagy, 2000; Tian et al., 2006) to adjust the experimental setup. Hence, depending on the promoter system chosen, the conditional

modulation/deletion of target genes can be initiated in a cell-/tissue-specific, in a time-specific manner or in a combination of both.

In this thesis, the *Tg(Pax6-cre,GFP)*^{2Pgr} (α-Cre) recombinase (Marquardt et al., 2001) was used to conditionally delete transforming growth factor receptor type 2 (*Tgfbr2*). This recombinase is under the control of the α-enhancer element of the Pax6 promotor and starts expression of the Cre at embryonic day 10.5, specifically in cells originating from the inner layer of the optic cup (Bäumer et al., 2002; Marquardt et al., 2001). Hence, we used the α-Cre to conditionally delete *Tgfbr2* in Müller cells and retinal neurons.

1.4 The TGFβ signaling pathway

The cytokine transforming growth factor β (TGFβ) and its signaling pathway have pluripotent functions and play a critical role in embryonic development, regulation of cell growth, differentiation and migration (Massagué, 2012b). Moreover, TGFβ has been shown to be involved in the caspase mediated apoptosis of cells and is reported to have neuroprotective properties (Braunger et al., 2013b; Walshe et al., 2009).

In mammals, three isoforms of TGFβ are known: TGFβ 1, 2 and 3. They are transcribed by different genes, but share a 71-79 % sequence identity (Huang et al., 2014), bind to the same receptors and are involved in cell differentiation, embryogenesis and cell growth. Besides, isoform 1 is known to act as a key player in immune response (Shull et al., 1992). TGFβ2 plays an essential role in angiogenesis and embryogenesis, and in particular in heart development (Boileau et al., 2012) and TGFβ3 is referred to be involved in processes of the secondary palate development (Taya et al., 1999). As a side note, TGFα carries a similar name suggesting a close relation to TGFβ, but there are no structural or functional similarities between the factors.

All three TGFβ ligands bind to the TGFβ receptor type 2 (TGFBR2), a serine/threonine kinase which recruits and phosphorylates the TGFβ receptor type 1 (TGFBR1) to build a heterodimere (Shi & Massagué, 2003; Xu et al., 2012). In the canonical/Mothers against decapentaplegic homolog (SMAD)-dependent signaling pathway (shown in Figure 3A), downstream SMAD2/SMAD3 get phosphorylated and form a complex with SMAD4. The SMAD2/SMAD3/SMAD4 complex translocates into the nucleus and acts as a transcriptional regulator of TGFβ target genes (Akhurst & Hata, 2012; Clayton et al., 2020). SMAD7 as a negative regulator of the canonical TGFβ signaling prevents the formation of the SMAD complexes and thus inhibits TGFβ-mediated transcriptional regulation, respectively (Yan et al., 2009).

In non-canonical, non-SMAD TGFβ signaling, different pathways are involved (Overview shown in Figure 3B). The proteins Rat-sarcoma-virus (RAS), Rapidly growing fibrosarcoma (RAF) and their downstream Mitogen-activated-protein (MAP)-Kinases can activate Extracellular-signal-regulated-

kinases (ERK1/2) to regulate target genes, e.g. in epithelial-mesenchymal transition (EMT). Another non-SMAD signaling pathway of TGFβ involves the Tumor-necrosis-factor (TNF) receptor-associated-factor (TRAF6), which is poly-ubiquinated after activation and recruits TAK1. TAK1 in turn can activate JNK/p38 regulating apoptosis and EMT. In addition, the Ras homologue (RHO)-like Guanosine triphosphatase (GTPase) dependent TGFβ signaling is also involved in EMT regulation, by inducing the dissolution of tight junctions during EMT. The last known non-canonical pathway of the TGFβ signaling activates the phosphatidylinositol-3-kinase (PI3K)/AKT and modulates growth arrest and EMT by activating Mechanistic target of rapamycin/Ribosomal protein S6 kinase (mTOR/S6K) (Clayton et al., 2020; Peng et al., 2022; Zhang, 2009). However, the PI3K/AKT pathway of the non-canonical TGFβ signaling can prevent SMAD-mediated apoptosis by an interaction of AKT with SMAD3 (Conery et al., 2004).

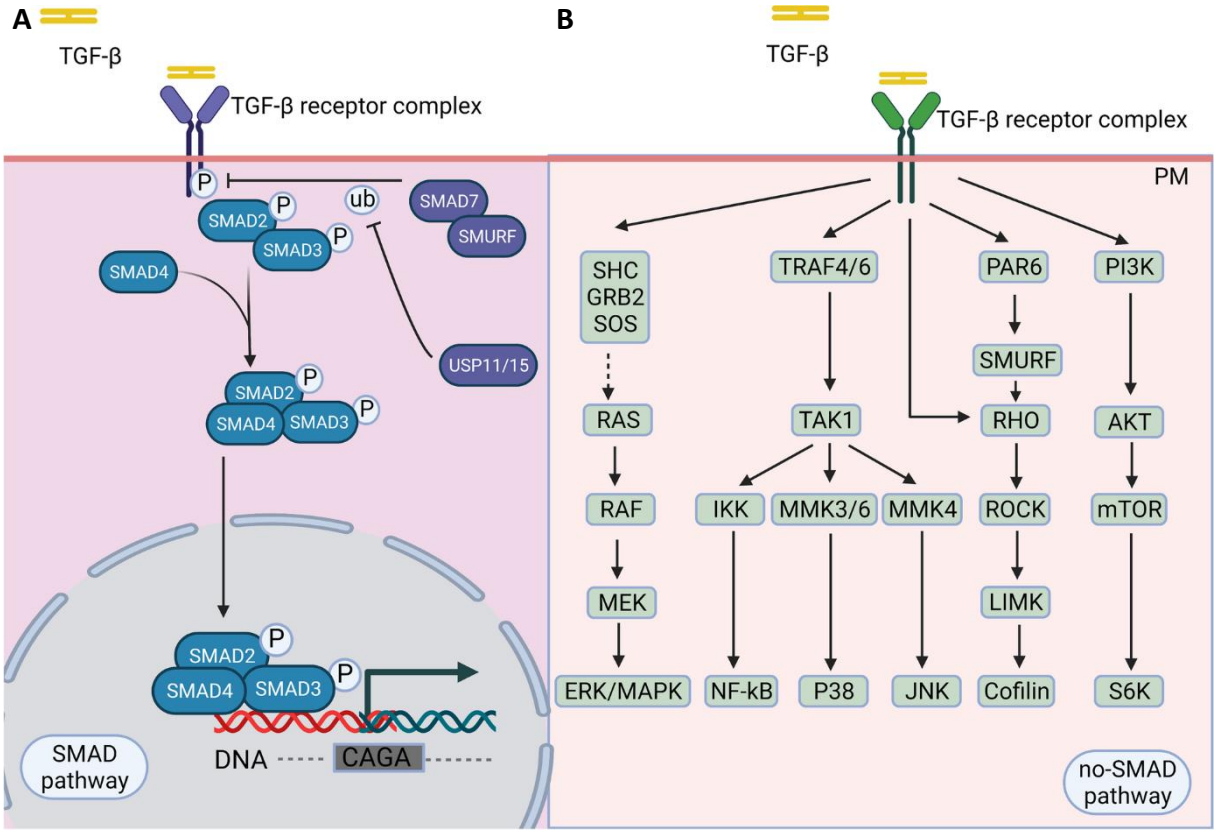

Figure 3: SMAD-dependent and SMAD-independent TGFβ signaling Pathways.

***(A)** Binding of TGFβ activates Tgfbr complex. Phosphorylated downstream SMAD proteins form the SMAD2/SMAD3/SMAD4 complex that translocates in the nucleus to activate canonical TGFβ signaling by transcriptional regulation of target genes. SMAD7 acts as a negative regulator as it prevents the formation of the SMAD2/SMAD3/SMAD4 complex and thus the transcription of TGFβ associated target gene. (**B**) Non-canonical TGFβ signaling induces SMAD-independent pathways including downstream factors like ERK, TRAF6, RHO or PI3K. Transforming growth factor β = TGFβ, Mothers against decapentaplegic homolog 2/3/4/7 = SMAD2/3/4/7, = ERK, Tumor-necrosis-factor receptor-associated-factor 6 = TRAF6, Ras homologue = RHO, phosphatidylinositol-3-kinase = PI3K. Figure from (Peng et al., 2022) CC BY 4.0 (https://creativecommons.org/licenses/by/4.0/legalcode).*

1.5 Aim of the Study

The overall aim in this thesis was to investigate the underlying molecular mechanisms of photoreceptor degeneration and in particular to study the impact of TGFβ signaling in this process. Therefore, we took advantage of different damage paradigms to mimic photoreceptor degeneration in mouse models. To gain more insight to the underlying mechanisms of diseases like RP:

…….. we will investigate the influence of different light intensities and exposure times on the degree of photoreceptor degeneration and the expression levels of reference genes

Therefore, we will use albino wildtype mice and treat the retina with different light intensities and exposure times. We will determine the amount of degenerating photoreceptors and evaluate the relative mRNA expression level of the reference genes glycerinaldehyd-3-phosphat-dehydrogenase (*Gapdh*), 60S ribosomal protein L32 (*Rpl32*), guanine nucleotide-binding protein subunit beta-2-like 1 (*Gnb2l*), ribosomal protein 9 (*Rps9*), actin-beta (*Actb*), ubiquitin C (*Ubc*) and TATA-binding protein (*Tbp*), which are all involved in basal cellular mechanisms and frequently used as reference genes in mRNA analyses.

…….. we aim to identify signaling pathways involved in retinal degeneration and characterize the specific cell types in which the signaling pathways are expressed.

We will use VPP mice as a model of autosomal dominant RP. First, we will validate the damage model by TUNEL-analysis in one-month-old animals and morphological and mRNA expression analyses of well-known neuroprotective factors in three-month-old animals. The glial response to the retinal degeneration will be determined by immunofluorescent staining against glial fibrillary acidic protein (GFAP) and ionized calcium-binding adapter molecule 1 (IBA1) in one-month-old animals. Retinal samples of three-month-old VPP and controls will be analysed by next generation RNA sequencing (RNAseq), followed by gene ontology analyses and weighted-correlation network analyses (WGCNA) to identify modules of dysregulated genes. Finally, we will combine *in situ* hybridizations and co-staining with GFAP and glutamine synthetase (GS) to characterize the location and cell types that express components of identified dysregulated pathways in the VPP model.

…….. we will investigate the role of TGFβ signaling in Müller cells and retinal neurons in retinal degeneration

We will generate a cell-type specific conditional deletion of *TGFβ receptor type 2* (*Tgfbr2*) in retinal neurons and Müller cells. Resulting α-Cre;*Tgfbr2* mouse line will be crossbred with the VPP mouse line to genetically induce photoreceptor degeneration. We will verify the successful deletion of *Tgfbr2* in retinal neurons and Müller cells by *in situ* hybridization and analyze the impact of TGFBR2 depletion on neurodegeneration by TUNEL-analysis in one-month-old and morphometric measurements of the outer nuclear layer in three-month-old "healthy" (without VPP transgene) and "diseased" (carrying the VPP transgene) mice. Samples of healthy and diseased *Tgfbr2* conditional knockout and control mice

will be analyzed by RNAseq to identify TGFβ-dependent molecular key factors that may modulate neuroprotection.

Chapter 2

2 Light Intensity-Dependent Dysregulation of Retinal Reference Genes

(Adapted from: **Christina B. Bielmeier**, Sabrina Schmitt and Barbara M. Braunger**. Light Intensity-Dependent Dysregulation of Retinal Reference Genes** published in the *Retinal Degenerative Diseases 2019.)*

2.1 Abstract

The degeneration of photoreceptors is a common hallmark of ocular diseases like retinitis pigmentosa (RP) or age-related macular degeneration (AMD). To experimentally induce photoreceptor degeneration, the light damage paradigm is frequently used. In this study we show that the exposure to high amounts of cool white light (10,000 lux, 1 h) resulted in a more than 11-fold higher apoptotic rate in the retina compared to light exposure with 5,000 lux for 30 min. Consequently, exposure to intense light resulted in a significant downregulation of retinal mRNA expression levels of the reference genes *Gapdh, Gnb2l, Rpl32, Rps9, Actb, Ubc* or *Tbp* compared to untreated controls. Investigators performing light-induced photoreceptor degeneration should be aware of the fact that higher light intensities will result in a dysregulation of reference genes

2.2 Introduction

The degeneration of photoreceptors is a common hallmark of ocular diseases like retinitis pigmentosa (RP) or age-related macular degeneration (AMD) finally resulting in an impaired vision or even blindness (Bhutto & Lutty, 2012; Bramall et al., 2010). To allow for detailed mechanistic understanding of the molecular mechanisms leading to the degeneration of photoreceptors, light damage has become a well-developed model (Organisciak & Vaughan, 2010).

In this study, we compared the exposure to 5,000 lux cool white light for 30 minutes (low) with the exposure to 10,000 lux for 1 hour (high) using Balb-C/CD1 albino mice. We report, that the exposure to the higher amounts of cool white light resulted in a more than 11-fold higher rate of apoptotic cells in the retina compared to the low exposure. Moreover, the low exposure did not affect the mRNA expression levels of seven investigated reference genes in the retina compared to untreated controls (= no light exposure). However, using the high light intensity of 10,000 lux for 1h resulted in a significant downregulation of all investigated reference genes.

2.3 Results

2.3.1 Validation of light-induced damage

To evaluate the extent of light-induced photoreceptor apoptosis, we used TUNEL labelling on retinal sections of wildtype albino mice that had been exposed to 5,000 lux for 30 min or 10,000 lux for 1h, respectively. Both groups showed a considerable number of apoptotic cells in the outer nuclear layer (ONL) of the central retina (Figure 4A,B). Animals that had been exposed to 5,000 lux for 30 min had an average number of 526.00 ±180.63 TUNEL-positive cells per mm^2 ONL (Figure 4C). However, animals exposed to 10,000 lux for 1 h (Figure 4A,B) had 6026.53 ± 1071.09 TUNEL-positive cells per mm^2 ONL stretching into the peripheral retina (Figure 4A,C).

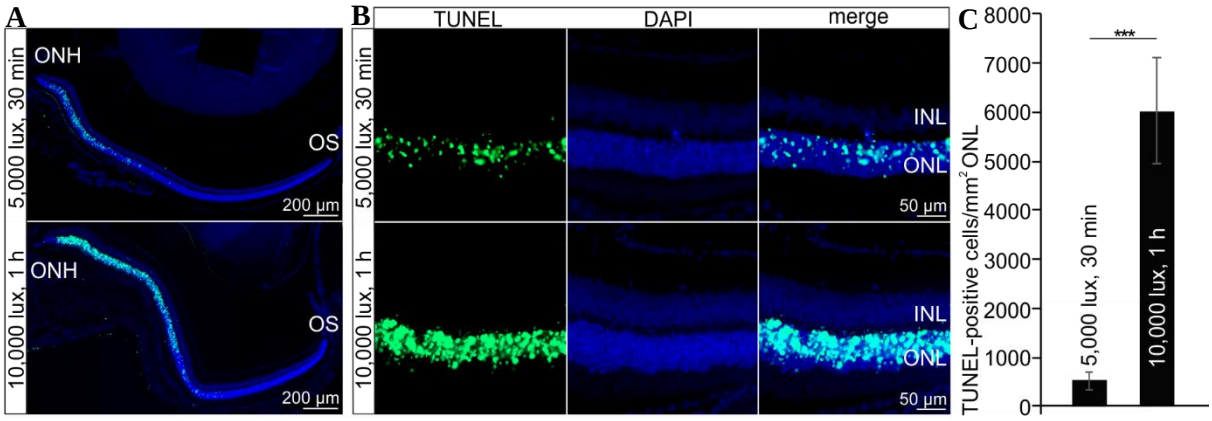

Figure 4: TUNEL-analysis of mice exposed to different light intensities and exposure time

*Retinal hemispheres (**A**) and detailed magnification (**B**) of mice exposed to 5,000 lux for 30 min (above) or 10,000 lux for 1 h (below) showing a considerable number of TUNEL-positive cells (green) in the ONL. (**C**) Exposure to 10,000 lux for 1h resulted in a 11.4-fold higher number of apoptotic cells compared to exposure to 5,000 lux for 30 min. Nuclei are DAPI stained (blue). OS=ora serrata; ONH=optic nerve head; INL=inner nuclear layer; ONL=outer nuclear layer. Data are mean ±SEM; n≥6; ***p≤0.001*

2.3.2 Dysregulation of reference genes following high light exposure

Quantitative realtime RT-PCR (qPCR) is commonly used to evaluate alterations in gene expression levels following light induced photoreceptor degeneration. In this study we aimed to identify reliable reference genes for qPCR. We investigated the expression level of glycerinaldehyd-3-phosphat-dehydrogenase (*Gapdh*), 60S ribosomal protein L32 (*Rpl32*), guanine nucleotide-binding protein subunit beta-2-like 1 (*Gnb2l*), ribosomal protein 9 (*Rps9*), actin-beta (*Actb*), ubiquitin C (*Ubc*) and TATA-binding protein (*Tbp*). When comparing the mRNA expression level in the retinae of untreated controls (= no light exposure) compared to mice exposed to 5,000 lux for 30 min, none of these genes showed a significant alteration ($p>0.05$) (Figure 5A). In contrast, when analyzing the mRNA expression levels of the same reference genes of untreated controls compared to mice exposed to 10,000 lux for 1h,

we detected a significant decrease in the expression of *Gapdh* (control: 1 ±0.009, light: 0.912 ±0.034, p=0.020), *Gnb2l* (control: 1 ±0.006, light: 0.937 ±0.020, p=0,007), *Rpl32* (control: 1 ±0.006, light: 0.950 ±0.011, p=0.001), *Rps9* (control: 1 ±0.004, light: 0.960 ±0.011, p=0.006), *Actb* (control: 1 ±0.007, light: 0.900 ±0.026, p=0.002), *Ubc* (control: 1 ±0.006, light: 0.950 ±0.022, p=0.043) and *Tbp* (control: 1 ±0.008, light: 0.875 ±0.027, $p \leq 0.001$) following light induced photoreceptor degeneration (Figure 5B).

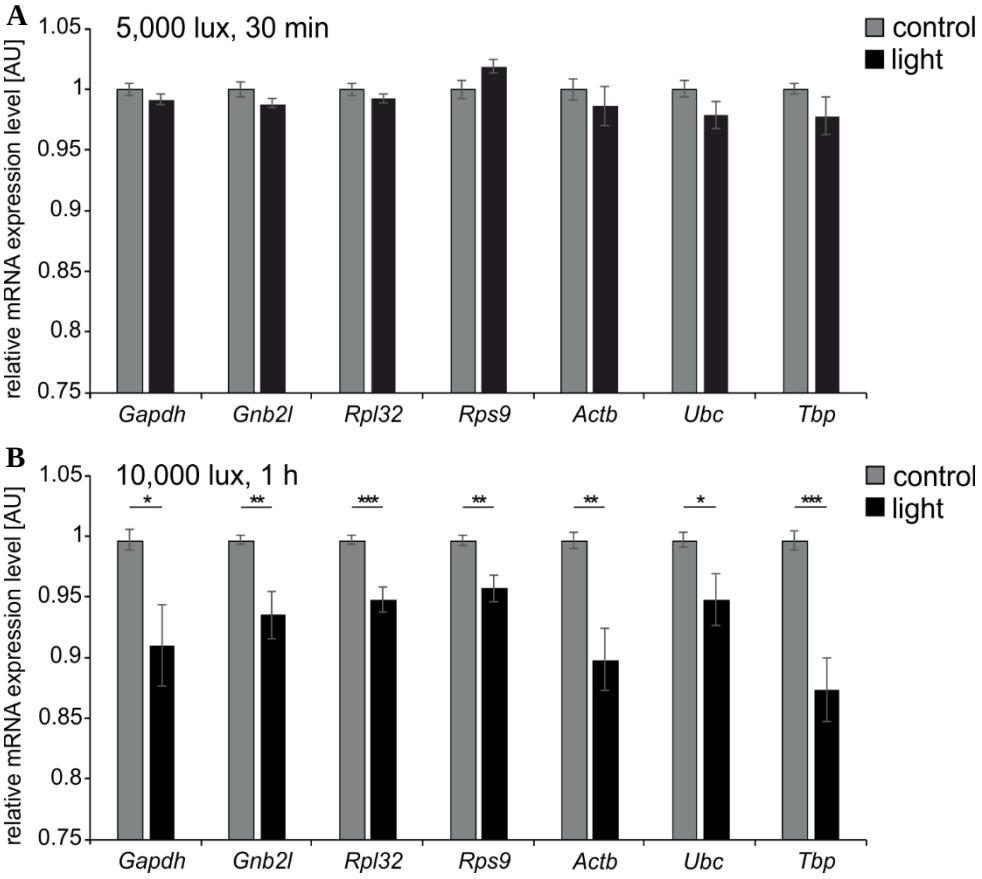

Figure 5: Relative mRNA analysis of reference genes in mice exposed to different light intensities and exposure time

*Relative mRNA expression levels of Gapdh, Gnb2l, Rpl32, Rps9, Actb, Ubc and Tbp in the retinae of untreated compared to light exposed mice. (A) The analyzed genes were not differentially regulated in animals exposed to 5,000 lux for 30 min. (**B**) Mice exposed to 10,000 lux for 1 h showed a significant downregulation in the relative mRNA expression levels of all reference genes. Data are mean ±SEM; n≥4; *p≤0.05, **p≤0.01, ***p≤0.001, AU = arbitrary unit.*

2.4 Discussion

Based on our results we conclude that (**1**) light exposure of albino animals to 5,000 lux for 30 min is sufficient to induce photoreceptor degeneration in the central retina. (**2**) The illumination with 10,000 lux for 1h results in a 11.4-fold higher number of apoptotic cells but also (**3**) significantly alters the gene expression levels of commonly used reference genes.

In our study, light-induced apoptotic photoreceptor cells were mainly localized in the central part of the retina, a characteristic distribution of apoptotic cells (LaVail et al., 1987; Rapp & Williams, 1980). However, animals exposed to 10,000 lux for 1h additionally showed apoptotic cells stretching to the mid-peripheral region of the retina (Figure 4A). This has already been reported by other groups following damage with higher light intensities (Thomas & Thummel, 2013).

qPCR is frequently used to evaluate signalling pathways that might be involved or contribute to the apoptosis of photoreceptors. Animals exposed to 10,000 lux for 1 h demonstrated increased apoptosis in the ONL that most likely resulted in a disruption of the cellular homeostasis. Consequently, we observed a dysregulation of genes involved in basal cellular mechanisms that are commonly used as reference genes for qPCR (Ginzinger, 2002). Previous studies already mentioned that the widely-used reference gene *Gapdh* was dysregulated following various experimental conditions (Kim & Kim, 2003; Kozera & Rapacz, 2013; Nakao et al., 2015). In contrast, *Tbp* has been reported to be very stable in glioblastoma cells and muscle atrophy (Nakao et al., 2015; Valente et al., 2009) and *Ubc* has been shown to be consistent in diverse liver diseases (Kim & Kim, 2003). Quite intriguingly, our study showed a significant downregulation of all analyzed reference genes in retinal tissue of mice exposed to high light intensities.

The threshold of light exposure that will result in dysregulation of reference genes, clearly also depends on the genetic background of the experimental animals and the individual experimental setup. However, investigators performing light-induced photoreceptor degeneration should be aware of the fact that excessive light intensities will result in a dysregulation of reference genes and that these effects need to be controlled for.

2.5 Materials and Methods

2.5.1 Animals and light damage paradigm

All procedures conformed to the tenets of the National Institutes of Health Guidelines on the Care and Use of Animals in Research, the EU Directive 2010/63/E, and the Uniform Requirements for manuscripts submitted to Biomedical journals. Wildtype albino mice (Balb-C/CD1) at the age of 6-8 weeks were tested to be homozygous for the leucine variant of the *Rpe65* gene (Wenzel et al., 2003). Light-induced photoreceptor degeneration was performed using diffuse cool white fluorescent light with an intensity of 5,000 lux for 30 min or 10,000 lux for 1 h and as described in (Braunger et al., 2013a). Dark-adapted Balb-C/CD1 animals served as controls. The mice were sacrificed after 6 h for mRNA analyses or 30 h for TUNEL analyses.

2.5.2 Terminal deoxynucleotidyl transferase dUTP nick end labelling (TUNEL)

Apoptotic cell death was assessed by terminal deoxynucleotidyl transferase-mediated dUTP nick end labelling using the Apoptosis Detection System (DeadEnd Fluorometric TUNEL, Promega) and our previously published protocol (Braunger et al., 2013a; Kugler et al., 2017).

TUNEL sections were analyzed using an Axio Imager Z1 microscope (Carl Zeiss) and the software ZENpro (Carl Zeiss). For quantitative analysis of apoptotic cells, the number of TUNEL-positive nuclei in mid-horizontal sections throughout the entire retina was counted and normalized to the area [mm²] of the outer nuclear layer.

2.5.3 relative mRNA expression analysis

RNA was isolated with TriFast (Peqlab) using the instructions by Peqlab. cDNA synthesis was performed using iScript cDNA Synthesis Kit (Bio-Rad) according to manufacturers' instructions and quantitative real-time RT-PCR analyses were performed as previously reported (Schlecht et al., 2017).

All oligonucleotides were purchased from Invitrogen (Carlsbad, CA) (Table 1) and the assays spanned exon-exon boundaries. CFX Manager™ Software and Excel was used to calculate relative expression of mRNA levels according to the $\Delta\Delta C_T$-method (Livak & Schmittgen, 2001).

Gene	Sequence
Actb	5` -ctaaggccaaccgtgaaaag- 3`
	5` -accagaggcatacagggaca- 3`
Gapdh	5` -tgtccgtcgtggatctga- 3`
	5` -cctgcttcaccaccttcttg- 3`
Gnb2l	5` -tctgcaagtacacggtccag- 3`
	5` -acgatgatagggttgctgc- 3`
Rpl32	5` -gctgccatctgttttacgg- 3`
	5` -gactggtgcctgatgaact- 3`
Rps9	5` -atccgccaacgtcacatta- 3`
	5` -tcttcactcggcctggac- 3`
Tbp	5` -caggagccaagagtgaagaac- 3`
	5` -ggaaataattctggctcatagctact- 3`
Ubc	5` -gtctgctgtgtgaggactgc- 3`
	5` -cctccagggtgatggtctta- 3`

Table 1: Oligonucleotides used for quantitative realtime RT-PCR

2.5.4 Statistical analysis

All results are expressed as mean ±SEM. A two-tailed Student's t-test was used for comparisons between the mean variables of two groups. *P* values ≤0.05 were considered to be statistically significant.

2.6 Acknowledgments

The authors wish to thank Elke Stauber, Angelika Pach, Silvia Babl and Margit Schimmel for the great technical assistance. This work was supported by PRO RETINA Deutschland e.V. (S.I.S., B.M.B.), the Jackstädt Foundation (B.M.B.) and BR 4957/3-1 (B.M.B.).

2.7 Author Contributions

Conceptualization: B.M.B.

Methodology: C.B.B., S.I.S., B.M.B.

Software: C.B.B., B.M.B.

Validation: B.M.B.

Formal analysis: C.B.B., B.M.B.

Investigation: C.B.B., B.M.B.

Resources: B.M.B.

Data curation: C.B.B., B.M.B.

Writing-original draft preparation: C.B.B., B.M.B.

Writing review and editing: C.B.B., S.I.S., B.M.B.

Visualization: C.B.B., B.M.B.

Supervision: B.M.B.

Project administration: B.M.B.

Funding acquisition: B.M.B.

Chapter 3

3 Transcriptional Profiling Identifies Upregulation of Neuroprotective Pathways in Retinitis Pigmentosa

(Adapted from: **Christina B. Bielmeier**, Saskia Roth, Sabrina Schmitt, Stefaniya K. Boneva, Anja Schlecht, Mario Vallon, Ernst R. Tamm, Süleyman Ergün, Andreas Neueder and Barbara M. Braunger**. Transcriptional Profiling Identifies Upregulation of Neuroprotective Pathways in Retinitis Pigmentosa** published in the *International Journal of Molecular Sciences 2021.)*

3.1 Abstract

Hereditary retinal degenerations like retinitis pigmentosa (RP) are among the leading causes of blindness in younger patients. To enable in vivo investigation of cellular and molecular mechanisms responsible for photoreceptor cell death and to allow testing of therapeutic strategies that could prevent retinal degeneration, animal models have been created. In this study, we deeply characterized the transcriptional profile of mice carrying the transgene rhodopsin V20G/P23H/P27L (VPP), which is a model for autosomal dominant RP. We examined the degree of photoreceptor degeneration and studied the impact of the VPP transgene-induced retinal degeneration on the transcriptome level of the retina using next generation RNA sequencing (RNAseq) analyses followed by weighted correlation network analysis (WGCNA). We furthermore identified cellular subpopulations responsible for some of the observed dysregulations using *in situ* hybridizations, immunofluorescence staining, and 3D reconstruction. Using RNAseq analysis, we identified 9256 dysregulated genes and six significantly associated gene modules in the subsequently performed WGCNA. Gene ontology enrichment showed, among others, dysregulation of genes involved in TGFβ regulated extracellular matrix organization, the (ocular) immune system/response, and cellular homeostasis. Moreover, heatmaps confirmed clustering of significantly dysregulated genes coding for

components of the TGFβ, G-protein activated, and VEGF signaling pathway. 3D reconstructions of immunostained/*in situ* hybridized sections revealed retinal neurons and Müller cells as the major cellular population expressing representative components of these signaling pathways. The predominant effect of VPP-induced photoreceptor degeneration pointed towards induction of neuroinflammation and the upregulation of neuroprotective pathways like TGFβ, G-protein activated, and VEGF signaling. Thus, modulation of these processes and signaling pathways might represent new therapeutic options to delay the degeneration of photoreceptors in diseases like RP.

3.2 Introduction

Retinitis pigmentosa (RP) is a hereditary form of retinal degeneration that results from mutations in any one of more than 70 known susceptibility genes (Hartong et al., 2006; Ruzickova & Stanek, 2017). Quite intriguingly, RP is considered as one of the most common hereditary diseases associated with mutations in core splicing proteins resulting in the altered regulation of gene expression (Ruzickova & Stanek, 2017). Even though RP is considered a rare genetic disorder, it is still among the major causes of blindness in younger patients (Buch et al., 2004; Farrar et al., 2002), caused by the progressive loss of rod and cone photoreceptor cells, respectively (Hartong et al., 2006).

Photoreceptors are the light sensitive neurons of the retina that are responsible for visual perception (Kolb, 1995). These cells consist of the outer and inner segments, which are connected through a cilium with the cell's perikaryal, located in the outer nuclear layer (ONL). They form a synaptic layer in the outer plexiform layer (OPL) of the retina to signal to the inner retinal neurons (Farrar et al., 2002; Kolb, 1995). Photoreceptor degeneration typically results in a thinning of the ONL concomitant with the loss of the inner and outer photoreceptor segments, resulting in an impaired visual function up to blindness. Based on the genetic heterogeneity of RP, it is still a challenge to understand and, more importantly, to inhibit the molecular mechanisms leading to the degeneration of photoreceptors, with the overall goal of delaying it.

Consequently, animal models mimicking photoreceptor degeneration are frequently used to gain insights into the impact of certain mutations on the degeneration of photoreceptors. Among these, the VPP mouse model is a well-known animal model for photoreceptor degeneration. VPP mice carry a rhodopsin transgene with three amino acid substitutions: Val-20 → Gly (V20G), Pro-23 → His (P23H), and Pro-27 → Leu (P27L) (VPP) (Naash et al., 1993), with the P23H mutation being the most prevalent mutation in U.S. patients suffering from autosomal dominant RP (Berson et al., 1991; Sung et al., 1991). Hemizygous VPP mice harbor two to five copies of the mutant rhodopsin transgene at a single integration site in addition to the wildtype rhodopsin gene (Naash et al., 1993). Transgene expression results in slowly progressing degeneration of rod and cone photoreceptors (Naash et al., 1993). In the current study, we first analyzed the morphology and apoptotic events in retinae of VPP mice. In humans, the various RP mutations of core splicing proteins result in an altered transcriptome (Ruzickova & Stanek, 2017). Therefore, we furthermore asked the question whether mutations of other genes, e.g., the rhodopsin gene, might also influence the retinal transcriptome with the overall aim to identify molecular key factors and signaling pathways that predominantly influence the course of photoreceptor degeneration. Thus, we studied the impact of the VPP mutation on the retinal transcriptome using RNAseq analyses, which has not been done so far.

In summary, we identified more than 9000 dysregulated genes. By performing gene correlation network analyses, we identified six significantly associated modules in VPP animals. Gene ontology enrichment

analyses showed, among others, involvement of components of the (ocular) immune system or response, respectively; transforming growth factor β (TGFβ) regulated extracellular matrix organization; and dysregulation of the cellular homeostasis. The progressive photoreceptor loss was highlighted by, e.g., reduced expression of photoreceptor specific transcripts, a downregulation of the rhodopsin mediated signaling pathway, and the reactivity of (micro)glial cells. In summary, our findings show that apoptosis; neuroinflammation; and the upregulation of neuroprotective pathways like TGFβ, endothelin-, and vascular endothelial growth factor (VEGF)-signaling are among the dominant effects following hereditary retinal degeneration in the VPP retina.

3.3 Results

3.3.1 Photoreceptor Degeneration in VPP Mice

To validate the VPP model, we quantified TUNEL-positive, apoptotic cells of one- month-old animals (Suppl Fig 1A–C; controls: 16.28 ± 3.08 apoptotic cells/mm^2 ONL, VPP: 173.57 ± 17.84 apoptotic cells/mm^2 ONL, $p < 0.001$) and performed morphometric analyses on semithin sections of the eyes of three-month-old control and VPP animals (Suppl Fig 1D–F) to show the beginning and more progressed photoreceptor degeneration in VPP mice (Naash et al., 1993).

We furthermore analyzed mRNA expression levels by qPCR of factors like *leukemia inhibitory factor* (*Lif*), *fibroblast growth factor 2* (*Fgf2*), and *endothelin 2* (*Edn2*) that are well-known to be upregulated in the context of retinal degeneration (Braunger et al., 2013;a Joly et al., 2008; Rattner & Nathans, 2005) and found them to be significantly upregulated in retinae of three-month-old VPP mice (*Lif* : 22.38 ± 4.13, $p = 0.008$; *Fgf2*: 13.17 ± 1.52, $p = 0.005$; *Edn2*: 46.33 ± 5.64, $p < 0.001$) compared with retinae of control littermates (*Lif*: 1.00 ± 0.18; *Fgf2*: 1.00 ± 0.14; *Edn2:* 1.00 ± 0.15) (Suppl Fig 1G).

3.3.2 Transcriptional Alterations in VPP Retinae: RNAseq and Weighted Correlation Network Analysis (WGCNA)

Subsequently, we applied next generation RNA sequencing (RNAseq) analyses to investigate the impact of VPP transgene expression and concomitant photoreceptor de- generation on the transcriptome of the retina in three-month-old VPP and control animals. Out of the total of 54,532 genes in the Ensembl gene annotation for mouse (Mus musculus GRCm38 v. 94), we found 30,796 genes to be expressed in the retina, of which 9256 were dysregulated (4636 down- and 4620 upregulated, Figure 6A, cut off criteria: Benjamin- Hochberg adjusted *p*-value (p_{adj}) < 0.05).

The top 30 dysregulated genes are shown inSuppl Table 2. Among others, genes regulating processes in neurotransmission like histidine decarboxylase *(Hdc);* galactosidase beta 1 like 3 *(Glb1l3),* which is associated with Leber's congenital amaurosis; as well as serine protease 56 *(Prss56),* which was reported to be involved in eye development, were significantly downregulated. Genes controlling scar formation, such as fibrinogen-like 2 *(Fgl2)* as well as apoptosis, e.g., caspase1 *(Casp1)* or bcl2-interacting killer (apoptosis-inducing) *(Bik),* were significantly higher expressed in VPP retinae. Furthermore, we found upregulation of quite a considerable number of genes associated with inflammatory or immune response functions such as C-X-C motif chemokine ligand 13 *(Cxcl13),* glial fibrillary acidic protein *(Gfap),* T-cell receptor T3 gamma chain *(Cd3g),* chemokine (C-C motif) ligand

5 *(Ccl5)*, and C-C motif chemokine ligand 2 *(Ccl2)*, as well as factors associated with the complement cascade like complement component factor i *(Cfi)*, *complement factor C4B*, and the *Serping1* gene.

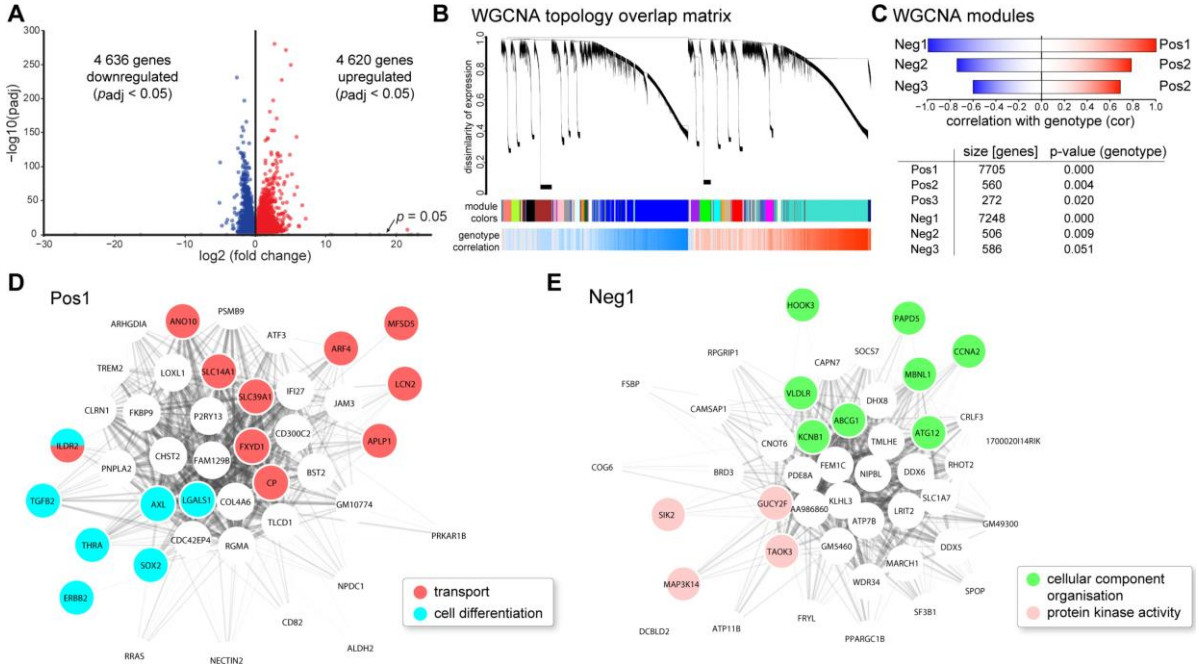

Figure 6: Transcriptome analysis of VPP mice

*(**A**) RNAseq analysis of three-month-old identified more than 4600 significantly down- and up-regulated genes, respectively (Benjamini–Hochberg adjusted p-values; padj). (**B**) Weighted correlation network analysis (WGCNA) showed large clusters of genes (modules) that were positively or negatively correlated with the genotype. Blue color in the panel below indicates lower expression and red color indicates higher expression in the VPP mice. (**C**) For each sign of correlation, three significantly correlated modules that changed in the VPP mice were identified. (**D,E**) Intra-module analysis of the Pos1 (**D**) and Neg1 I modules. The 50 highest connected (intramodular connectivity) genes are shown. Coloring of the genes corresponds to significantly enriched gene ontology terms.*

Gene ontology enrichment showed, among others, involvement of TGFβ regulated extracellular matrix organization, response to cytokine stimuli, and disturbed cellular homeostasis in VPP retinae (Table 2). Photoreceptor loss was indicated by a lower expression level of rhodopsin signaling pathway components (Table 2). Moreover, we performed weighted gene correlation network analysis (WGCNA) to identify genotype-specific patterns of dysregulation, upstream regulators, and involved signaling pathways. WGCNA clusters co-regulated genes into modules based on their similarity of expression. As this approach does not rely on the traditional dysregulation analysis and the problem of correction for multiple comparisons, more subtle changes and patterns can be identified. In addition, biological key players, e.g., regulatory proteins driving a certain pathway, for a given module can be found by the intra-module analysis. The topology overlay matrix, which represents the co-regulation of expression, for VPP and control animals, as well as the identified modules (clusters of co-regulated genes as shown by their colors in Figure 6B) and their correlation of expression with the genotype, are illustrated in Figure 6B.

The analysis identified six significantly associated modules (three positively correlated with the genotype, i.e., higher expressed in the VPP animals (Pos1, 2, 3) and three negatively correlated, i.e., lower expressed in the VPP animals (Neg1, 2, 3) (Figure 6D,E and Suppl Fig 2A-D). The Pos1 module was significantly enriched for genes involved in cellular transport and differentiation (Figure 6D and Table 3. In the Pos2 module, we found significant clustering of genes regulating necroptosis, protein transport, organelle organization, cellular homeostasis, and the ribosome (Suppl Fig 2A and Table 3). The Pos3 module (Suppl Fig 2B and Table 3) showed enrichment for bone morphogenetic protein (BMP) signaling pathway components. In the Neg1 module, we observed significant clustering of genes regulating cellular component organization and protein kinase activity (Figure 6E and Table 3). The Neg2 module (Suppl Fig 2C and Table 3) was enriched for genes involved in nucleotide homeostasis and the Neg3 module showed significant enrichment for genes encoding for ribosomal proteins and transport proteins (Suppl Fig 2D and Table 3).

Dysregulation Analysis	**Enriched Pathways** **1: BioPlanet 2019, 2: Reactome 2016, 3: NCI-Nature 2016**	**Gene Ontology Enrichment** **(Biological Process 2018)**	**Potential Regulators** **1: ChEA 2016; 2: Encode TF ChIP-seq 2015**
4620 upregulated genes ($p_{adj} < 0.05$)	1: Platelet activation, signaling, and aggregation 98.77; Axon guidance 92.59; TGF-beta regulation of extracellular matrix 89.40; Integrin cell surface interactions 80.66; PI3K class IB pathway in neutrophils 69.39 2: Platelet activation, signaling, and aggregation 98.99; Integrin cell surface interactions 84.30; Hemostasis 73.18, EPH-Ephrin 62.44; Axon guidance 56.40 3: Integrin family cell surface interactions 61.52, S1P3 pathway 54.91, CXCR4-mediated signaling events 53.30, LPA receptor mediated events 52.65, S1P1 pathway 48.70	extracellular matrix organization 93.21, neutrophil activation involved in immune response 78.28, cellular response to cytokine stimulus 72.40, regulation of cell migration 69.84, vascular endothelial growth factor receptor signaling pathway 68.22	1: SUZ12 268.86, MTF2 160.06, WT1 96.47 2: EZH2 98.33, EP300 96.32, MYOD1 30.74

4636 downregulated genes ($p_{adj} < 0.05$)	1: Messenger RNA processing 141.05, Visual signal transduction: rods 57.92, Global genomic nucleotide excision repair 45.63, Mitotic G2-G2/M phases 42.06, RNA polymerase II transcription 40.22, 2: Assembly of the primary cilium 107.65, mRNA splicing—major pathway 73.55, Activation of the phototransduction cascade 69.44, DNA repair 61.73, Cell cycle 58.51 3: Visual signal transduction: Rods 57.92, Fanconi anemia pathway 27.00, ATR signaling pathway 16.33, Regulation of Telomerase 13.58, ATM pathway 12.73, p38 MAPK signaling pathway 11.53	mRNA processing 168.47, DNA repair 93.72, cilium assembly 68.84, termination of RNA polymerase II transcription 55.78, rhodopsin mediated signaling pathway 48.90	1: CREM 212.80, FOXO3 172.49, KDM5B 152.04 2: KAT2A 233.47, GABPA 199.23, E2F4 196.15

Table 2: Enrichment analysis for dysregulated genes derived from the VPP RNAseq analysis

Enriched pathways and potential upstream regulators were predicted using the indicated databases. For gene ontology enrichment, only the top five non-redundant significantly enriched biological process terms are shown. The numbers following the terms are the combined score as calculated by Enrichr. Only terms with a combined score >5 were considered.

Dysregulation Analysis	Enriched Pathways 1: BioPlanet 2019, 2: Reactome 2016, 3: NCI-Nature 2016	Gene Ontology Enrichment (Biological Process 2018)	Potential Regulators 1: ChEA 2016; 2: Encode TF ChIP-seq 2015
Pos1 (7705 genes)	**1:** Axon guidance 36.18, T helper cell surface molecules 32.25, Platelet activation, signaling, and aggregation 29.28, Alpha-V beta-3 integrin/OPN pathway 27.52, PI3K class IB pathway in neutrophils 25.55 **2:** Integrin cell surface interactions 31.84, Platelet activation, signaling, and aggregation 29.71, Ephrin signaling 27.88, Extracellular matrix organization 27.76, Signal amplification 24.50, Semaphorin interactions 20.52 **3:** Osteopontin-mediated events 27.52, Beta3 integrin cell surface interactions 25.55, S1P2 pathway 25.22, S1P3 pathway 24.00, LPA receptor mediated events 20.74	extracellular matrix organization 44.07, sprouting angiogenesis 27.06, ephrin receptor signaling pathway 24.92, response to cytokine 24.09, vascular endothelial growth factor receptor signaling 23.91	1: SUZ12 67.13, MTF2 35.24, JARID2 25.08 2: EZH2 14.15, EP300 6.68
Pos2 (560 genes)	**1:** Respiratory electron transport 148.50, Ketone body metabolism 70.09, Cap-dependent translation initiation 50.22, Nef-mediated CD8 downregulation 42.88, Cytoplasmic ribosomal proteins 39.30 **2:** Respiratory electron transport 128.38, Eukaryotic translation elongation 57.24, Nef mediated CD8 down-regulation 42.88, Orexin and neuropeptides FF and QRFP bind to their respective receptors 35.11, Ketone body metabolism 35.11 **3:** Validated nuclear estrogen receptor alpha network 15.80, JNK signaling in the CD4+ TCR pathway 14.61,	respiratory electron transport chain 114.12, SRP-dependent cotranslational protein targeting to membrane 57.24, negative regulation of peptide 56.44, negative regulation of membrane potential 53.81, negative regulation of necroptotic process 53.81	1: EKLF 13.21, THRA 7.02, GATA1 6.80 2: HCFC1 6.41

	PDGF receptor signaling network 11.03, Alpha-synuclein signaling 9.45, Visual signal transduction: Cones 6.22		
Pos3 (272 genes)	**1:** Adrenoceptors 82.98, Phospholipase C delta-1 interactions in phospholipid-associated cell signalling 39.93, Serotonin and melatonin biosynthesis 39.93, FGFR1b ligand binding and activation 39.93, Pyrimidine biosynthesis 31.12 **2:** Adrenoceptors 82.98, Free fatty acid receptors 39.93, Arachidonate production from DAG 39.93, Serotonin and melatonin biosynthesis 39.93, FGFR1b ligand binding and activation 31.12 **3:** Signaling events mediated by the Hedgehog family 22.30, IL4-mediated signaling events 11.14, IL23-mediated signaling events 9.57, Circadian rhythm pathway 8.25, BMP receptor signaling 7.68	spinal cord dorsal/ventral patterning 365.39, osteoblast development 97.81, positive regulation of catenin import into nucleus 97.81, DNA replication-dependent nucleosome organization 71.54, septin ring assembly 39.82	1: FOXP1 17.13, BP1 6.21 2: n.s.
Neg1 (7248 genes)	**1:** Messenger RNA processing 59.45, Global genomic nucleotide excision repair 25.86, RNA polymerase II C-terminal domain phosphorylation and interaction with capping enzyme 22.43, Visual signal transduction: rods 21.50, Non-coding RNA metabolism 19.92 **2:** Assembly of the primary cilium 57.92, Processing of intronless pre-mRNAs 42.06, Processing of capped intron-containing Pre-mRNA 37.93, Homologous DNA Pairing and Strand Exchange 33.07, Activation of the phototransduction cascade 30.84 **3:** Fanconi anemia pathway 21.85, Visual signal transduction: Rods 21.50, ATR signaling pathway 5.94, Regulation of Telomerase 5.36, p38 MAPK signaling pathway 5.30	mRNA processing 70.46, DNA repair 38.32, ciliary basal body-plasma membrane docking 29.59, DNA-templated transcription, termination 26.90, histone lysine demethylation 22.88	1: FOXO3 51.83, YY1 27.21, CREB1 23.28 2: KAT2A 105.06, GABPA 89.64, E2F4 56.05
Neg2 (506	**1:** Signaling by FGFR1 fusion mutants 56.25, Activation of NOXA and translocation to mitochondria 16.74, Polo-like kinase 3 (PLK3) pathway 16.74,	left/right pattern formation 49.64, viral RNA genome replication 21.96,	1: n.s. 2: n.s.

genes)	Cyclin B2-mediated events 16.74, Tachykinin receptors bind tachykinins 16.74 **2:** Signaling by cytosolic FGFR1 fusion mutants 61.27, Heme biosynthesis 25.15, Golgi cisternae pericentriolar stack reorganization 17.20, Defective ABCA3 causes pulmonary surfactant metabolism dysfunction type 3 (SMDP3) 16.74, Hyaluronan biosynthesis and export 16.74 **3:** PLK3 signaling events 16.74, Canonical NF-kappaB pathway 7.46, TNF receptor signaling pathway 5.68, TRAIL signaling pathway 5.22, Signaling mediated by p38-gamma and p38-delta 5.04	DNA replication-independent nucleosome organization 19.36, mRNA splice site selection 18.87, positive regulation of vascular smooth muscle cell proliferation 17.20	
Neg3 (586 genes)	**1:** Cytoplasmic ribosomal proteins 195.82; Spliceosomal assembly 176.30; Translation 169.55; Respiratory electron transport, ATP biosynthesis by chemiosmotic coupling, and heat production by uncoupling proteins 137.50; Apoptotic factor-mediated response 104.27 **2:** Eukaryotic translation initiation 251.77; Mitochondrial translation 208.25; Cytochrome c-mediated apoptotic response 170.73; rRNA processing 135.64; Respiratory electron transport, ATP synthesis by chemiosmotic coupling, and heat production by uncoupling proteins 129.02 **3:** PLK3 signaling events 13.51, DNA-PK pathway in nonhomologous end joining 10.86, HIV-1 Nef: Negative effector of Fas and TNF-alpha 7.31, C-MYC pathway 5.73	mitochondrial translation 175.43, mitochondrial electron transport, ubiquinol to cytochrome c 125.37, translation 123.40, rRNA metabolic process 122.84, activation of cysteine-type endopeptidase activity involved in apoptotic process by cytochrome c 104.27	1: JARID1A 89.00, ETS1 71.54, EKLF 44.12 2: EP300 54.49, GABPA 48.40, KAT2A 46.47

Table 3: Enrichment analysis for WGCNA modules derived from the VPP RNAseq analysis

Enriched pathways and potential upstream regulators were predicted using the indicated databases. For gene ontology enrichment, only the top five non-redundant significantly enriched biological process terms are shown. The numbers following the terms are the combined score as calculated by Enrichr. Only terms with a combined score >5 were considered. Terms in bold font were also identified in the enrichment analysis of the dysregulated gene lists (combined score > 5). N.s. = no significant enrichment.

3.3.3 Dysregulation of Potentially Neuroprotective Pathways in VPP Retinae: VEGF-, TGFβ-, and G-protein Mediated Signaling

As a follow up to our previously published studies (Braunger et al., 2015; Braunger et al., 2013a; Braunger et al., 2013b) on the neuroprotective properties of signaling pathways such as transforming growth factor (TGF)β signaling, G-protein activated signaling, and vascular endothelial growth factor (VEGF) mediated signaling, we investigated their potential regulation in the VPP model. Quite intriguingly, our RNAseq data analysis (Suppl Table 2) showed a significant upregulation of genes encoding for components of the G-protein activated signaling family. Here, we particularly focused on endothelin signaling, as our group and others recently showed that endothelin 2 *(Edn2)* and endothelin receptor b *(Ednrb)* are upregulated following photoreceptor damage (Braunger et al., 2013a; Joly et al., 2008; Rattner & Nathans, 2005; Schmitt et al., 2019). In accordance, the RNAseq data (Suppl Table 2) of the VPP retinae showed a significant increase in *Ednrb* (1.28-fold, p_{adj} = 0.0074) and *Edn2* (22.12-fold, p_{adj} = 8.68×10^{-87}) expression. We furthermore observed an upregulation of factors involved in TGFβ signaling (e.g., *Tgfβ receptor type 1 (Tgfbr1)*: 1.15-fold, p_{adj} = 0.013; *Tgfbr2*: 2.23-fold, p_{adj} = 2.18×0^{-23}; *Tgfβ1*: 2.24, p_{adj} = 1.24×10^{-12}; *Tgfβ2*: 1.51-fold, p_{adj} = 2.20×10^{-20}). Of note, *Tgfβ2* was additionally identified as one of the hub genes in the Pos1 module. Vascular endothelial growth factor (VEGF) receptor signaling pathway was identified in the gene ontology enrichment analysis of the significantly upregulated genes and the RNAseq data (Suppl Table 2) showed an increased expression of *Vegfr1 (Flt1)*: 1.25-fold, p_{adj} = 4.75×10^{-7}, *Vegfr2 (Kdr)*: 2.14-fold, p_{adj} = 1.40×10^{-41}; *Vegfb*: 1.20-fold, p_{adj} = 0.00013; and *Vegfc*: 1.46-fold, p_{adj} = 9.31×10^{-5} (Suppl Table 2).

Thus, we aimed to investigate the impact of these signaling pathways (TGFβ-, G- protein activated, and VEGF- signaling) in the VPP model in detail. Unsupervised hierarchical clustering of the samples that we generated on basis of the Reactome pathway database (Wu et al., 2010) for the VEGF (Figure 7A), TGFβ (Figure 7B) and G-protein mediated signaling pathways (Figure 7C) demonstrated a perfect separation of the genotypes, highlighting the dysregulation of these pathways in the VPP animals. Furthermore, k-mer analysis (three k-mer groups indicated by numbers on the left side of each heatmap) showed clusters of tightly co-regulated genes. We highlighted some genes of particular interest (e.g., which are known to be involved in neuroprotective or immune modulating processes or to be involved in regulatory functions) in each pathway on the right side of each heatmap. The heatmaps including the full labelling are shown in Suppl Fig 3. To further analyze sub-groups of dysregulated pathways, we transformed the Reactome pathways into functional interaction networks (Figure 7D–F). We colored the genes of each network according to their dysregulation: white indicates no significant regulation, red genes were up- and blue genes were significantly down-regulated, respectively. The size of each node corresponds to the log2-fold change of regulation. The fully labeled networks are shown in Suppl Fig 4. This analysis identified distinct sub-clusters of dysregulated genes, e.g., endothelin *2 (Edn2)* and

endothelin receptor b *(Ednrb)* in the G-protein activated signaling pathway network (Figure 7E and Suppl Fig 4C) or *Tgfbr2* in the TGFβ family signaling network (Figure 7D and Suppl Fig 4B) and Vegfr2/kinase insert domain receptor *(Kdr)* in the VEGF signaling network (Figure 7F and Suppl Fig 4A).

In addition to the quantitative information from the RNAseq data derived from whole retinae, and to further validate our results, we next performed mRNA *in situ* hybridization and/or immunofluorescence staining to identify cell types expressing transcripts of interest. Using a specific probe against *Edn2*, we detected *Edn2* most prominently in the ONL in the control retina. However, we also observed distinct *Edn2* signals in the INL and some rather sparse signals in the GCL (Figure 8A). VPP retinae showed significantly higher *Edn2* expression in the RNAseq data (22.12-fold, $p_{adj} = 8.68 \times 10^{-87}$; Figure 8B, Suppl Table 2, Suppl Fig 1G) and accordingly showed a marked increase of *Edn2* signals in particular in the degenerating ONL and in the INL, but the signals in the GCL remained sparse (Figure 8A). To identify specific cell types expressing *Edn2*, we combined *in situ* hybridization with immunofluorescence staining. We used glial fibrillary acidic protein (GFAP) as a marker for astrocytes and reactive Müller cells. GFAP is a major intermediate filament particularly expressed in astrocytes (Sofroniew & Vinters, 2010) and upregulated in response to retinal trauma in astrocytes and Müller cells (Bringmann et al., 2006; Sofroniew & Vinters, 2010). Moreover, immunofluorescence staining for glutamine synthetase (GS) was used to label Müller cells (Lewis et al., 1988). When performing GFAP/GS/*Edn2* co-labelling, we observed the characteristic GFAP staining pattern for astrocytes in the nerve fiber layer for both groups (Suppl Fig 5A,B). Consistent with the observed upregulation of *Gfap* in VPP retinae as determined by RNAseq analysis (17.05-fold, $p_{adj} = 3.87 \times 10^{-78}$), immunofluorescence staining showed an increased GFAP signal intensity, indicating an enhanced protein expression, in the nerve fiber layer and an additional stripe-like staining pattern stretching through the retina, which represents the characteristic morphological appearance of reactive Müller cells. Of note, unlike apoptosis and ONL thinning (Suppl Fig 1A,D,E), which were both more prominent in the central retina, we could not detect a difference in GFAP reactivity between the central (Suppl Fig 5A,B)and the peripheral (Suppl Fig 5A,C) parts of the retina (VPP animals ($n = 3$): GFAP-intensity central retina: 26,653.88 mean gray value/mm^2; GFAP-intensity peripheral retina 50,308.26 mean gray value/mm^2, $p = 0.10$). In the 3D reconstruction of *Edn2*/GFAP/GS co-labelled sections, we observed some *Edn2* signals in GFAP-positive astrocytes (Figure 8C and Suppl Fig 6C) and in GS-positive resting and GFAP/GS-positive reactive Müller cells, respectively (Figure 8D and Suppl Fig 6D). However, we observed the majority of the *Edn2* signals in neurons of the INL and ONL (Figure 8A).

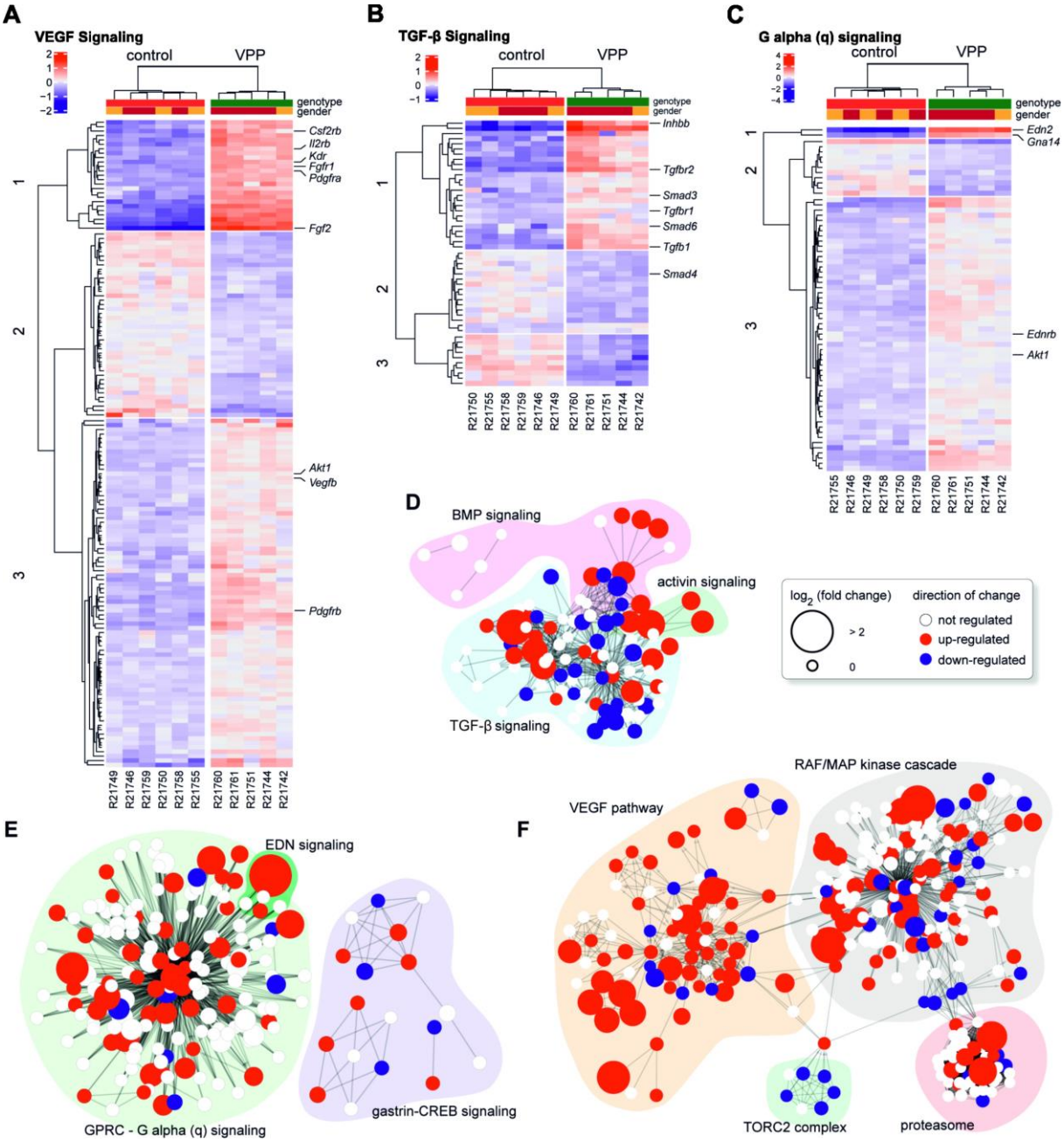

Figure 7: Pathway analyses of transcriptomic changes in VPP mice

*(**A**–**C**) Heatmaps showing the significantly dysregulated genes in the Reactome pathways VEGF signaling (**A**), TGFβ signaling (**B**), and G alpha (q) signaling (**C**). For each heatmap, the genotypes separate perfectly, as indicated by the unsupervised clustering above the heatmaps. Colors (red: upregulated, blue: downregulated) represent the deviation of the mean expression for each gene, independent of genotype. K-mer analysis into three groups revealed clusters of tightly co-regulated genes. Some interesting genes (e.g., neuroprotective or immune modulating function, directly involved in the intracellular signaling) are highlighted on the right. To further visualize sub-groups of pathways that were dysregulated, we converted the Reactome pathways into functional interaction networks. For each network, genes were colored according to their dysregulation state: white—not significantly dysregulated; red—significantly upregulated; and blue—significantly downregulated. The size of the nodes corresponds to the log2-fold change of regulation. The network for TGFβ signaling is shown in (**D**), G alpha (q) signaling is shown in I, and VEGF signaling is shown in (**F**); R21742-61 = RNAseq sample number.*

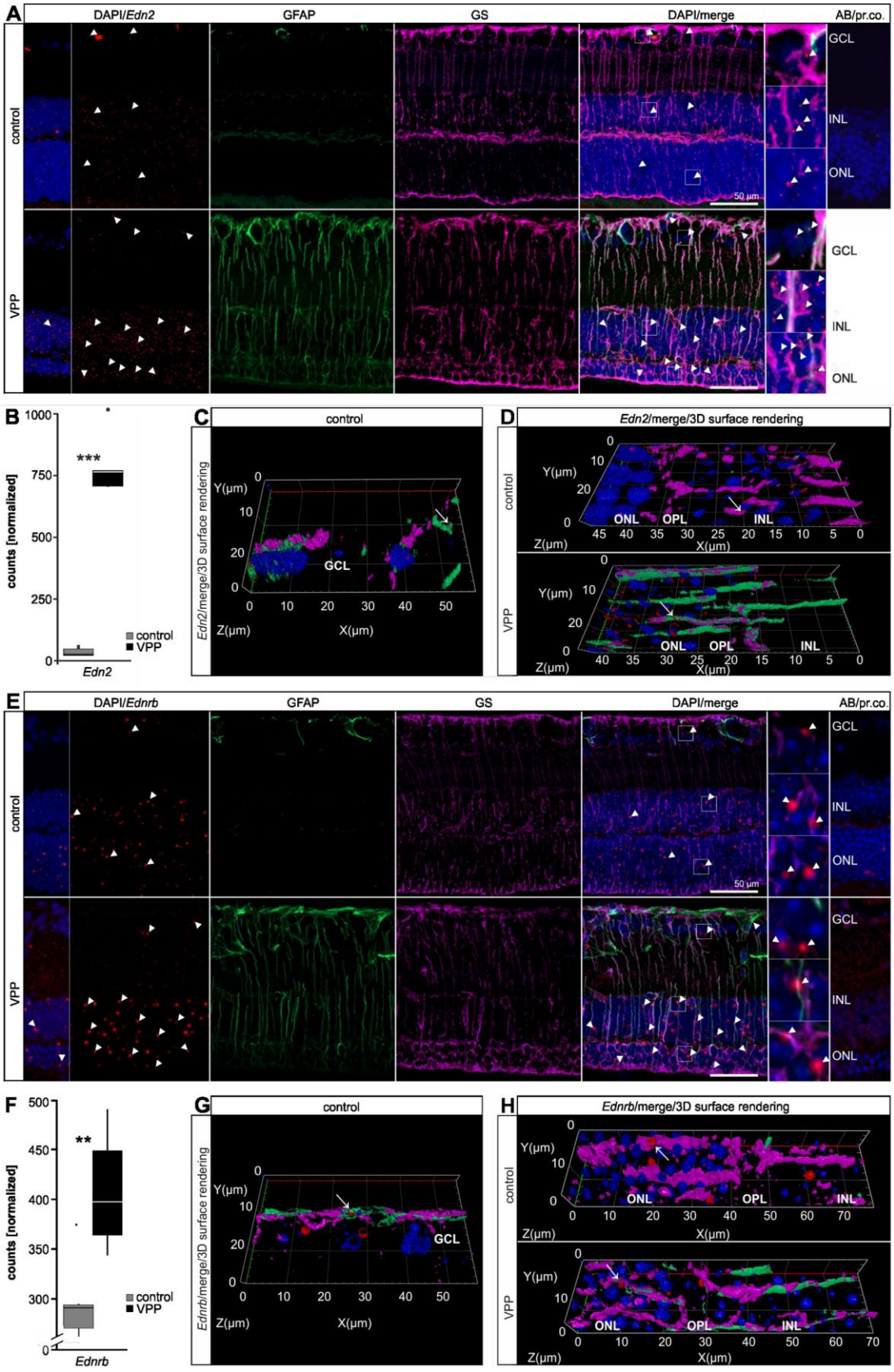
A
DAPI/Edn2
GFAP
GS
DAPI/merge
AB/pr.co.
control
VPP
GCL
INL
ONL
50 µm
B
counts [normalized]
***
control
VPP
Edn2
C
control
Edn2/merge/3D surface rendering
Y(µm)
Z(µm)
X(µm)
GCL
D
Edn2/merge/3D surface rendering
control
VPP
ONL
OPL
INL
E
DAPI/Ednrb
F
**
Ednrb
G
H
Ednrb/merge/3D surface rendering

Figure 8: Upregulation of endothelin signaling in VPP mice

*(**A**) In situ hybridization for Edn2 (red, arrowheads) and GFAP (green)/GS (purple) immunofluorescence co-labeling in the retinae of three-month-old animals. Nuclei were DAPI-stained (blue). In the VPP retina, the number of the Edn2 signals (red, arrowheads) was increased and the Müller cells were GFAP/GS-positive. The boxed areas in the merge image are shown in high resolution on the right. (**B**) Boxplots showing the extracted Edn2 expression data from the RNAseq as normalized counts for control and VPP genotypes. Control n = 6; VPP n = 5; *** $p_{adj} = 8.68 \times 10^{-87}$. (**C**,**D**) Higher magnification of the GCL (**C**) and ONL/OPL/INL region (**D**) depicted as 3D reconstruction (Edn2/merge/3D surface rendering). (**C**) Edn2 signals (red, arrow) partly overlapped with GFAP (green)-positive astrocytes. (**D**) Edn2 punctae (red, arrow) overlapped to some extent with GS (purple)-positive resting (control animal, arrow) and GFAP (green)/GS (purple)-positive reactive (VPP animal, arrow) Müller cells. In situ hybridization for Ednrb (red, arrowheads) and GFAP (green)/GS (purple) immunofluorescence co-labeling in the retinae of three-month-old animals. Nuclei were DAPI-stained (blue). In the VPP retina, the Müller cells were GFAP/GS-positive. The boxed areas in the merge image are shown in high resolution on the right. (**F**) Boxplots showing the extracted Ednrb expression data from the RNAseq as normalized counts for control and VPP genotypes. Control n = 6; VPP n = 5; ** $p_{adj} = 0.0074$. (**G**,**H**) Higher magnification of the GCL (**G**) and ONL/OPL/INL region (**H**) depicted as a 3D reconstruction (Ednrb/merge/3D surface rendering). (**G**) Ednrb signals (red, arrow) partly overlapped with GFAP (green)-positive astrocytes. (**H**) Ednrb punctae (red, arrow) overlapped to some extent with GS (purple)-positive resting (control animal, arrow) and GFAP (green)/GS (purple)-positive reactive (VPP animal, arrow) Müller cells. Edn2 = endothelin2; Ednrb = endothelin receptor type B; GCL = ganglion cell layer; INL = inner nuclear layer; OPL = outer plexiform layer; ONL = outer nuclear layer; GFAP = glial fibrillary acidic protein; GS = glutamine synthetase; AB/pr. Co. = antibody/probe control.*

Ednrb mRNA *in situ* hybridization showed specific signals in the INL and ONL and some defined signals in the GCL in control retinae (Figure 8E). We furthermore observed some *Ednrb* expression in GFAP-positive astrocytes (Figure 8G and Suppl Fig 6E) and in GS-positive resting Müller cells (Figure 8H and Suppl Fig 6F). In VPP retinae, *Ednrb* was significantly upregulated (1.29-fold, $p_{adj} = 0.007$; Figure 8F) in the RNAseq data (Suppl Table 2). In the 3D reconstruction of the *Ednrb*/GFAP/GS labelling, we detected pronounced *Ednrb* signals in the INL and ONL that overlapped to some extent with GFAP-/GS-positive reactive Müller cells (Figure 8E,H and Suppl Fig 6F). Yet, *Ednrb* signals were visible in the INL and ONL that did not overlap with GFAP/GS, indicating its further expression in neuronal cells.

Tgfbr2 was significantly upregulated (2.23-fold, $p_{adj} = 2.18 \times 10^{-23}$; Figure 9B) in VPP retinae in the RNAseq data (Suppl Table 2). To further supplement the quantitative information and potentially identify cell types in which it is upregulated, we performed *Tgfbr2 in situ* hybridization. Control retinae showed distinct signals in the INL and ONL and some scattered punctae in the GCL (Figure 9A and Suppl Fig 6G,H). In VPP retinae, the number of *Tgfbr2* punctae increased in the INL and ONL. 3D reconstruction of immunofluorescence co-labelling confirmed its expression in only some isolated GFAP-positive astrocytes (Figure 9C and Suppl Fig 6G) and its association with resting, GS-positive, and reactive GFAP-/GS-positive Müller cells, respectively (Figure 9D and Suppl Fig 6H). Yet, we also observed *Tgfbr2 in situ* hybridization in the neuronal cell layers of the retina, in particular in the INL and ONL, that did not overlap with GFAP-/GS-positive Müller cells, indicating additional expression in neuronal cells (Figure 9A).

Vegfr2 mRNA *in situ* hybridization in control retinae showed numerous signals in the INL that partly overlapped with GS-positive resting Müller cells (Figure 9E and Suppl Fig 6J). Moreover, we detected *Vegfr2* mRNA in the ONL and isolated signals in the GCL that overlapped to some extent with GFAP-positive astrocytes (Figure 9E,G and Suppl Fig 6I). Our RNAseq analysis showed *Vegfr2* to be significantly upregulated in VPP retinae (2.00-fold, $p_{adj} = 1.40 \times 10^{-41}$; Figure 9F; Suppl Table 2) and, accordingly, *Vegfr2 in situ* hybridization showed an increase in expression in the INL and ONL (Figure 9E). 3D reconstruction of co-labelling showed its association with and expression in GFAP-/GS-positive reactive Müller cells (Figure 9H and Suppl Fig 6J). Moreover, we detected *Vegfr2* signals in the neuronal layers of the retina, again in particular in the INL and ONL, that did not overlap with GFAP-/GS-positive Müller cells, indicating additional expression in neuronal cells (Figure 9E).

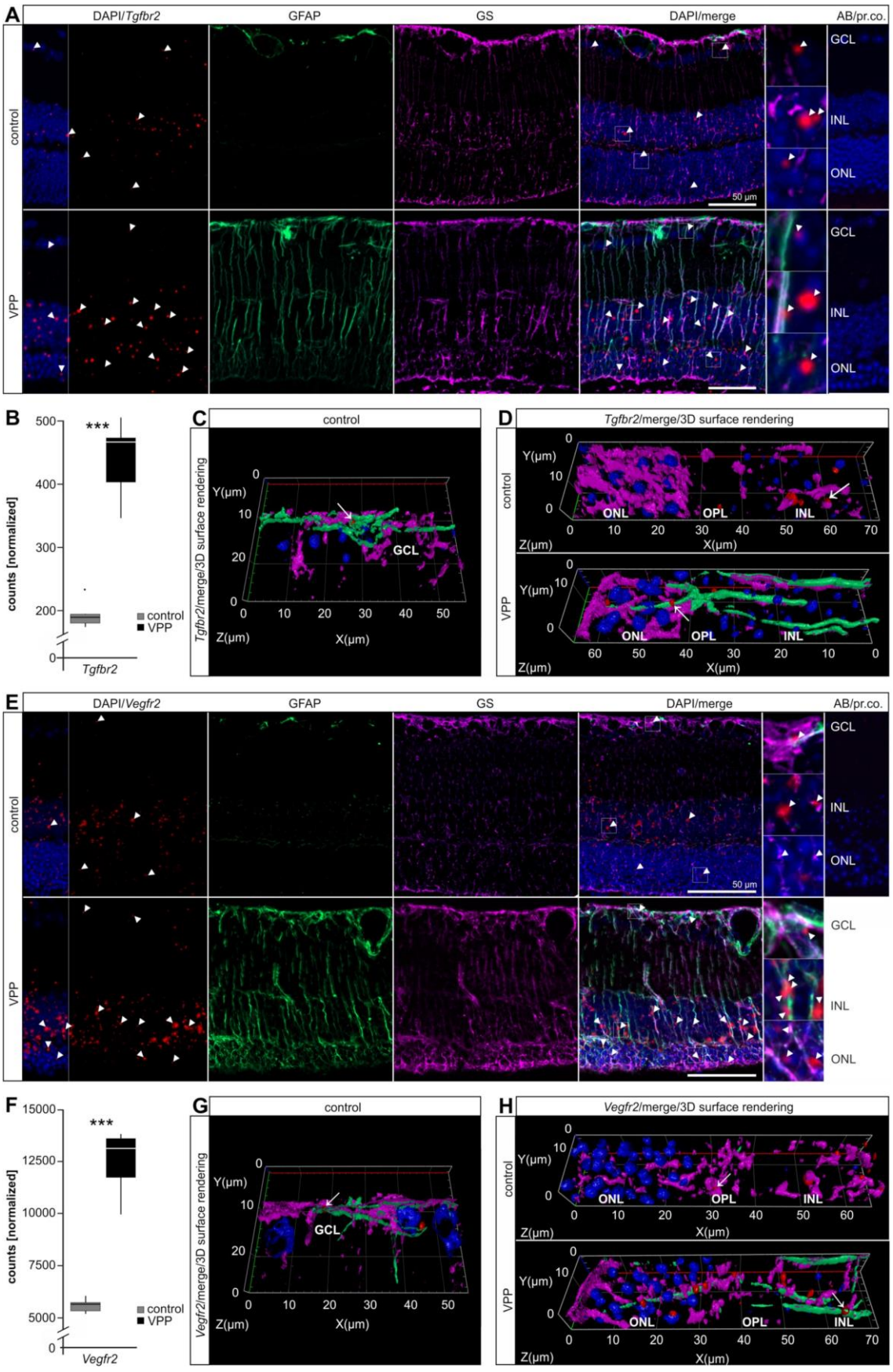
A
DAPI/Tgfbr2
GFAP
GS
DAPI/merge
AB/pr.co.
control
VPP
GCL
INL
ONL
50 µm
B
***
counts [normalized]
control
VPP
Tgfbr2
C
control
Tgfbr2/merge/3D surface rendering
Y(µm)
Z(µm)
X(µm)
GCL
D
Tgfbr2/merge/3D surface rendering
control
VPP
ONL
OPL
INL
E
DAPI/Vegfr2
F
***
Vegfr2
G
control
H
Vegfr2/merge/3D surface rendering

Figure 9: Upregulation of TGFβ- and VEGF-signaling in VPP mice

*(**A**) In situ hybridization for Tgfbr2 (red, arrowheads) and GFAP (green)/GS (purple) immunofluorescence co-labeling in the retinae of three-month-old animals. Nuclei were DAPI-stained (blue). In the VPP retina, the number of Tgfbr2 signals (red, arrowheads) in the ONL and INL was increased and the Müller cells were GFAP/GS-positive. The boxed areas in the merge image are shown in high resolution on the right. (**B**) Boxplots showing the extracted Tgfbr2 expression data from the RNAseq as normalized counts for control and VPP genotypes. Control n = 6; VPP n = 5; *** padj = 2.18 × 10−23. (**C**,**D**) Higher magnification of the GCL (**C**) and ONL/OPL/INL region (**D**) depicted as 3D reconstruction (Tgfbr2/merge/3D surface rendering). (**C**) Tgfbr2 signals (red, arrow) showed only scattered co-labeling with GFAP (green)- positive astrocytes. (**D**) Tgfbr2 punctae (red, arrow) partly associated with GS (purple)-positive resting (control animal, arrow) and GFAP (green)/ GS (purple)-positive reactive (VPP animal, arrow) Müller cells. In situ hybridization for Vegfr2/Kdr (red, arrowheads) and GFAP (green)/GS (purple) immunofluorescence co-labeling in the retinae of three-month-old animals. Nuclei were DAPI-stained (blue). The number of Vegfr2 signals (red, arrowheads) was increased in the VPP retina and the Müller cells were GFAP/GS-positive. The boxed areas in the merge image are shown in high resolution on the right. (**F**) Boxplots showing the extracted Vegfr2/Kdr expression data from the RNAseq as normalized counts for control and VPP genotypes. Control n = 6; VPP n = 5; *** padj = 1.40 × 10−41. (**G**,**H**) Higher magnification of the GCL (**G**) and ONL/OPL/INL region (H) depicted as a 3D reconstruction (Vegfr2/merge/3D surface rendering). (**G**) Vegfr2 signals (arrow) showed some co-labeling with GFAP (green)-positive astrocytes. (**H**) Vegfr2 signals partly overlapped with GS (purple)-positive resting (control animal, arrow) and GFAP (green)/GS (purple)-positive reactive (VPP animal, arrow) Müller cells. Tgfbr2 = transforming growth factor beta receptor type 2; Vegfr2 = vascular endothelial growth factor receptor 2; GCL = ganglion cell layer; INL = inner nuclear layer; OPL = outer plexiform layer; ONL = outer nuclear layer; AB/pr. Co. = antibody/probe control.*

3.3.4 The Glial Response to Photoreceptor Degeneration in VPP Mice

As we observed a significant upregulation of several genes modulating glial reactivity (e.g., glial fibrillary acidic protein (*Gfap*), serine protease inhibitor A3N (*Serpina3n*), lipocalin 2 (*Lcn2*), we performed qPCR analyses on retinal samples to determine the relative *Gfap* expression levels (control: 1.00 ± 0.19, VPP: 8.89 ± 0.63, $p < 0.001$) as well as the expression levels of the microglia/macrophage marker ionized calcium-binding adapter molecule 1 (*Iba1*, control: 1.00 ± 0.11, VPP: 6.56 ± 1.03, $p = 0.015$) and the chemokine (C-C motif) ligand 2 (*Ccl2*, control: 1.00 ± 0.11, VPP: 68.74 ± 5.11, $p < 0.001$), the latter being reported to stimulate the migration and reactivity of microglia cells (Feng et al., 2017; Rutar et al., 2011a) (Suppl Fig 5D). In accordance, our RNAseq data showed increased *Iba1* (5.51-fold, $p_{adj} = 1.12 \times 10^{-23}$ expression levels), which we further validated using an anti-IBA1 labeling to visualize myeloid cells, e.g., microglia and recruited macrophages, in the retinae of control and VPP animals (Suppl Fig 5E,F). In controls, we observed ramified IBA1-positive cells in their typical localization in the nerve fiber layer and the inner (IPL) and outer plexiform layers (OPL). In contrast, in VPP retinae, IBA1-positive cells changed their shape from ramified microglia towards amoeboid, reactive microglia in particular in the OPL, and thus in very close association with the degenerating photoreceptors. Moreover, we observed an accumulation of amoeboid-shaped, IBA1-positive cells in the sub-neuroretinal space in close proximity to the retinal pigment epithelium (RPE) (Suppl Fig 5E,F).

Taken together, these results showed a pronounced reactivity of macro- and microglial cells in response to photoreceptor degeneration. To identify the origin of the significantly elevated *Ccl2* expression in VPP retinae and to supplement the quantitative information from the RNAseq (*Ccl2*: 67.51-fold increase, $p_{adj} = 8.05 \times 10^{-14}$; Figure 10B) and qPCR data (Suppl Fig 5D), we performed *Ccl2* mRNA *in situ* hybridization on retinal sections combined with immunofluorescence co-labeling of glial cells. In

control retinae, we observed a rather low number of *Ccl2* punctae in the inner nuclear layer (INL) and the ONL, and a few signals in the retinal ganglion cell layer (GCL) (Figure 10A and Suppl Fig 6A,B). The number of *Ccl2* punctae was markedly increased in the INL and ONL of the VPP retinae (Figure 10A). When performing 3D reconstruction of *Ccl2*/GFAP/GS co-labelled sections, we observed sparse overlap of *Ccl2* in GFAP-positive astrocytes (Figure 10C and Suppl Fig 6A) and more frequent overlap in GS-positive resting and in GFAP-/GS-positive reactive Müller cells (Figure 10D and Suppl Fig 6B). However, we also detected *Ccl2* mRNA expression in cells other than Müller glia and astrocytes in the neuronal layers of the retina (GCL, INL, and ONL), pointing towards additional expression in retinal neurons (Figure 10A).

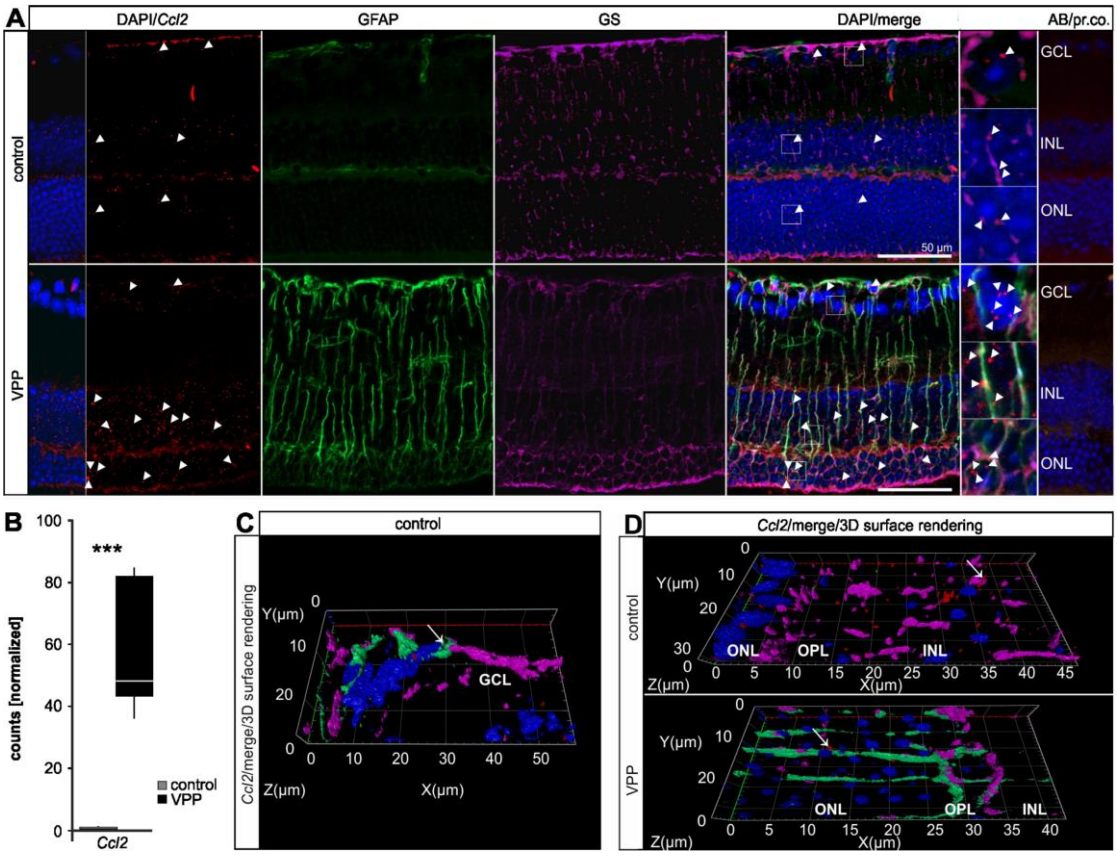

Figure 10: Upregulation of Ccl2 in VPP mice

*(**A**) In situ hybridization for Ccl2 (red) and GFAP (green)/GS (purple) immunofluorescence co-labeling in the retinae of three-month-old animals. Nuclei were DAPI-stained (blue). In the control retina, a rather discrete Ccl2 signal (arrowheads) was visible. In the VPP retina, the number of the Ccl2 punctae increased (arrowheads) and the Müller cells were GFAP/GS-positive. The boxed areas in the merge image are shown in high resolution on the right. (**B**) Boxplots showing the extracted Ccl2 expression data from the RNAseq as normalized counts for control and VPP genotypes. Control n = 6; VPP n = 5; *** $p_{adj} = 8.05 \times 10^{-14}$. (**C**,**D**) Higher magnification of the GCL (**C**) and ONL/OPL/INL region (**D**) depicted as a 3D reconstruction (Ccl2/merge/3D surface rendering). (**C**) One of the few overlaps of the Ccl2 signals (red, arrow) with GFAP (green)-positive astrocytes. (**D**) Ccl2 punctae (red, arrow) partially overlapped with GS (purple)-positive resting (control animal, arrow) and GFAP (green)/ GS (purple)-positive reactive (VPP animal, arrow) Müller cells. GCL = ganglion cell layer; INL = inner nuclear layer; OPL = outer plexiform layer; ONL = outer nuclear layer; Ccl2 = CC-chemokine ligand 2; GS = glutamine synthetase; AB/pr. Co. = antibody/probe control; AU = arbitrary unit.*

3.4 Discussion

The present data confirm that the VPP model displays the major phenotypic characteristics of the human disease retinitis pigmentosa. Briefly, we demonstrate, in comprehensive transcriptome-wide analyses of retinae from three-month-old VPP mice, (**1**) an extensive dysregulation of genes modulating apoptosis, processes in scar formation, and components of the (ocular) immune system or response, respectively; (**2**) a strong genotype-dependent clustering of genes regulating the VEGF, TGFβ, and G-protein activated signaling pathway; (**3**) the expression of regulatory genes in neurons as well as resting and reactive glia cells; and (**4**) a dysregulation of extracellular matrix organization and cellular homeostasis in WGCNA analyses.

3.4.1 The Transcriptional Response to Photoreceptor Degeneration Leads to Increased Expression of Genes Regulating Inflammatory or Immune Response Functions

Neuroinflammation is a common hallmark of the pathogenesis of neurodegenerative diseases like Alzheimer's, Parkinson's, multiple sclerosis, or retinal degenerations (Chen et al., 2016; Cuenca et al., 2014; Mullins et al., 2012). Following a neurotoxic event, neuronal stress signals mediate reactivity of microglial cells, leading to their proliferation, migration, and the secretion of specific cytokines and chemokines that can exert neurotoxic or neuroprotective effects (Cuenca et al., 2014; Stoll et al., 2000). Sustained reactivity of microglia promotes chronic inflammation and may cause irreversible neuronal cell death (Cuenca et al., 2014; Hanisch & Kettenmann, 2007; Langmann, 2007). Thus, the accumulation of reactive IBA1-positive cells in the OPL and in the sub-neuroretinal space in VPP retinae strongly indicates an ongoing neuroinflammatory process. Moreover, in the top 30 dysregulated genes, we found a considerable number of genes associated with inflammatory or immune response functions, respectively. Gene ontology enrichment analyses also pointed towards an upregulation of the cellular response to cytokine stimuli, again indicating an ongoing neuroinflammation. These findings are in accordance with previously published data, which describe upregulation of factors like *Lif, Ccl2 (Mcp-1), Ccl28,* interleukin-1 *(Il-1),* complement component 1q *(C1q),* and complement factor H *(CFH)* in retinae of genetic mouse models of RP (Bales et al., 2018; Joly et al., 2008; Lohr et al., 2006; Rohrer et al., 2007a; Rohrer et al., 2007b; Samardzija et al., 2006a; Samardzija et al., 2006b). Quite intriguingly, microarray data from the retina of one RP patient carrying two mutations in the *ABCA4* gene showed, among others, an increased expression of complement system genes (*complement factor B, complement C2*), several cytokines, and cytokine receptors (*IL-6, CXCL10, CXCL2*), respectively, indicating a neuroinflammatory process in human RP (Mullins et al., 2012). We as well as others (Feng et al., 2017; Rutar et al., 2011a) have shown that *Ccl2* is expressed in Müller cells and photoreceptors in the healthy retina and upregulated upon retinal damage, contributing to the recruitment of microglia/infiltrative

macrophages (Rutar et al., 2012; Rutar et al., 2011a). However, conflicting data exist concerning the exact role of *Ccl2* in the context of neurodegeneration. Recently, Joly and colleagues showed that the retinal morphology of double mutant mice expressing the VPP trans- gene on a *Ccl2* null background (VPP; $Ccl2^{-/-}$) did not differ from that of transgene VPP mice on a wildtype background (Joly et al., 2008). In contrast, Rutar and colleagues demonstrated that siRNA-mediated knock down of *Ccl2* resulted in a significantly lower number of apoptotic photoreceptors in rats after light-induced photoreceptor degeneration and (Rutar et al., 2012; Rutar et al., 2011a). Based on our data, we hypothesize that, in VPP retinae, the elevated *Ccl2* expression in Müller cells and in the ONL contributes to the attraction/migration and reactivity of microglial cells in this particular region.

In our comprehensive analyses, we furthermore detected a considerable number of genes encoding for components of the complement system, which is part of the innate immune system. Various complement factors have been reported to be upregulated in retinae of human patients suffering from RP or in retinae of mice following genetically or light-induced photoreceptor degeneration in mice (Hadziahmetovic et al., 2012; Lohr et al., 2006; Rohrer et al., 2007a; Rohrer et al., 2007b; Rutar et al., 2012; Schäfer et al., 2017; Silverman et al., 2019). Activation of the complement system promotes microglia/infiltrative macrophages migration and eventually complement activated lysis (Lohr et al., 2006; Rutar et al., 2011b). Still, conflicting data exist regarding the exact role of complement system activation and its impact on photoreceptor degeneration. Mice with a deficiency in complement factor D are protected from light-induced photoreceptor degeneration (Rohrer et al., 2007a), indicating a detrimental role for photoreceptor survival, but the deficiency in complement component 3 (C3) or complement receptor 3 (CR3) in a genetic mouse model of photoreceptor degeneration increases microglia-mediated neurotoxicity to photoreceptors (Silverman et al., 2019). Thus, the detailed function of the complement system and its specific role in microglia and Müller cells and its contribution to photoreceptor degeneration has yet to be elucidated. Nevertheless, based on our transcriptome-wide data, we conclude that the significant upregulation of genes associated with inflammatory or immune response functions leads to neuroinflammation in VPP retinae, potentially contributing to the degeneration of photoreceptors.

3.4.2 The Transcriptional Response to Photoreceptor Degeneration Leads to the Upregulation of Neuroprotective Factors and Pathways

We additionally analyzed the impact of the VPP model on neuroprotective path- ways like TGFβ, G-protein, and VEGF signaling (Saint-Geniez et al., 2008). Recently, our group and others showed that, in response to retinal injury, endothelin 2 (*Edn2*) is expressed by photoreceptors concomitant with elevated expression of endothelin receptor b (*Ednrb*) and *Gfap*, the latter indicating the reactivity of Müller cells, and an increased expression of *Lif* and *Fgf2* (Boneva et al., 2016; Braunger et al., 2013a; Joly et al., 2008; Rattner & Nathans, 2005; Schmitt et al., 2019). Our RNAseq data, *in situ* hybridizations,

immunofluorescence staining, and qPCR analyses confirmed this observation for the VPP model of retinal degeneration. It is of interest to note that our co-labelling experiments showed expression not only of *Ednrb*, but also of *Tgfbr2* and *Vegfr2* in resting and reactive Müller cells, clearly indicating the close interplay of neuronal and glial cells. Furthermore, we previously showed that *Edn1*, *Edn2*, *Ednra*, and *Ednrb* are significantly upregulated following induced ocular traumata (Schmitt et al., 2019). Yet, in VPP retinae, only *Edn2* and *Ednrb* were upregulated. These inconsistent results might well be explained by the different activation patterns of signaling pathways depending on the actual cause of cell death, i.e., light-induced versus genetically-induced cell death (Samardzija et al., 2006b).

3.4.3 The Transcriptional Response to Photoreceptor Degeneration Leads to Expression of Pro-Apoptotic Factors and Extracellular Matrix Organization

Our transcriptome analyses also showed upregulation of factors associated with apoptosis (*Casp1, Bik*) and scar formation such as fibrinogen like 2 *(Fgl2)* and *Tgfβ1*. A well-described characteristic of TGFβ signaling is its contribution to wound healing, tissue fibrosis, and scar formation (Penn et al., 2012; Saika, 2006). Accordingly, "TGF-β regulated organization of extracellular matrix" was a major hit in our gene ontology analysis and might well be the result of a healing response following photoreceptor degeneration in VPP retinae. We furthermore identified the isoform *Tgfβ2* as one of the central hub genes in the WGCNA module Pos1. Gene ontology analysis of the Pos1 module showed enrichment for genes involved in cell differentiation. TGFβ signaling modulates manifold processes, e.g., the regulation of early development, cell-cycle control, and cell differentiation (Goumans et al., 2009; Goumans & Mummery, 2000; Massagué, 2004). Moreover, we recently showed that the deletion of TGFβ signaling results in the development of retinal microaneurysms and choroidal neovascularization (Braunger et al., 2015; Schlecht et al., 2017), clearly emphasizing its potential to regulate angiogenic processes. Furthermore, TGFβ signaling contributes to extracellular matrix reorganization in ocular diseases such as primary open angle glaucoma (Fuchshofer, 2011; Fuchshofer & Tamm, 2009, 2012). However, AAV-mediated delivery of TGFβ1 rescued degenerating cones in mouse models of RP (Wang et al., 2020) and TGFβ signaling protects retinal neurons from programmed cell death during retinal development (Braunger et al., 2013b), thus highlighting its neuroprotective properties (Tesseur et al., 2017).

The observed gliosis of astrocytes and Müller cells, as indicated, e.g., by elevated *Gfap* expression levels and the characteristic stripe-like staining pattern of GFAP in retinal sections, is a typical reaction of neuronal tissue to various neurotoxic insults (Bringmann et al., 2006; Giaume et al., 2007) and eventually results in a glial scar. Quite intriguingly, recently published data suggest a major and interactive role of glial cells such as astrocytes contributing to neurodegeneration and their cell-specific targeting resulted in

accelerated functional recovery compared with untreated animals (Kitchen et al., 2020; Sylvain et al., 2021).

The identified dysregulation of genes involved in neuroinflammation, neuroprotection, apoptosis, scar formation, and wound healing and the corresponding WGCNA data are not only of interest for researchers working on retina, but might well be of interest for scientists working with other neuronal tissues.

In the future, using material from mouse models of RP or humanized 3D culture models (retinal organoids) combined with advanced transcriptomic techniques such as imaging-based in situ cell-type identification/mapping combined with single-cell RNA- sequencing will allow to create a molecularly annotated and spatially dedicated cell atlas of transcriptional changes related to RP (Moffitt et al., 2016, 2018). Moreover, the use of high-throughput screening and computer-aided drug design can provide novel insights with the overall aim to find new treatment options for neurodegenerative diseases such as RP (Aldewachi et al., 2021; Salman et al., 2021).

3.5 Conclusion

The parallel expression of VPP mutant and wildtype rhodopsin (Naash et al., 1993) results in a significant increase in apoptosis and thinning of the ONL to half of its thickness in retinae of three-month-old VPP animals. Intriguingly, in our transcriptome-wide analyses, we found more than 9,000 dysregulated genes in retinae of VPP mice. The predominant changes in gene expression point towards induction of apoptosis, scar formation, neuroinflammation, and the upregulation of neuroprotective pathways like TGFβ, G-protein activated (e.g., endothelin), and VEGF signaling in VPP retinae. Using *in situ* hybridization combined with cell-type specific markers, we could show that regulatory factors such as *Ccl2*, *Edn2*, *Tgfbr2*, *Ednrb*, and *Vegfr2* were also expressed in glial cells in addition to neurons. Albeit the relevance of the identified pathways needs further investigation using, e.g., different (cell-type specific) knockout mouse lines, it is tempting to speculate that modulation of neuroinflammation and neuroprotective pathways in general or, e.g., in glial cells, is a promising target for the development of new therapeutic options to delay the degeneration of photoreceptors in diseases like RP.

3.6 Materials and Methods

3.6.1 Mice

The mice were on a 129 SV background and kept in a 12 h light/dark cycle. Mice of both sexes were used for the experiments. Mice, carrying two floxed *Tgfbr2* alleles at chromosome 9 (Chytil et al., 2002), thus representing functional wildtype mice, were crossbred with hemizygous VPP mice (Naash et al., 1993). The resulting offspring expressed either wildtype rhodopsin (named as control mice = VPP negative animals) or the VPP transgene (referred to as VPP mice), a rhodopsin mutant with point mutations at positions V20G, P27L, and P23H, in addition to wildtype rhodopsin. The VPP mutation results in a progressive retinal neurodegeneration (Naash et al., 1993). For genotyping, the following primers were used: 5'-agactgacatggggaggaattcccaga- 3, (sense) and 5-gagctgctcgaagtgactccgacc-3, (antisense). The thermal cycle protocol was denaturation at 94 ˚C for 30 s, annealing at 68 ˚C for 45 s, and elongation at 72 ˚C for 45 s for 35 cycles.

3.6.2 Microscopy and Morphometric Analyses (Spider Diagram)

The enucleated eyes were fixed for 24 h in 2.5% paraformaldehyde (PFA)/2.5% glutaraldehyde in sodium cacodylate buffer and processed as described previously (Kugler et al., 2017). Then, 1 µm thick semithin meridional sections were cut and stained according to Richardson (Richardson et al., 1960). The sections were analyzed on an Axio Imager Z1 microscope (Carl Zeiss, Jena, Germany) using Zeiss Zen software (Carl Zeiss, Jena, Germany). The thickness of the outer nuclear layer (ONL) was measured and the mean values were plotted a as spider diagram, as described previously in (Boneva et al., 2016; Braunger et al., 2015). It is of interest to note that there was no sex-specific difference in the ONL thickness of VPP (male (n = 3) versus female (n = 3)) and control (male (n = 3) versus female (n = 3)) animals.

3.6.3 Immunofluorescence and RNA/Basescope® In situ hybridization

Eyes were fixed for 4 h in 4% PFA, washed extensively in phosphate buffer (PB, 0.1 M, pH 7.4), and embedded in paraffin according to standard protocols. Paraffin sections (6 µm thick) were deparaffinized. Glial fibrillary acidic protein (GFAP) (Agilent Dako, Santa Clara, CA, USA), ionized calcium-binding adapter molecule 1 (IBA1) (Wako, Ō saka, Japan), and glutamine synthetase (GS) (Millipore, Temecula, California, USA) immunofluorescent staining were performed as described in (Braunger et al., 2015). For *in situ* hybridization (ACD, Newark, USA), paraffin sections were pretreated with retrieval reagent and protease according to the user manual. RNAscope® Fluorescent Multiplex Reagent Kit was used to hybridize chemokine (C-C motif) ligand 2 (*Ccl2*) (ACD catalog number: 311791) and Endothelin 2

(*Edn2*) (ACD catalog number: 418221) and BaseScope™ Detection Reagent Kit v2—RED was used to label Vegf receptor type 2 (*Vegfr2*) (ACD catalog number: 860711), endothelin receptor type b (*Ednrb*) (ACD catalog number: 706471), and TGFβ receptor type 2 (*Tgfbr2*) (ACD catalog number: 845871). The sections were analyzed on an Axio Imager Z1 microscope with the Apotome.2 function (Carl Zeiss, Jena, Germany) using Zeiss Zen software (Carl Zeiss, Jena, Germany).

To determine Müller cell reactivity of the peripheral and central part of the retina, we measured GFAP fluorescence intensity in the area of the peripheral and central 20% of the retina, which we defined as comparable to the measurements for the spider diagrams (Boneva et al., 2016; Braunger et al., 2015).

3.6.4 RNA Isolation and Quantitative Real-Time RT-PCR (qPCR)

TriFast (Peqlab, Erlangen, Germany) was used to isolate total mRNA from retinal tissue and cDNA was synthesized using the iScript cDNA Synthesis Kit (Bio-Rad Laboratories, Inc., Hercules, CA, USA) following the manufacturer's instructions. QPCR analyses were performed on a CFX Realtime PCR Detection System (Bio-Rad Laboratories, Inc., Hercules, CA, USA) and as previously described (Schlecht et al., 2017). All oligonucleotides (Suppl Table 1) were designed to span exon-intron boundaries and purchased from Invitrogen (Carlsbad, CA, USA). CFX Manager™ Software and Excel were used to analyse relative mRNA expression levels according to the $\Delta\Delta C_T$-method (Livak & Schmittgen, 2001). The geometric mean value of the reference genes ubiquitin c *(Ubc)* and guanine nucleotide binding protein subunit beta2 like 1 *(Gnb2l1)* was used for normalization. To perform RNA sequencing, total RNA of pooled retinae (right and left eye) was purified using the Rneasy Mini Kit by Qiagen (Venlo, The Netherlands).

3.6.5 RNA Sequencing

Library preparation and RNAseq were performed at the service facility 'KFB—Center of Excellence for Fluorescent Bioanalytics' (Regensburg, Germany. www.kfb-regensburg.de, accessed on 11 June 2021). Library preparation and RNAseq were carried out as described in the Illumina TruSeq Stranded mRNA Sample Preparation Guide, the Illumina NextSeq 500 System Guide (Illumina, Inc., San Diego, CA, USA), and the KAPA Library Quantification Kit—Illumina/ABI Prism User Guide (Kapa Biosystems, Inc., Woburn, MA, USA). In brief, 250 ng of total RNA was used for purifying the poly-A containing mRNA molecules using poly-T oligo-attached magnetic beads. Following purification, the mRNA was fragmented to an average insert size of 200–400 bases using divalent cations under elevated temperature (94 °C for 4 min). Next, the cleaved RNA fragments were reverse transcribed into first strand cDNA using reverse transcriptase and random hexamer primers. Actinomycin D was added to improve strand specificity by preventing spurious DNA-dependent synthesis. Blunt-ended second strand cDNA was

synthesized using DNA Polymerase I, Rnase H, and dUTP nucleotides. The incorporation of dUTP, in place of dTTP, quenched the second strand during the later PCR amplification, because the polymerase does not incorporate past this nucleotide. The resulting cDNA fragments were adenylated at the 3' ends; the indexing adapters were ligated; and, subsequently, specific cDNA libraries were created by PCR enrichment. The libraries were quantified using the KAPA SYBR FAST ABI Prism Library Quantification Kit. Equimolar amounts of each library were sequenced on a NextSeq 500 instrument controlled by the NextSeq Control Software (NCS) v2.2.0, using a 75 Cycles High Output Kit with the single index, paired-end (PE) run parameters. Image analysis and base calling were done by the Real Time Analysis Software (RTA) v2.4.11. The resulting .bcl files were converted into .fastq files with the CASAVA Software v1.8.2.

3.6.6 Bioinformatics

For all samples, at least 30 million reads were analyzed. Fastq files were quality controlled with FastQC v0.11.5 (http://www.bioinformatics.babraham.ac.uk/projects/fastqc/ (Accessed on June 2021)). All files passed quality control. The reads were aligned against Ensembl Mus musculus GRCm38 version 94 using STAR aligner v2.5.3a (Dobin et al., 2013). One sample (R21753) showed poor read alignments of less than 30% and was removed from further analyses. Reads were quantified using salmon v0.8.2 (Patro et al., 2017). All subsequent analyses were conducted in R v3.5.1. Samples were screened for outliers using PCA and clustering analysis. One sample (R21741) was identified as an outlier and removed from further analyses. Thus, the final sample number was six control and five VPP retinae. Transcriptional dysregulation was computed using tximport v1.10.0 (Soneson e al., 2015) and DESeq2 v1.22.1 (Love et al., 2014) with genotype as the variable of interest and sex of the mice as a covariate and using ashr (Stephens, 2017) as the fold change shrinkage estimator. The Benjamini–Hochberg procedure was used to correct for multiple comparisons (*p*-adjusted; p_{adj}). For correlation network analysis, we used the normalized and variance stabilized counts from the DESeq2 analysis. Batch correction for sex was applied with limma v3.38.3 (Ritchie et al., 2015) keeping genotype as the variable of interest. The normalized, transformed, and batch corrected counts were used to construct a weighted gene correlation network using WGCNA v1.66 (Langfelder et al., 2013; Langfelder & Horvath, 2008). Heatmaps and k-mer analysis were carried out using ComplexHeatmap v2.3.2 (Gu et al., 2016). Visualization was carried out using cytoscape v3.7.2 (http://cytoscape.org, accessed on 11 June 2021) with the Reactome FI app v7.2.1 (Wu et al., 2010). Ontology analysis was carried out using the Enrichr website (Chen et al., 2013; Kuleshov et al., 2016). Scripts are available upon request.

3.6.7 Statistics

All results that are displayed in bar graphs are expressed as means ± SEM. Data were screened for outliers using the Grubb's outlier test in graph pad prism. Comparisons between the means of two groups were made by a two-tailed Student's t-test. $P \leq 0.05$ was considered as statistically significant.

3.7 Acknowledgments

The authors wish to thank Esther Asan for her helpful suggestions. We thank Alla Ganscher, Elke Stauber, Angelika Pach, Silvia Babl, and Margit Schimmel for the great technical assistance and Christoph Möhle and Thomas Stempfl of the Kompetenzzentrum für Bioanalytik, University of Regensburg for the RNA sequencing analysis. Furthermore, the authors acknowledge support by the High Performance and Cloud Computing Group at the Zentrum für Datenverarbeitung of the University of Tübingen, the state of Baden-Württemberg through bwHPC, and the German Research Foundation (DFG) through grant no INST 37/935-1 FUGG.

3.8 Supplementary Material

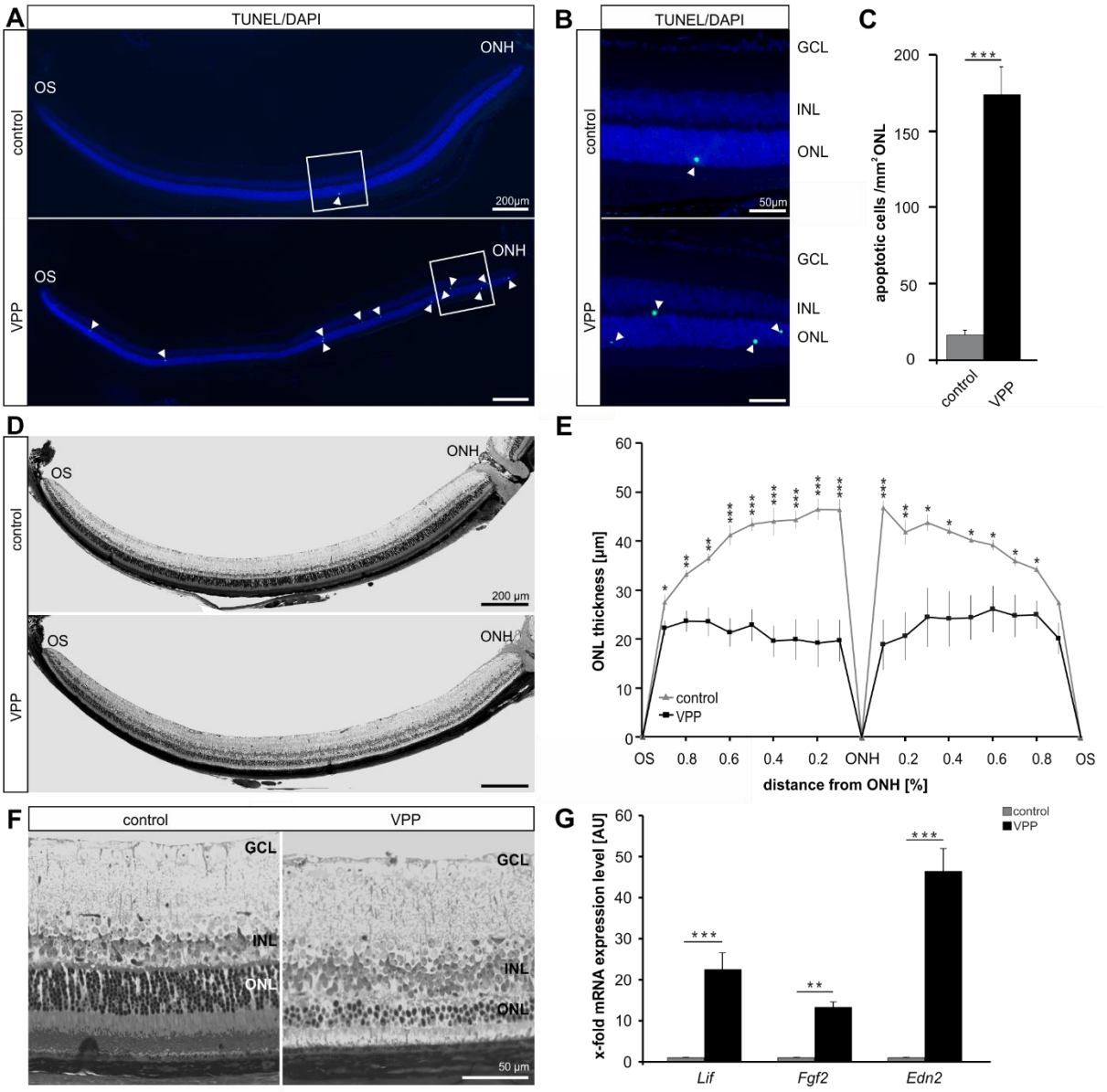

Suppl Fig 1: Apoptosis, retinal morphology/morphometry and the expression of neuroprotective factors in VPP and control mice

***(A**,**B**) Mid-horizontal sections of TdT-mediated dUTP-biotin nick end (TUNEL)-labeled (green, arrowheads) retinae of one-month-old control and VPP animals (**A**) Detailed magnification (**B**) of the boxed areas in (**A**). Cell nuclei were stained with DAPI (blue). (**C**) Total number of TUNEL-positive cells normalized to mm² ONL. Controls: n = 11; VPP: n = 11. (**D**) Richardson-stained, mid-horizontal semithin sections of the posterior eye segment of three-month-old control and Vpp mice. (**E**,**F**) The detailed magnification of the central retina (**F**) shows a regular morphology of control and a strongly thinned ONL in VPP animals. The thickness of the ONL was measured on mid-horizontal semithin sections at defined measure points and the mean values were plotted in the spider-diagram in I. Controls n = 5; VPP: n = 5. (**G**) Relative mRNA expression levels of Lif, Fgf2 and Edn2 are significantly upregulated in VPP mice compared to controls. Controls: n = 4; VPP: n = 8. AU= arbitrary unit; GCL = ganglion cell layer; INL = inner nuclear layer; ONL = outer nuclear layer; ONH = optic nerve head; OS = ora serrata. Data are means ± SEM; *p≤0.05, **p≤0.01, ***p≤0.001.*

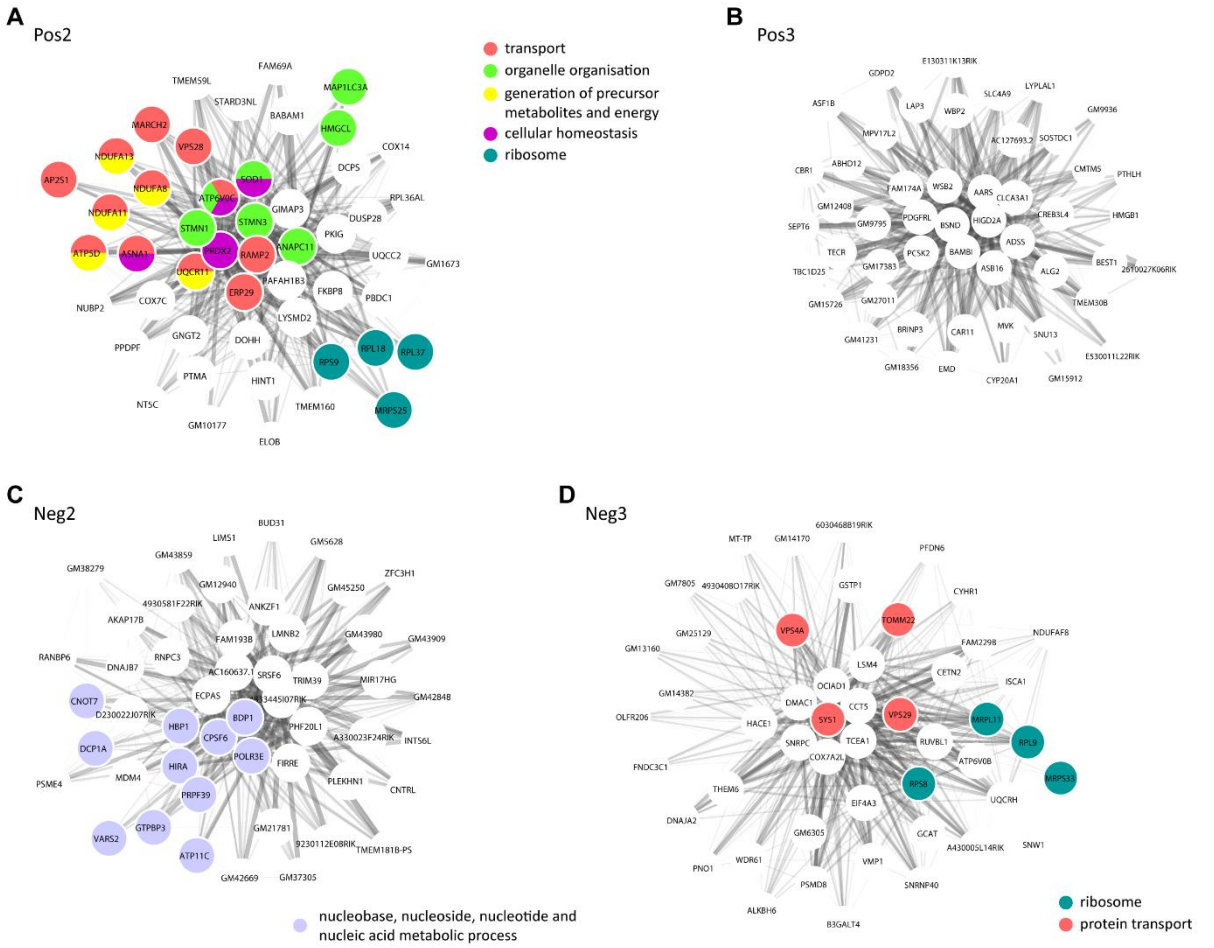

Suppl Fig 2: WGCNA analysis of VPP mice

*This figure supplements Figure 6. Intra-module analysis of the Pos2 (**A**), Pos 3 (**B**) and Neg2 (**C**), Neg 3 (**D**) modules in Vpp animals show the 50 highest connected (intramodular connectivity) genes. Coloring of the genes corresponds to significantly enriched gene ontology terms.*

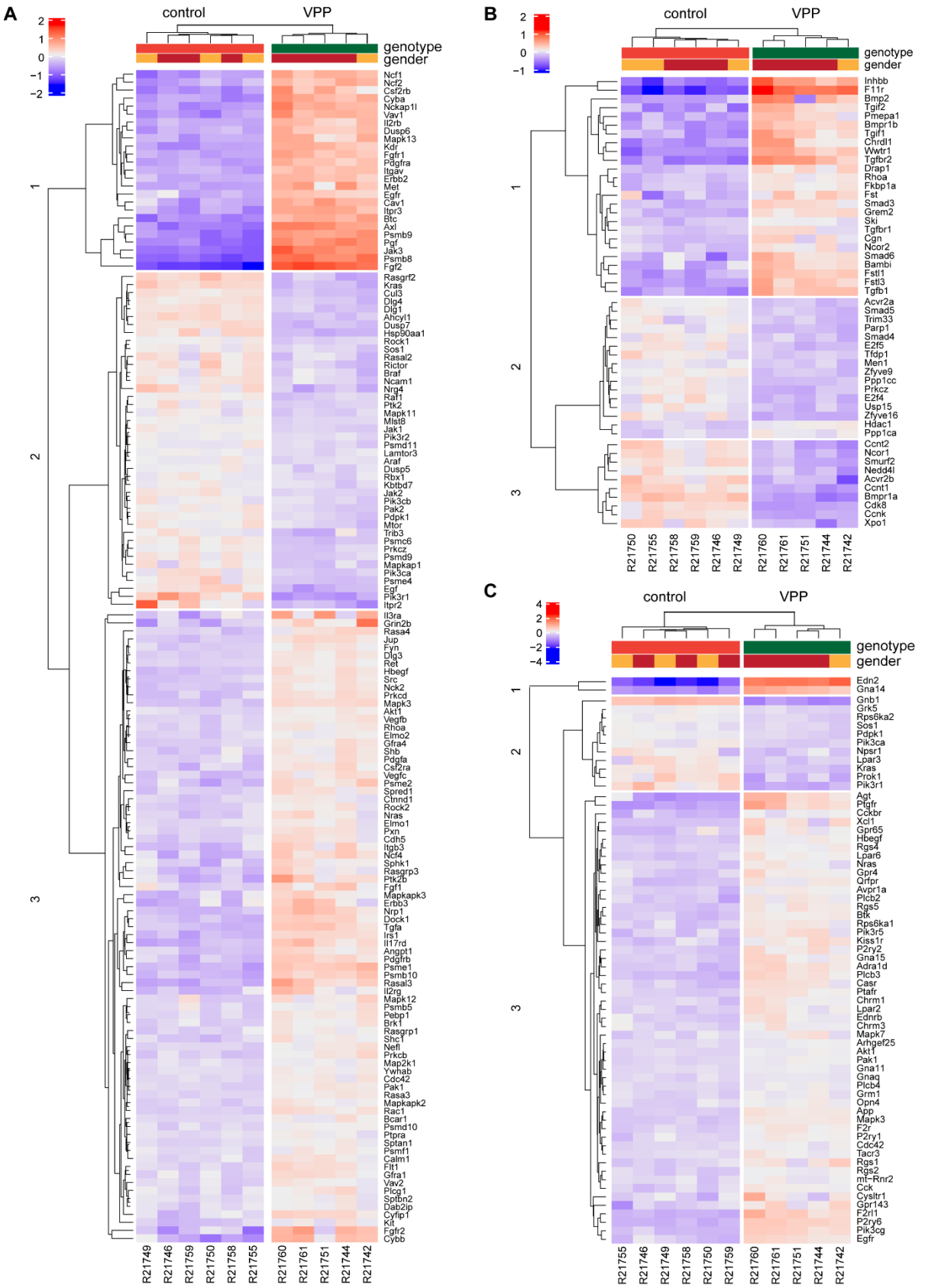

Suppl Fig 3: Heatmaps of pathway analysis of transcriptomic changes in the VPP mice

*Heatmaps showing the significantly dysregulated genes in the Reactome pathways VEGF signaling (**A**), TGF-beta signaling (**B**) and G alpha (q) signaling (**C**). For each heatmap, the genotypes separate perfectly, as indicated by the clustering above the heatmaps. K-mer analysis into 3 groups revealed clusters of tightly co-regulated genes.*

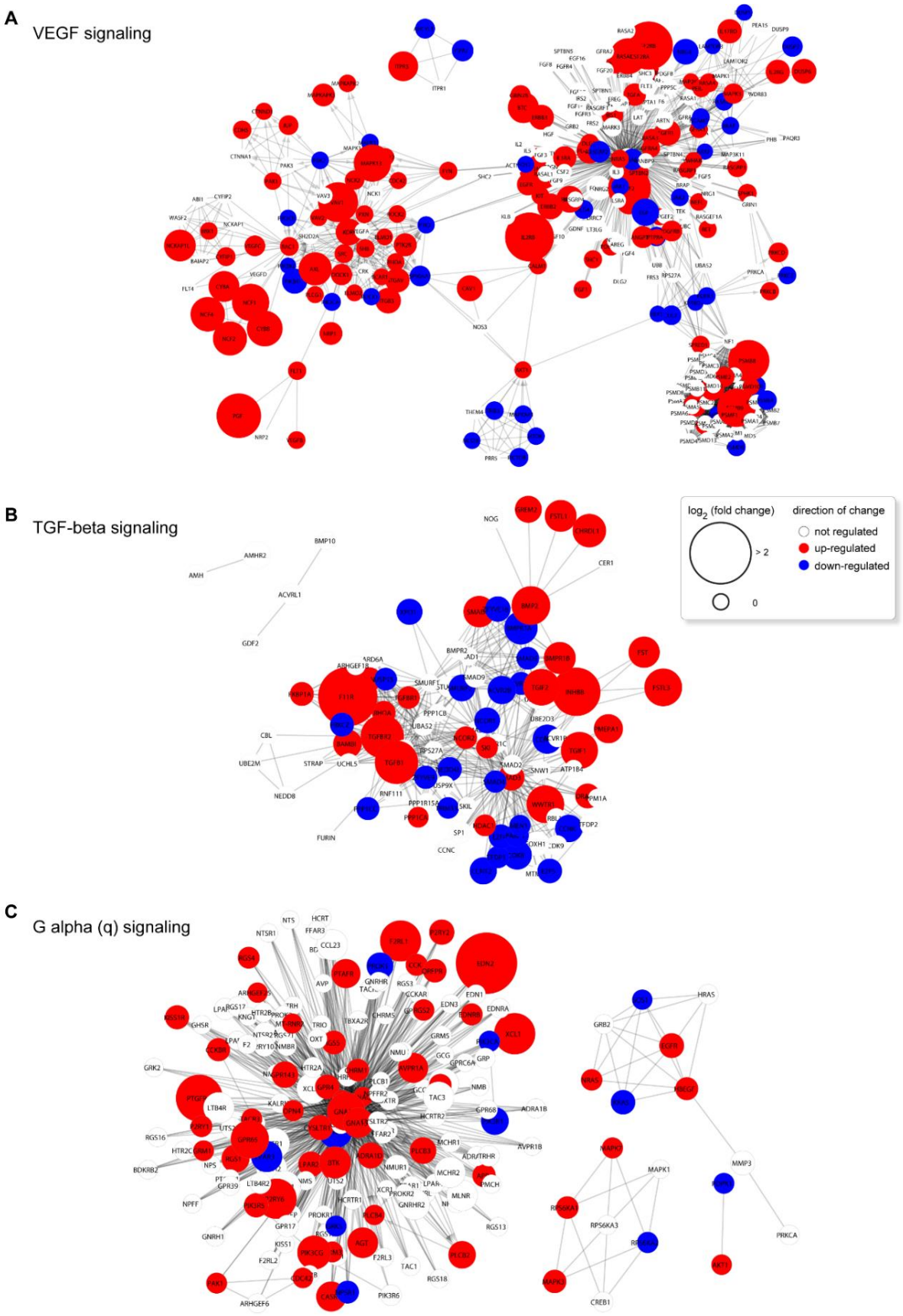
A
VEGF signaling
B
TGF-beta signaling
log2 (fold change)
direction of change
not regulated
up-regulated
down-regulated
> 2
0
C
G alpha (q) signaling

Suppl Fig 4: Pathway analysis of transcriptomic changes in the VPP mice

*Reactome pathways were converted into functional interaction networks. The network for VEGF signaling is shown in (**A**), TGF-beta signaling is shown in (**B**) and G alpha (q) signaling is shown in (**C**). For each network genes were colored according to their dysregulation state: white – not significantly dysregulated; red – significantly up-regulated and blue – significantly down-regulated. The size of the nodes corresponds to the log2-fold change of regulation.*

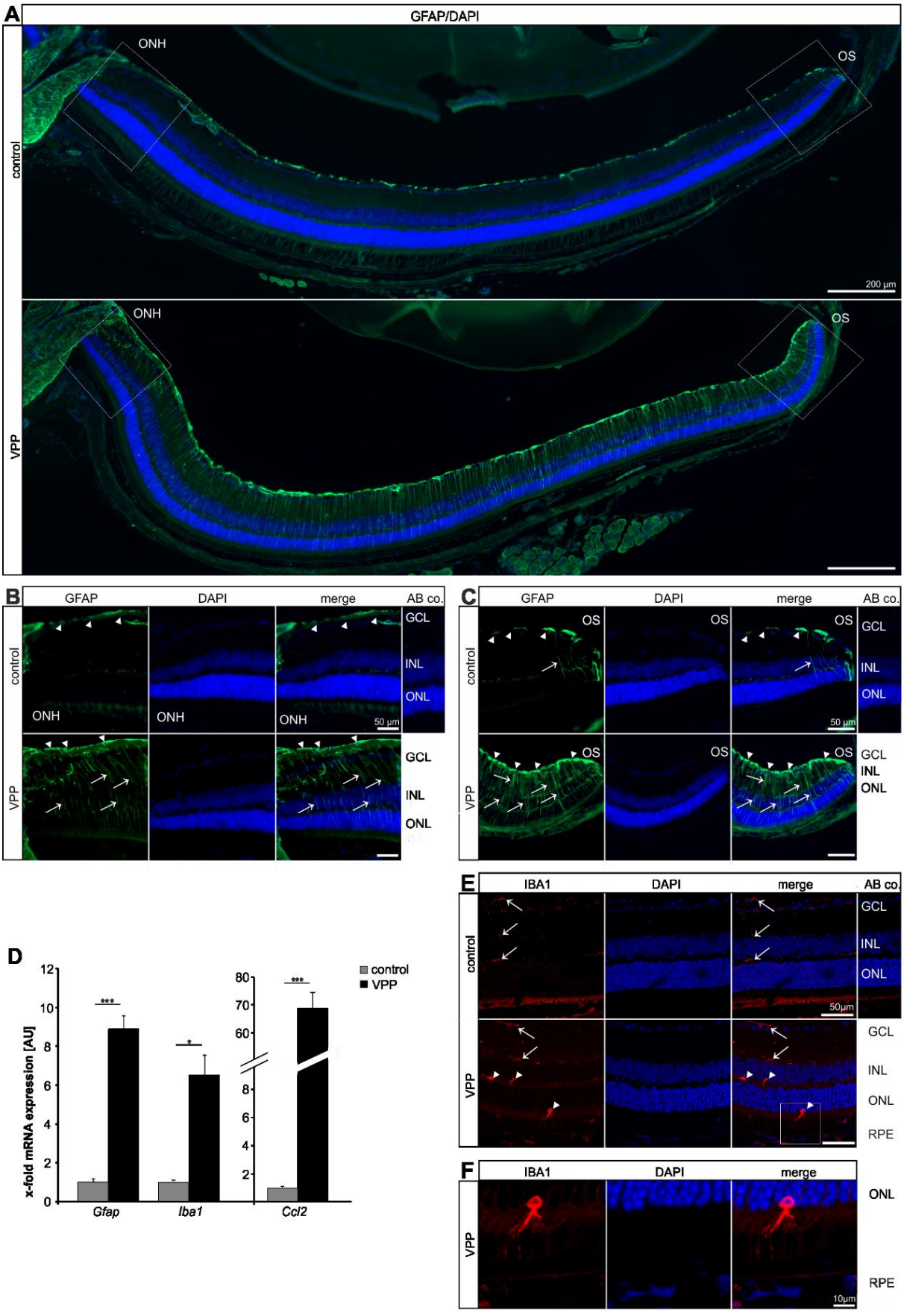
A
GFAP/DAPI
control
VPP
ONH
OS
200 µm
B
GFAP
DAPI
merge
AB co.
GCL
INL
ONL
50 µm
C
D
control
VPP
x-fold mRNA expression [AU]
Gfap
Iba1
Ccl2
E
IBA1
RPE
50µm
F
10µm

Suppl Fig 5: The glial response to photoreceptor degeneration in the VPP model

*(**A**) Immunofluorescence staining against GFAP (green) on mid-horizontal sections of one-month-old eyes. Cell nuclei were DAPI-stained (blue). (**B**,**C**). The detailed magnification of the central (B) and peripheral (**C**) retina the characteristic GFAP staining (green, arrowheads) pattern in the nerve fiber layer which was more intense in the VPP retina with an additional radial staining pattern (arrows), indicating reactivity of Müller cells. Cell nuclei were DAPI-stained (blue). (**D**). QPCR analyses for mRNA of retinal Gfap, Iba1 and Ccl2 in three-month-old animals. Controls: Gfap: n = 8, Iba1: n = 8, Ccl2: n = 9; VPP: Gfap: n = 8, Iba1: n = 7, Ccl2: n = 7. Data are means ± SEM, student`s t-test. *p ≤ 0.05, ***p ≤ 0.001. (**E**,**F**) Immunoreactivity for IBA1 (red, arrows, arrowheads) in retinae of one-month-old animals. Ramified IBA1-positive cells (arrows) were identified in the control retina. In the VPP retina, the IBA1-positive cells in the outer plexiform layer (OPL) showed a non-ramified phenotype (arrowheads) and IBA1-positive cells were visible in the sub-neuroretinal space (arrowheads). Nuclei were DAPI-stained (blue). (**F**) shows the boxed area of I with the amoeboid, reactive microglia cell in high magnification. GCL = ganglion cell layer; INL = inner nuclear layer; ONL = outer nuclear layer; OS = ora serrata; ONH = optic nerve head; GFAP/Gfap = glial fibrillary acidic protein; IBA1/Iba1 = ionized calcium-binding adapter molecule 1; Ccl2 = CC-chemokine ligand 2; AB co.= antibody control; AU = arbitrary unit.*

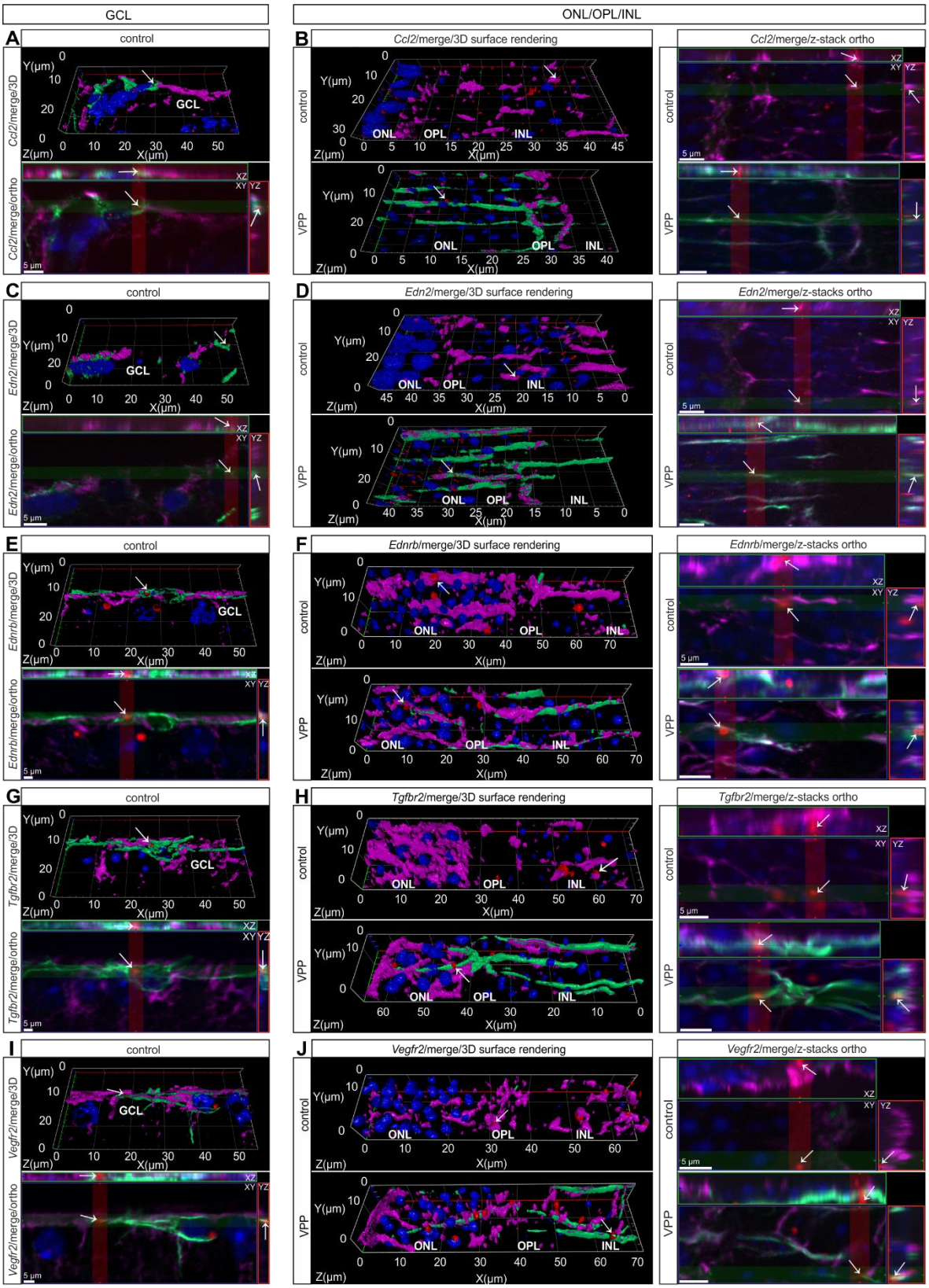
GCL
ONL/OPL/INL
A
control
Ccl2/merge/3D
Ccl2/merge/ortho
B
Ccl2/merge/3D surface rendering
Ccl2/merge/z-stack ortho
C
Edn2/merge/3D
Edn2/merge/ortho
D
Edn2/merge/3D surface rendering
Edn2/merge/z-stacks ortho
E
Ednrb/merge/3D
Ednrb/merge/ortho
F
Ednrb/merge/3D surface rendering
Ednrb/merge/z-stacks ortho
G
Tgfbr2/merge/3D
Tgfbr2/merge/ortho
H
Tgfbr2/merge/3D surface rendering
Tgfbr2/merge/z-stacks ortho
I
Vegfr2/merge/3D
Vegfr2/merge/ortho
J
Vegfr2/merge/3D surface rendering
Vegfr2/merge/z-stacks ortho
GCL
ONL
OPL
INL
control
VPP
XZ
XY
YZ
5 µm

Suppl Fig 6: z-stacks and corresponding 3D reconstructions

***(A-J)** The 3D reconstructions (…/merge/3D surface rendering) from Figure 8, 9 and 10 are shown here with their corresponding z-stacks (…/merge/(z-stacks)ortho) in the ortho (orthogonal section) view. The ortho view allows to analyze z-stacks in detail, as it shows the top view (X/Y axis) and additionally the section views of the X/Z axes (top, framed in green) and Y/Z axes (right, framed in red). The in situ hybridizations (red, arrows) for Ccl2 (**A**,**B**), Edn2 (**C**,**D**), Ednrb (**E**,**F**), Tgfbr2 (**G**,**H**) and Vegfr2/Kdr (**I**,**J**) and GFAP (green)/ GS (purple) co-labeling in the retinae of three-month-old animals are shown. Nuclei were DAPI-stained (blue). The images from the GCL region are shown in (**A**,**C**,**E**,**G**,**I**) and the images from the ONL/OPL/INL region are shown in (**B**,**D**,**F**,**H**,**J**). Ortho = orthogonal section; GCL=ganglion cell layer; INL=inner nuclear layer; OPL= outer plexiform layer; ONL=outer nuclear layer; GFAP=glial fibrillary acidic protein; GS=glutamine synthetase; Ccl2=CC-chemokine ligand 2; Edn2 = endothelin2; Ednrb = endothelin receptor type B; Tgfbr2 = transforming growth factor beta receptor type 2; Vegfr2 = vascular endothelial growth factor receptor 2.*

Gene	Species	Orientation	Sequence 5´-3´
Ccl2	Mus musculus	sense	catccacgtgttggctca
		antisense	gatcatcttgctggtgaatgagt
Edn2	Mus musculus	sense	acctcctccgaaagctgag
		antisense	tttcttgtcacctctggctgta
Fgf2	Mus musculus	sense	ccaaccggtaccttgctatg
		antisense	ccagtcgttcaaagaagaaacac
Gfap	Mus musculus	sense	tcgagatcgccacctacag
		antisense	gtctgtacaggaatggtgatgc
Gnb2l1	Mus musculus	sense	tctgcaagtacacggtccag
		antisense	acgatgatagggttgctgc
Iba1	Mus musculus	sense	ggatttgcagggaggaaaag
		antisense	tgggatcatcgaggaattg
Lif	Mus musculus	sense	aaacggcctgcatctaagg
		antisense	agcagcagtaagggcacaat
Ubc	Mus musculus	sense	gtctgctgtgtgaggactgc
		antisense	cctccagggtgatggtctta

Suppl Table 1: Oligonucleotides for qPCR

3.9 Digital Supplementary Material on CD-R

Suppl Table 2: DEseq2 analysis of VPP animals compared to controls

Suppl Table 3: WGCNA modules of VPP animals compared to controls

3.10 Author Contributions

Conceptualization: A.N., B.M.B.

Methodology: C.B.B., S.R., S.I.S., S.K.B., A.S., M.V., A.N., B.M.B.

Software: A.N.

Validation: A.N., B.M.B.

Formal analysis: C.B.B., S.R., S.I.S., S.K.B., A.S., A.N., B.M.B.

Investigation: C.B.B., S.R., S.I.S., S.K.B., A.S., A.N., B.M.B.

Resources: E.R.T., S.E., B.M.B.

Data curation: C.B.B., S.R., S.I.S., S.K.B., A.S., M.V., A.N., B.M.B.

Writing-original draft preparation: C.B.B., A.N., B.M.B.

Writing review and editing: C.B.B., S.R., S.I.S., S.K.B., A.S., M.V., E.R.T., S.E., A.N., B.M.B.

Visualization: C.B.B., A.N., B.M.B.

Supervision: E.R.T., S.E., B.M.B.

Project administration: A.N., B.M.B.

Funding acquisition: A.N., B.M.B.

Chapter 4

4 Deficiency in Retinal TGFβ Signaling Aggravates Neurodegeneration by Modulating Pro-Apoptotic and MAP Kinase Pathways

(Adapted from: **Christina B. Bielmeier**, Sabrina I. Schmitt, Nikolai Kleefeldt, Stefaniya K. Boneva, Anja Schlecht, Mario Vallon, Ernst R. Tamm, Jost Hillenkamp, Süleyman Ergün, Andreas Neueder and Barbara M. Braunger**. Deficiency in Retinal TGFβ Signaling Aggravates Neurodegeneration by Modulating Pro-Apoptotic and MAP Kinase Pathways** published in the *International Journal of Molecular Sciences 2022)*

4.1 Abstract

Transforming growth factor β (TGFβ) signaling has manifold functions such as regulation of cell growth, differentiation, migration, and apoptosis. Moreover, there is increasing evidence that it also acts in a neuroprotective manner. We recently showed that TGFβ receptor type 2 (*Tgfbr2*) is upregulated in retinal neurons and Müller cells during retinal degeneration. In this study we investigated if this upregulation of TGFβ signaling would have functional consequences in protecting retinal neurons. To this end, we analyzed the impact of TGFβ signaling on photoreceptor viability using mice with cell type-specific deletion of *Tgfbr2* in retinal neurons and Müller cells (*Tgfbr2*$^{\Delta OC}$) in combination with a genetic model of photoreceptor degeneration (VPP). We examined retinal morphology and the degree of photoreceptor degeneration, as well as alterations of the retinal transcriptome. In summary, retinal morphology was not altered due to TGFβ signaling deficiency. In contrast, VPP-induced photoreceptor degeneration was drastically exacerbated in double mutant mice (*Tgfbr2*$^{\Delta OC}$; VPP) by induction of pro-apoptotic genes and dysregulation of the MAP kinase pathway. Therefore, TGFβ signaling in retinal neurons and Müller cells exhibits a neuroprotective effect and might pose promising therapeutic options to attenuate photoreceptor degeneration in humans.

4.2 Introduction

Retinal degeneration is among the leading causes of blindness worldwide (Buch et al., 2004; Farrar et al., 2002) . Intriguingly, a multitude of different causative pathomechanisms such as various genetic mutations in patients suffering from retinitis pigmentosa (Hartong et al., 2006; Ruzickova & Stanek, 2017) or as a consequence of age-related macular degeneration (AMD) (Ambati & Fowler, 2012; de Jong, 2006) and systemic diseases like diabetes (Antonetti et al., 2012), promote degeneration of retinal neurons such as the rod and cone photoreceptor cells. Photoreceptor cells are the light-sensitive cells of the retina and as such are responsible for visual perception (Kolb et al., 1995). Morphologically, these cells exhibit an outer segment that is connected through a cilium with the inner segment, a perikaryon which is located in the outer nuclear layer (ONL) and a synaptic ending located in the outer plexiform layer (OPL) of the retina (Bielmeier et al., 2021; Kolb et al., 1995). Photoreceptor degeneration typically results in a thinning of the ONL concomitant with the loss of the inner and outer segments, resulting in a loss of visual function up to complete blindness (Ambati & Fowler, 2012; Farrar et al., 2002). Due to the multiple pathomechanisms of photoreceptor degeneration, it is still challenging to understand and intervene in the molecular mechanisms leading to their degeneration, with the overall goal of mitigating it. We recently analyzed the retinal transcriptome of the VPP mouse model, a genetic mouse model carrying a transgenic rhodopsin V20G/P23H/P27L (VPP), which results in photoreceptor degeneration as observed in autosomal dominant retinitis pigmentosa (Bielmeier et al., 2021; Naash et al., 1993). In the course of that study we aimed to identify molecular key factors and signaling pathways that predominantly influence the course of photoreceptor degeneration (Bielmeier et al., 2021). Amongst other findings, our data indicated a clustering of significantly dysregulated genes coding for components of potentially neuroprotective pathways such as the transforming growth factor β (TGFβ) signaling pathway (Bielmeier et al., 2021). Moreover, we particularly identified a significant upregulation of TGFβ receptor type 2 (TGFBR2) during photoreceptor degeneration (Bielmeier et al., 2021).

TGFβ signaling controls a plethora of cellular responses such as proliferation, differentiation, tissue homeostasis, morphogenesis and regeneration (Massagué, 2012a). In addition, there is increasing evidence that it also has neuroprotective properties (Braunger et al., 2013b; Gabriel et al., 2003; Ma et al., 2008; Park et al., 2008; Walshe et al., 2009, 2011). TGFβ signaling is initiated by binding of specific ligands (e.g., TGFβ1–3) to the type II transmembrane receptor (TGFBR2), a serine/threonine kinase that builds a heterodimer with the further signaling of the type I receptor (TGFBR1) (Shi & Massagué, 2003). Upon activation, TGFBR2 phosphorylates the TGFBR1 kinase domain resulting in phosphorylation of its intracellular downstream effectors SMAD2 and SMAD3 (Lewis et al., 1988). Subsequently, SMAD2/SMAD3 form a complex with SMAD4 and translocate into the nucleus to promote the activation of the canonical TGFβ signaling pathway (Clayton et al., 2020) through transcriptional regulation of TGFβ-dependent target genes (Massagué, 2000). In contrast, non-canonical TGFβ

signaling pathways involves the activation of various branches of MAP kinase (MAPK) pathways, Rho-like GTPase signaling pathways, and phosphatidylinositol-3-kinase (PI3K)/AKT pathways that regulate target genes (Clayton et al., 2020; Zhang, 2009).

We have previously identified retinal neurons and Müller cells as the cell populations in which Tgfbr2 was notably upregulated following photoreceptor degeneration (Bielmeier et al., 2021). Therefore, in this study we conditionally deleted TGFβ signaling specifically in retinal neurons and Müller cells. To induce photoreceptor degeneration, we used the VPP mouse model (Bielmeier et al., 2021; Naash et al., 1993) and asked the question whether additional deletion of TGFβ signaling in this model might result in a higher susceptibility of photoreceptors to VPP-induced degeneration and what the changes on the retinal transcriptome would be. In summary, we provide evidence for an important role of TGFβ signaling for photoreceptor survival. Deletion of TGFβ signaling in retinal neurons and Müller cells sensitizes the retinal neurons to degeneration, potentially through ferroptosis, and enhances neurodegeneration by shifting the MAPK signaling pathway towards its pro-apoptotic side.

4.3 Results

4.3.1 Deletion of TGFβ Signaling in Retinal Neurons and Müller Cells in Health and Disease

In this study, we investigated the impact of TGFβ signaling on the retina in healthy and neurodegenerative retinae with the overall aim of identifying TGFβ-dependent molecular key factors promoting neuroprotection (Figure 11). *Tgfbr2*$^{\Delta OC}$ and *Tgfbr2*$^{fl/fl}$ mice (see material and methods) were crossbred with hemizygous VPP mice to obtain double mutant mice with a genetically induced photoreceptor degeneration (Naash et al., 1993). The resulting offspring analyzed in this study were as follows: Mice (expressing wildtype rhodopsin and carrying *Tgfbr2*$^{fl/fl}$ alleles); *Tgfbr2*$^{\Delta OC}$ mice (expressing wildtype rhodopsin and harboring a Cre-mediated deletion of *Tgfbr2* in retinal neurons and Müller cells); *Tgfbr2*$^{fl/fl}$;VPP mice (henceforth termed 'VPP mice'; expressing the VPP rhodopsin mutant protein) and *Tgfbr2*$^{\Delta oc}$;VPP mice (henceforth termed 'double mutant mice'; expressing the VPP transgene in combination with Cre-mediated deletion of *Tgfbr2* in retinal neurons and Müller cells).

Tgfbr2$^{\Delta OC}$ mice allowed us to analyze the effects of deletion of TGFβ signaling in otherwise healthy retinae by analyzing the morphology and transcriptomic changes of *Tgfbr2*$^{\Delta OC}$ mice in comparison to control mice (Figure 11, left side). In addition, we analyzed the effects of the deletion of TGFβ signaling (*Tgfbr2*$^{\Delta OC}$) in conjunction with a model of retinal degeneration (VPP). To this end, we compared morphological and molecular changes in the double mutants, in which TGFβ signaling was additionally deleted, to those of the VPP mice (Figure 11, right side).

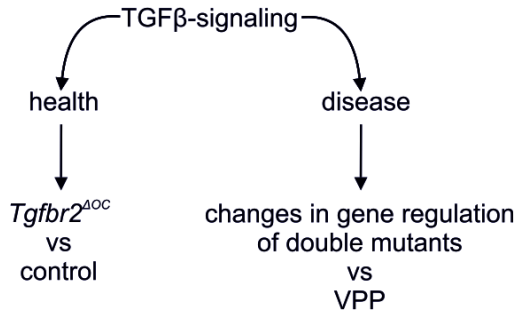

Figure 11: Schematic depicting the two experimental conditions that we addressed in this study.

*The role of TGFβ signaling in the adult, healthy retina (**left**) and its role in disease, such as VPP-induced photoreceptor degeneration (**right**).*

4.3.2 Deletion of TGFβ Signaling in Healthy Retinae Is Not Sufficient to Cause Morphological Changes

First, we studied the retinal morphology of *Tgfbr2*$^{\Delta oc}$ and control animals to investigate whether the deletion of *Tgfbr2* might have an impact on it. The verification of the successful deletion of TGFBR2 and its downstream effector pSMAD3 in *Tgfbr2*$^{\Delta oc}$ retinae has already been published in (Braunger, et al., 2013b). In the current project, we additionally performed *Tgfbr2 in situ* hybridization on retinal sections and show that *Tgfbr2* signals were dramatically reduced in *Tgfbr2*$^{\Delta oc}$ retinae (Suppl Fig 7).

When analyzing the number of degenerating, TUNEL-positive photoreceptor cells in the outer nuclear layer (ONL) of one-month-old mice, we did not find significant differences in their number (controls: 16.69 ± 2.94, n = 9; Tgfbr2$^{\Delta oc}$: 15.98 ± 5.29, n = 9, p = 0.9) (Figure 12A-C). Moreover, the morphology of retinae from three-month-old mice did not show obvious morphological alterations between control and Tgfbr2$^{\Delta OC}$ animals. Morphometric analyses of the thickness of ONL revealed a largely comparable ONL thickness between control and Tgfbr2$^{\Delta OC}$ mice (Figure 12D-F).

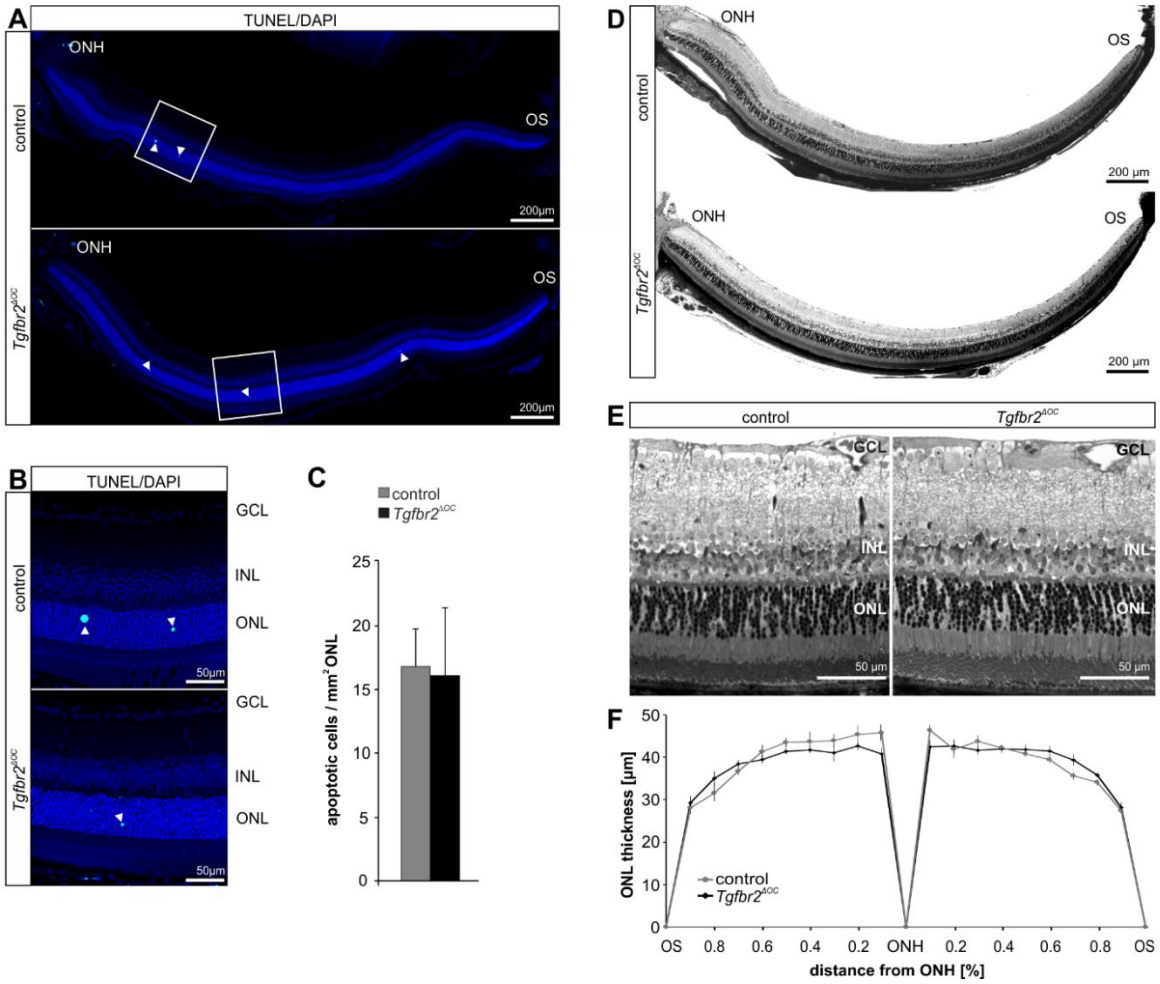

Figure 12: Cell death, retinal morphology and morphometry in Tgfbr2$^{\Delta oc}$ mice

***(A,B)** Mid-horizontal sections of TdT-mediated dUTP-biotin nick end (TUNEL)-labeled (green, arrowheads) retinae of one-month-old control and Tgfbr2$^{\Delta OC}$ animals (**A**). Detailed magnification (**B**) of the boxed areas in (**A**). Cell nuclei were stained with DAPI (blue). (**C**). Total number of TUNEL-positive cells normalized to mm^2 ONL. Controls: n = 9; Tgfbr2$^{\Delta OC}$: n = 9. (**D**) Richardson-stained, mid-horizontal semithin sections of the posterior eye segment of three-month-old control and Tgfbr2$^{\Delta OC}$ mice. (**E**,**F**) The detailed magnification of the central retina I shows a regular morphology of control and Tgfbr2$^{\Delta oc}$ animals. The thickness of the ONL was measured on mid-horizontal semithin sections at defined measure points and the mean values were plotted in the spider-diagram in (**F**). Controls n = 6; Tgfbr2$^{\Delta OC}$: n = 13. GCL = ganglion cell layer; INL = inner nuclear layer; ONL = outer nuclear layer; ONH = optic nerve head; OS = ora serrata. Data are means ± SEM. No significant changes were detected (Student's t-test).*

4.3.3 Deletion of TGFβ Signaling in Healthy Retinae Is Not Sufficient to Induce Major Transcriptional Changes

To investigate the impact of TGFβ signaling on the retinal transcriptome in healthy retinae (Figure 11, left side), we performed RNA sequencing (RNAseq) analyses of control (*Tgfbr2$^{fl/fl}$*) and *Tgfbr2$^{\Delta OC}$* retinae. Out of the total of 54,532 genes in the Ensembl gene annotation for mouse (Mus musculus GRCm38 v. 94) we found 30,796 genes to be expressed in the retina.

Only 22 genes were differentially expressed in *Tgfbr2$^{\Delta OC}$* retinae compared to control animals (12 down- and 10 upregulated, Figure 13A, cut off criteria: Benjamin-Hochberg adjusted *p*-value (p_{adj}) < 0.05,Suppl Table 4). Amongst others, myosin VIIA (*Myo7a*) which is a member of the myosin gene family and associated with the mouse shaker-1 phenotype and the human Usher syndrome 1B (Lévy et al., 1997) was significantly downregulated in *Tgfbr2$^{\Delta oc}$* retinae. Moreover, HD Domain Containing 3 (*Hddc3*) and triggering receptor expressed on myeloid cells 2 *(Trem2)* were significantly upregulated in *Tgfbr2$^{\Delta OC}$* retinae. *Hddc3* (also known as *Mesh1*) is expressed in a broad range of cells in the body (www.proteinatlas.org, accessed on 01/12/2021) with attributed functions e.g., in body growth, resistance to starvation and ferroptosis (Ding et al., 2020; Sun et al., 2010). *Trem2* constitutes an innate immune receptor, preferentially expressed by microglia, and involved in inflammation and microglial-mediated phagocytosis of e.g., apoptotic neurons (Kleinberger et al., 2014).

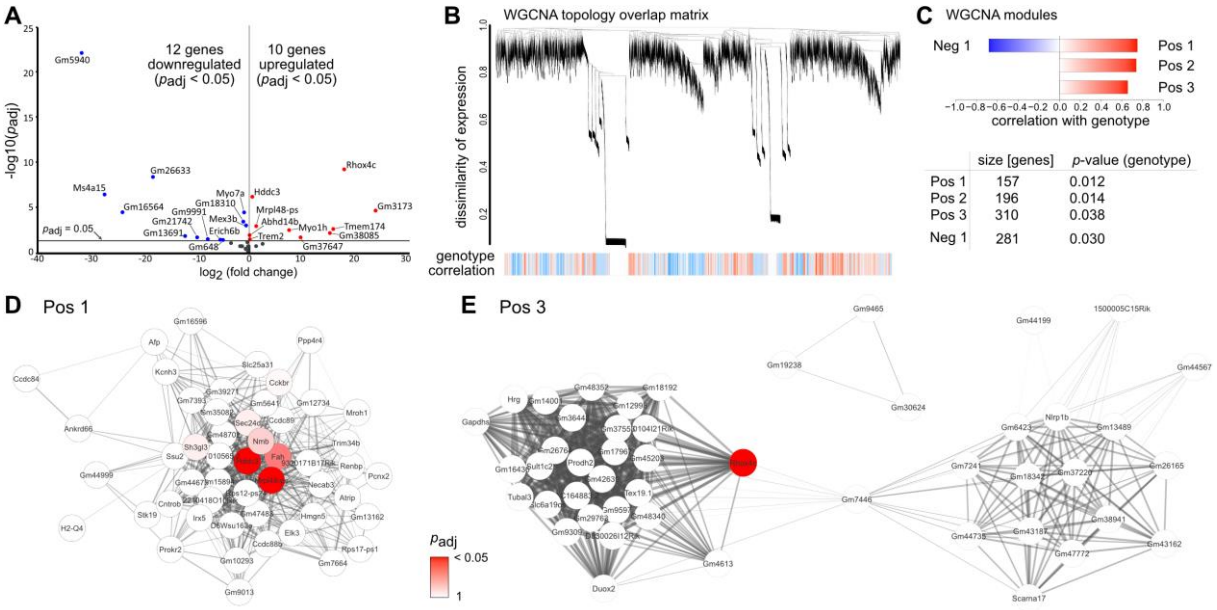

Figure 13: Transcriptome analysis: TGFβ effects in the adult, healthy retina

*(**A**) RNAseq analysis identified 12 significantly down- and 10 significantly up-regulated genes, respectively, in retinae of three-month-old Tgfbr2$^{\Delta OC}$ animals (Benjamini-Hochberg adjusted p-values; p_{adj}). (**B**) WGCNA analysis of Tgfbr2$^{\Delta OC}$ and control animals. Blue color in the lower panel (genotype correlation) indicates lower expression and red color indicates higher expression in Tgfbr2$^{\Delta OC}$ mice. (**C**) Three positively correlated modules (indicating higher expression in Tgfbr2$^{\Delta OC}$ animals) and one negatively correlated module (indicating lower expression in Tgfbr2$^{\Delta OC}$ animals) were identified to be significantly associated with the genotype. (**D**,**E**) Intra-module analysis of the Pos1 (**D**) and Pos3 I modules. The 50 highest connected (intramodular connectivity) genes with the 500 strongest connectivities per module are shown. Red colored genes were shown to be significantly upregulated in the DESeq2 analysis. The intensity of the fill color is inversely related to the adjusted p-value in the DESeq2 analyses.*

Moreover, we did not detect significant alterations in the expression of Müller glia cell specific markers such as Glutamine Synthetase *(Glul)*, Integrin beta-1 (*Itgb1*, also known as *Cd29*) or Retinaldehyde-binding Protein 1 *(Rlbp1*, also known as cellular Retinaldehyde-binding Protein *(Cralbp))* in *Tgfbr2*$^{\Delta OC}$ animals compared to controls (Suppl Table 4), indicating that cellular maintenance and homeostasis of Müller glia cells was not affected by the deletion of TGFβ signaling.

As gene ontology analyses and pathway enrichment analyses do not work reliably for small sets of genes, we performed weighted gene correlation network analysis (WGCNA) to potentially identify more subtle genotype-specific patterns of dysregulation, potential upstream regulators and involved signaling pathways in *Tgfbr2*$^{\Delta OC}$ retinae.

WGCNA identifies co-regulated genes by clustering them into modules based on their similarity of expression. This approach is able to uncover more subtle changes and patterns as it does not rely on the traditional dysregulation analysis and the problem of correction for multiple comparisons. Additionally, the network analysis allows the identification of biological key players, e.g., regulatory proteins driving a certain pathway.

The topology overlay matrix, demonstrating the co-regulation of gene expression for *Tgfbr2*$^{\Delta OC}$ and control animals, as well as the identified modules (clusters of co-regulated genes) are shown in Figure 13B,C. The analysis identified four significantly associated modules (three positively correlated with the genotype, i.e., higher expression in *Tgfbr2*$^{\Delta OC}$ retina (Pos1, 2, 3) and one negatively correlated, i.e., lower expression in *Tgfbr2*$^{\Delta OC}$ retina (Neg1) (Figure 13D and E and Suppl Fig 8A,B).

The Pos1 module contained 157 genes, and amongst those, the HD Domain Containing 3 *(Hddc3)* and mitochondrial ribosomal protein L48 pseudogene *(Mrpl48ps)* were central hub genes in WGCNA analyses and significantly dysregulated in Deseq2 analyses (Figure 13D (dysregulated genes are highlighted in red) and Suppl Table 4,5). In the Pos2 module, we found a clustering of 196 genes and in the Neg1 module a clustering of 310 genes, (Suppl Fig 8A,B and Suppl Table 4,5). However, none of them were dysregulated in Deseq2 analyses (Suppl Fig 8A,B and Suppl Table 4,5). The Pos3 module contained 281 genes with Reproductive Homeobox 4C (*Rhox4c*) as the only significantly upregulated gene in this module Figure 13E and Suppl Table 4,5).

In summary, WGCNA analyses did not detect a significant enrichment of genes coding for certain biological processes or pathways, which is consistent with our dysregulation analysis (DESeq2). We therefore conclude that deletion of TGFβ signaling in retinal neurons and Müller cells in the adult and healthy retina affects the retinal transcriptome only very mildly.

4.3.4 Deletion of TGFβ Signaling Increases the Susceptibility of Photoreceptors to Vpp-Induced Neurodegeneration

Next, we investigated whether deletion of TGFβ signaling in retinal neurons and Müller cells might impact the susceptibility of photoreceptors to VPP-induced degeneration. When analyzing the number of degenerating photoreceptor cells in the outer nuclear layer (ONL) of one-month-old VPP and double mutant mice, both groups demonstrated significantly more TUNEL-positive cells in the ONL (VPP mice: 205.76 ± 16.89, $n = 10$; double mutant mice: 245.61 ± 35.59, $n = 7$) compared to control (16.69 ± 2.94, $n = 9$, $p < 0.001$) and compared to *Tgfbr2*$^{\Delta OC}$ retinae (15.98 ± 5.29, $n = 9$, $p < 0.001$). Yet, double mutant mice (Figure 14A–C) demonstrated a slightly higher number of degenerating photoreceptors compared to VPP mice, although this alteration did not reach significance. Next, we analyzed whether the observed transcriptional alterations and the slight increase in degenerating photoreceptor cells might impact the retinal morphology of three-month-old double mutant animals. As expected, mice carrying the VPP transgene showed a significant thinning of the ONL (Figure 14D,E) compared to controls ($p < 0.02$) and *Tgfbr2*$^{\Delta oc}$ mice ($p < 0.001$), confirming the expected VPP-induced degeneration of photoreceptors (Bielmeier et al., 2021; Naash et al., 1993). Intriguingly, double mutant retinae demonstrated a significantly thinner ONL compared to VPP retinae ($p < 0.03$) (Figure 14D–F), showing

that deletion of TGFβ signaling in retinal neurons and Müller cells exacerbates VPP-induced photoreceptor degeneration.

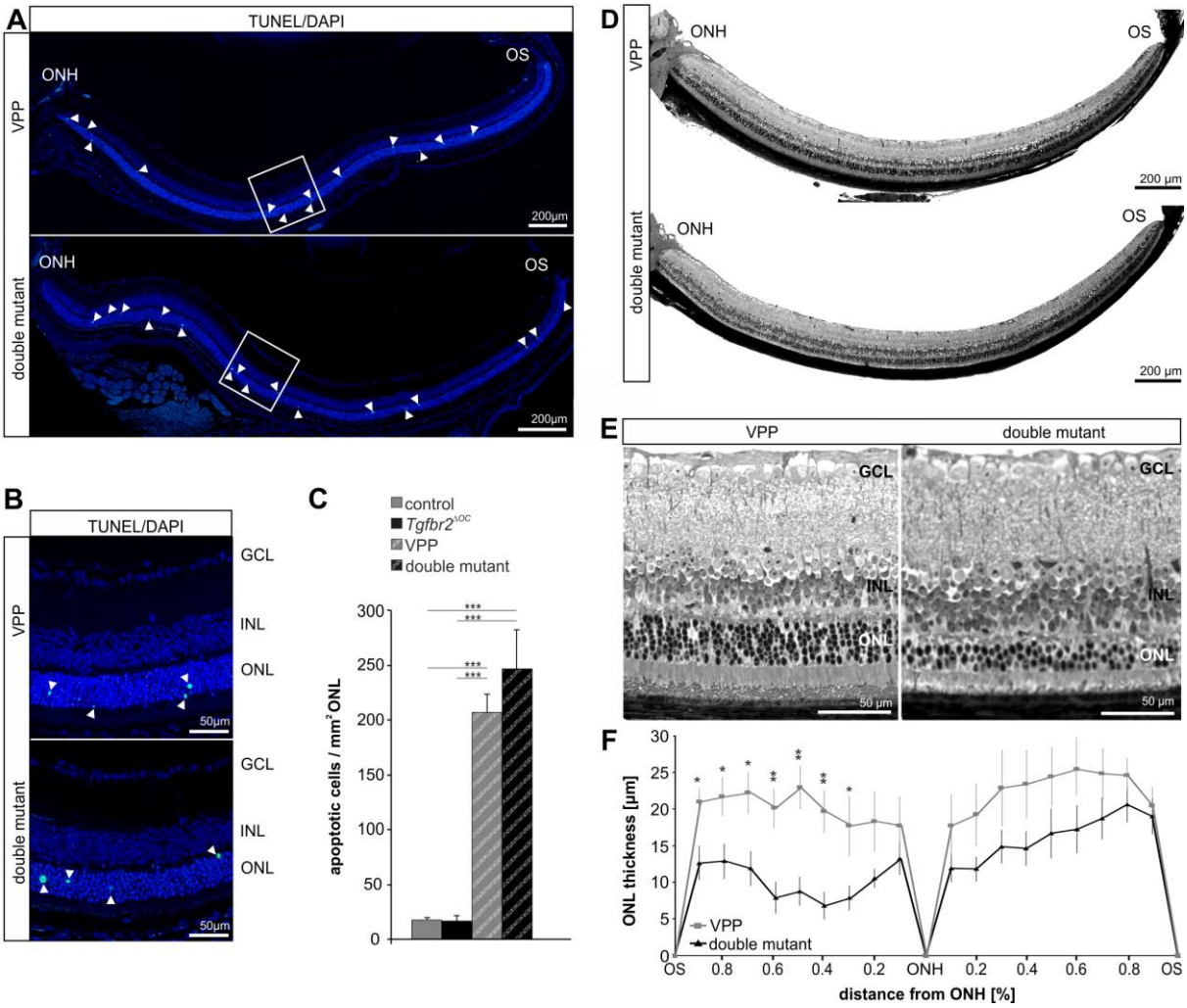

Figure 14: TGFβ signaling affects cell death, retinal morphology and morphometry in neurodegenerative retinae.

***(A)** Mid-horizontal sections of one-month-old TdT-mediated dUTP-biotin nick end (TUNEL)-labeled (green, arrowheads) retinae (**A**) and detailed magnification (**B**) of the boxed areas in (**A**). Cell nuclei were stained with DAPI (blue). (**C**) Total number of TUNEL-positive cells normalized to mm² ONL. VPP n = 10; double mutant n = 7. Data are means ± SEM. ANOVA with Bonferroni post-hoc analysis; *** p < 0.001. (**D**) Richardson-stained, mid-horizontal semithin sections of three-month-old VPP and double mutant mice. I The detailed magnification of the central retina shows the thinner ONL in the double mutant animal compared to the ONL of the VPP animal. (**F**) The thickness of the ONL was measured on mid-horizontal semithin sections from VPP and double mutant retinae at defined measure points and the mean values were plotted in the spider-diagram. Controls n = 9; VPP n = 6. GCL = ganglion cell layer; INL = inner nuclear layer; ONL = outer nuclear layer; ONH = optic nerve head; OS = ora serrata. Data are means ± SEM. Student's t-test. * p ≤ 0.05, ** p ≤ 0.01*

4.3.5 TGFβ-Mediated Effects on Vpp-Induced Transcriptomic Alterations

We have previously shown that VPP mice display huge alterations of the retinal transcriptome with thousands of significantly dysregulated genes (Bielmeier et al., 2021). To investigate TGFβ-mediated effects during VPP-induced photoreceptor degeneration (as illustrated in Figure 11, right side), we analyzed changes in the regulation patterns of gene expression in the retinae of double mutant animals (VPP plus TGFβ signaling deletion) in comparison to the gene regulation patterns in VPP mice (Figure 15A). To this end, we clustered significantly dysregulated genes (Benjamin-Hochberg adjusted *p*-value $p_{adj} < 0.05$) of any of the two genotype analyses (double mutant vs. controls mice and VPP vs. control mice) into genotype/regulation specific groups. We found that 647 genes were regulated in the double mutant mice, but not in the VPP mice (Table 4). In contrast, 2,106 genes were regulated in the VPP mice, but not in the double mutant mice (Table 5). While deletion of TGFβ signaling led to the aforementioned changes in the gene regulation patterns, the majority, namely 7,148 significantly dysregulated genes, were similarly regulated in both double mutant and VPP mice (Suppl Fig 9).

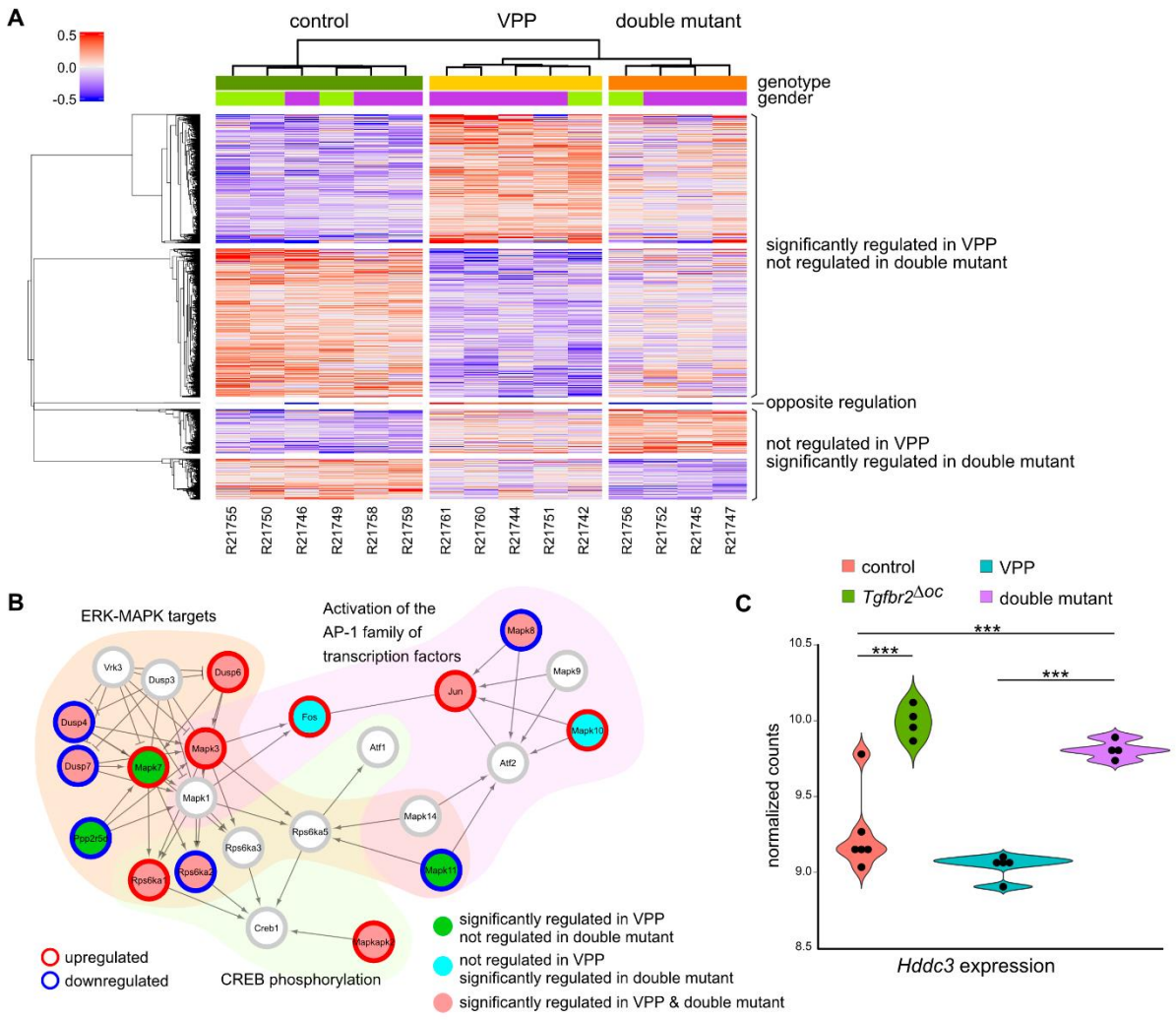

Figure 15: Transcriptome analysis: TGFβ effects in VPP-induced neurodegeneration.

*(**A**) Heatmap showing the deviation of expression from the mean of all significantly dysregulated genes in any of the pairwise comparisons: VPP and double mutant, respectively, against control retinae. Significantly dysregulated genes, which were significantly dysregulated (up- or down-regulated) in the same way in both comparisons are not shown here, but can be found in Suppl Fig 9. R21742-R21761 = RNAseq sample number. (**B**) Visualization of the Reactome MAPK targets/ Nuclear events mediated by MAP kinases signaling pathway. We converted the Reactome pathway into functional interaction networks. For each network, genes were colored according to the comparison (see legend) and their dysregulation state (white—not significantly dysregulated; red—significantly upregulated; and blue—significantly downregulated). (**C**) Violin blots with individual data points showing Hddc3 gene expression data from the RNAseq as normalized counts for control, Tgfbr2$^{\Delta OC}$, VPP and double mutant animals. ANOVA with Bonferroni post-hoc analysis; *** $p < 0.001$.*

Dysregulation Analysis	**Enriched Pathways 1: WikiPathways 2019 Mouse; 2: KEGG 2019 Mouse; 3: BioPlanet 2019**	**Gene Ontology Enrichment (Biological Process 2021)**	**Potential Regulators 1: ChEA; 2: Encode TF ChIP-seq 2015**
310 genes significantly downregulated in double mutant, not regulated in VPP	1: Electron Transport Chain 20.83, Oxidative phosphorylation 18.40, Translation Factors 12.91, Proteasome Degradation 12.00, Cytoplasmic Ribosomal Proteins 8.45 2: Oxidative phosphorylation 18.90, Ribosome 16.84, RNA polymerase 13.09, Ubiquitin mediated proteolysis 11.34, Thermogenesis 8.26 3: Chemiosmotic coupling formation of ATP 134.04, Valine, leucine and isoleucine biosynthesis 62.79, Cytoplasmic ribosomal proteins 29.21, Cap-dependent translation initiation 24.60, Activation of mRNA upon binding of the cap-binding complex and eIFs, and subsequent binding to 43S 21.53	tRNA pseudouridine synthesis 181.21, regulation of stem cell division 107.93, sarcomere organization 75.56, phosphorylated carbohydrate dephosphorylation 62.79, inositol phosphate dephosphorylation 62.79	1: HCFC1 19.91, JARID1A 18.65, YY1 10.50, BCL3 7.26 2: KAT2A 43.14, EP300 19.63, SIN3A 19.63, POLR2AphosphoS5 17.07, MYC 16.31

337 genes significantly upregulated in double mutant, not regulated in VPP	1: Serotonin and anxiety 24.32, Dysregulated miRNA Targeting in Insulin/PI3K-AKT Signaling 12.95, IL-6 signaling Pathway 11.43, Oxidative Stress 11.37, Matrix Metalloproteinases 10.69 2: Dopaminergic synapse 32.52, cAMP signaling pathway 17.02, IL-17 signaling pathway 13.61, Circadian entrainment 11.43, Aldosterone synthesis and secretion 10.74 3: Activation of the AP-1 family of transcription factors 65.31, Erythropoietin-mediated neuroprotection through NF-kB 55.58, Signaling by Robo receptor 52.51, Inactivation of APC/C via direct inhibition of the APC/C complex 51.87, Kinesins 33.65	sinoatrial node cell differentiation 230.87, microtubule nucleation by microtubule organizing center 230.87, negative regulation of synapse organization 230.87, aromatic amino acid transport 161.57, snoRNA localization 161.57	1: SUZ12 30.34, JARID2 20.32, MTF2 17.81, EZH2 15.66, RING1B 15.25, 2: POLR2A 9.20

Table 4: Gene ontology and pathway enrichment analysis of genes that were only dysregulated in the double mutant mice.

Enriched pathways and potential upstream regulators were predicted using the indicated databases. For gene ontology enrichment, only the top five non-redundant significantly enriched biological process terms are shown. The numbers following the terms are the combined score as calculated by Enrichr. Only terms with a combined score > 5 were considered.

Dysregulation Analysis	Enriched Pathways 1: WikiPathways 2019 Mouse; 2: KEGG 2019 Mouse; 3: BioPlanet 2019	Gene Ontology Enrichment (Biological Process 2021)	Potential Regulators 1: ChEA; 2: Encode TF ChIP-seq 2015
1127 genes significantly downregulated in VPP, not regulated in double mutant	1: mRNA processing 15.87, Mismatch repair 11.66, Fatty Acid Biosynthesis 5.53, Eukaryotic Transcription Initiation 5.25 2: Basal transcription factors 23.11, RNA transport 18.65, Nucleotide excision repair 15.19, Mismatch repair 12.78, Lysine degradation 10.73 3: Small interfering RNA (siRNA) biogenesis 96.77, Cytoskeletal remodeling regulation and cell spreading by IPP complex components 48.54, RNA polymerase II C-terminal domain phosphorylation and interaction with capping enzyme 48.54, ATM-mediated phosphorylation of repair proteins 39.86, NOSTRIN-mediated endothelial NOS trafficking 39.86	mRNA cleavage involved in gene silencing by miRNA 161.54, cellular lipid biosynthetic process 96.77, snRNA modification 96.77, transcription-dependent tethering of RNA polymerase II gene DNA at nuclear periphery 96.77, mRNA splice site selection 76.01	1: KDM5B 36.25, CREM 24.91, FOXO3 20.56, BCL3 18.68 ERG 17.39 2: GABPA 59.59, KAT2A 49.90, MAX 44.05, FLI1 32.08, HCFC1 27.13
979 genes significantly upregulated in VPP, not regulated in double mutants	1: Glutathione metabolism 20.55, Fatty Acid Biosynthesis 16.81, Prostaglandin Synthesis and Regulation 15.42, ACE Inhibitor Pathway 14.90, Heme Biosynthesis 14.90 2: Folate biosynthesis 38.75, Propanoate metabolism 15.42, Oxidative phosphorylation 14.95,	negative regulation of T cell migration 199.52, blood vessel endothelial cell proliferation involved in sprouting angiogenesis 120.22, basement membrane assembly 116.02, dolichyl diphosphate biosynthetic process 82.52, tetrahydrobiopterin metabolic process 73.01	1: SUZ12 12.02, THRA 10.23, SOX9 8.81, SRY 6.88, MTF2 5.96 2: n.s.

	beta-Alanine metabolism 14.38,	
	Nitrogen metabolism 12.71	
	3: Bile salt and organic anion SLC transporters 60.31,	
	Catalytic cycle of mammalian FMOs 49.72,	
	Kit receptor transcriptional targets 49.72,	
	Second messenger role in netrin-1 signaling 37.78,	
	Tetrahydrobiopterin (BH4) biosynthesis, recycling, salvage and regulation 37.78,	
	Cell cycle negative regulation by p75 neurotrophin receptor 33.66	

Table 5: Gene ontology and pathway enrichment analysis of genes that were only dysregulated in the VPP mice.

Enriched pathways and potential upstream regulators were predicted using the indicated databases. For gene ontology enrichment, only the top five non-redundant significantly enriched biological process terms are shown. The numbers following the terms are the combined score as calculated by Enrichr. Only terms with a combined score > 5 were considered. N.s. = no significant enrichment.

The analysis of the double mutant specific gene regulation patterns can be found in Table 4 and Suppl Table 4: 'VPPnot_doubleDown' and 'VPPnot_doubleUp'. Gene ontology and pathway enrichment analyses showed that, amongst other findings, an activation of the activator protein 1 (AP-1) family of transcription factors' in double mutants (Table 4). This pathway is part of the Reactome pathway 'mitogen-activated protein kinase (MAPK) targets Nuclear events mediated by MAP kinases' (Figure 15B). We found significant upregulation of the neuronal specific *Mapk10* (also known as c-Jun N-terminal kinase 3 (*JNK3*)) and *Fos* (Fos proto-oncogene, also known as AP-1 transcription factor subunit) in double mutants (Figure 15B, turquoise dots). Moreover, the 'interleukin (IL) -6 signaling pathway' was amongst the top hits in the pathway enrichment analyses (Table 4). IL6 is a pleotropic cytokine and is involved in a multitude of central nervous system (CNS) pathologies including injury and neurodegeneration. In addition, 'negative regulation of synapse organization' was also amongst the top hits in the pathway enrichment analyses (Table 4), potentially indicating a reduced number of existing synapses in double mutant retinae as a result of increased neurodegeneration.

In contrast, 2,106 genes were significantly dysregulated in VPP mice, but not in double mutant mice (Table 5 and Suppl Table 4: 'VPPdown_doubleNot' and 'VPPup_doubleNot'). In these clusters, gene ontology enrichment analyses indicated, amongst others, downregulation of genes controlling e.g., processes in mRNA processing and biology and an upregulation of genes that clustered e.g., for negative

regulation of T cell migration, and cell cycle negative regulation by p75 neurotrophin receptor (Table 5). In addition, we found a significant downregulation of *Mapk11* (Figure 15B, green dots), which is one of the p38 MAPKs (Cuadrado & Nebreda, 2010), while *Mapk7* (Figure 15B, green dots), which is a component of the ERK signaling pathway and associated with AP1 signaling (Drew et al., 2012), was significantly upregulated in VPP mice but not in double mutants.

Interestingly, we identified only two genes that were oppositely regulated in double mutant and VPP mice: mitochondrial ribosomal protein L48 pseudogene (*Mrpl48-ps*; $\log_2$ fold changes: VPP: −0.60, double mutant: 1.38) and myosin VIIa (*Myo7a*; $\log_2$ fold changes: VPP: 0.41, double mutant: −0.41) (Suppl Table 6). *Myo7a* is amongst others critical for renewal of the outer photoreceptor disks, distribution and migration of RPE melanosomes and phagosomes (Gibbs et al., 2004). As mentioned above, mutations in *Myo7a* are associated with the Usher syndrome I, a genetically heterogeneous condition that is characterized by congenital sensorineural deafness, absent vestibular function and prepubertal onset of progressive retinitis pigmentosa leading to blindness (Kremer et al., 2006).

Moreover, *Hddc3*, which was significantly higher expressed in *Tgfbr2*$^{\Delta oc}$ retinae (see above), was also significantly higher expressed in double mutant retinae compared to control, or VPP only mutant retinae (Figure 15C).

4.4 Discussion

The data of this study show that the deficiency of TGFβ signaling in retinal neurons and Müller cells in adult, healthy mice affects the retinal transcriptome only very mildly and does not result in obvious morphological alterations in the post-developmental retina. However, during VPP-induced photoreceptor degeneration, upregulation of genes involved in neurodegeneration and downregulation of genes essential for cellular maintenance and homeostasis were exacerbated by the additional deletion of TGFβ signaling. These effects culminate in enhanced vulnerability and degeneration of photoreceptors, resulting in a significantly thinner ONL.

4.4.1 TGFβ Signaling in Retinal Development and in the Healthy, Adult Retina

TGFβ signaling has a plethora of different functions such as cell-cycle control, cell differentiation, and regulation of early development (Goumans et al., 2009; Goumans & Mummery, 2000; Massagué, 2004; Schlecht et al., 2021). As the Cre recombinase in *Tgfbr2*$^{\Delta OC}$ retinae is constitutively expressed from embryonic day 10.5 in all cells deriving from the inner layer of the optic cup e.g., retinal neurons and Müller cells (Marquardt et al., 2001), we addressed potential developmental-related aspects in the *Tgfbr2*$^{\Delta OC}$ model in one of our previously published manuscripts (Braunger et al., 2013b). We showed that *Tgfbr2*$^{\Delta OC}$ animals exhibited a higher degree of degenerating neurons particularly affecting the inner retinal neurons (retinal ganglion cells and neurons of the INL) during developmental programmed cell death of the retina (Braunger et al., 2013b). Consequently, adult *Tgfbr2*$^{\Delta OC}$ retinae harbor mild, developmental-related alterations, such as a reduced number of retinal ganglion cells or neurons of the INL (Braunger et al., 2013b). However, only a negligible percentage of photoreceptors undergo programmed cell death during retinal development (Cepko et al., 1996). Accordingly, thicknesses of the ONL between control and *Tgfbr2*$^{\Delta OC}$ of two-month-old animals (Braunger et al., 2013b) and three-month-old animals (data of this publication, Figure 13F) were largely comparable.

Given the manifold properties of TGFβ signaling in cellular homeostasis, it was surprising to detect only 22 dysregulated genes in the RNAseq analyses of healthy, adult *Tgfbr2*$^{\Delta OC}$ animals when compared to control mice. This finding clearly indicates that in the healthy, post-developmental retina, TGFβ signaling is not essential for cellular maintenance and homeostasis of retinal neurons and Müller cells. However, our transcriptome analyses were performed using total retinal tissue, a mixed tissue containing cell types such as microglial cells, endothelial cells, perivascular cells, and astrocytes, which were not affected by the deletion of TGFβ signaling in *Tgfbr2*$^{\Delta OC}$ animals. Therefore, subtle transcriptional changes affecting e.g., only Müller cells or a subpopulation of retinal neurons might not have been detected by our approach. Still, we found genes like myo7a (*Myosin7A*), which is associated with Usher syndrome (Lévy et al., 1997), to be dysregulated in *Tgfbr2*$^{\Delta OC}$ retinae. Thus, it is reasonable to speculate

that dysregulation of TGFβ signaling might have an impact on the cellular 'buffer capacity' against cytotoxic insults potentially aggravating the course of human diseases such as Usher syndrome, as well.

4.4.2 TGFβ Signaling Mediated Effects in Retinal Neurodegeneration

We described the molecular effects of VPP-induced photoreceptor degeneration on the retinal transcriptome using RNAseq analyses in our previously published manuscript (Bielmeier et al., 2021). In this study, the deletion of TGFβ signaling in VPP-induced photoreceptor degeneration resulted in a dysregulation of more than 600 genes in double mutant retinae, which were not differentially expressed in the VPP retinae alone. Gene ontology analyses showed, amongst others, an upregulation of the AP-1 family of transcription factors associated signaling in double mutant retinae. AP-1 transcription factor is associated with a broad range of apoptosis-related interactions (Ameyar et al., 2003). In particular, in our data *Mapk11* was significantly downregulated in VPP retinae but not in double mutants. MAPK11 is one of the p38 MAPKs and plays an important role in cellular responses to, for example, proinflammatory cytokines or physical stress (Cuadrado & Nebreda, 2010), and in the regulation of Tumor necrosis factor (TNF) expression in monocytic cells (Mahlknecht et al., 2004).

Moreover, *Mapk10* and *Fos* were significantly upregulated in double mutant retinae (Figure 15B). MAPK10 plays a regulatory role during neuronal apoptosis (Ying et al., 2006), and the transcription factor Fos, which is part of the AP-1 transcription factor complex, and as such orchestrates expression of target genes that e.g., regulate neuronal cell death versus survival (Curran & Morgan, 1995; Zhang et al., 2002).

In contrast, MAPK7, which is a component of the ERK signaling pathway and associated with AP-1 signaling (Figure 15B) (Drew et al., 2012), was significantly upregulated in VPP retinae but not in double mutants. MAPK7 (also known as ERK5) regulates gene expression upon activation in response to various growth factors such as the neurotrophins nerve growth factor (NGF) and brain derived neuroprotective factor (BNDF), or in response to oxidative stress, finally contributing to anti-apoptotic signaling (Drew et al., 2012). Thus our data indicate that a deficiency of TGFβ signaling in retinal neurons and Müller cells results in an imbalance of MAPK associated signaling pathways, finally shifting its impact towards the pro-apoptotic side. It is reasonable to assume that this effect is directly related to TGFβ signaling, as particularly non-canonical TGFβ signaling regulates the transcription of target genes, amongst others, through activation of MAPK pathways (Clayton et al., 2020).

Moreover, gene ontology analyses suggested an upregulation of 'cell cycle negative regulation of p75 neurotrophin receptor' in VPP, but not in double mutant retinae. P75 neurotrophin receptor is one of the neurotrophin receptors, mediating predominately pro-apoptotic effects (Garcia et al., 2017; Schlecht et al., 2021). We have recently demonstrated that expression of the neurotrophin Ngf is dependent upon TGFβ2 treatment in vitro and is significantly enhanced in the juvenile retina of a mouse model with

increased TGFβ signaling activity (Braunger et al., 2013b). Hence, the fact that 'p75 neurotrophin receptor' was amongst the genes that were upregulated in VPP but not regulated in double mutant retinae might point towards an interaction of neurotrophin and TGFβ signaling, as postulated in previously published manuscripts from our group (Braunger et al., 2013b; Schlecht et al., 2021) and others (Krieglstein & Unsicker, 1996; Ma et al., 2019; Sometani et al., 2001).

Hddc3 was more highly expressed in *Tgfbr2*$^{\Delta OC}$. This effect persisted in the comparison of double mutant and VPP retinae, where *Hddc3* expression was also induced in the double mutants due to the deletion of TGFβ signaling. Published data show that overexpression of HDDC3 (also known as MESH1) sensitize cells to ferroptosis (Ding et al., 2020). Another study links ferroptosis to neuronal cell death (Qin et al., 2021). Taken together, deficiency of TGFβ signaling in retinal neurons and Müller cells might sensitize the retina towards ferroptosis associated neuronal cell death. Accordingly, our data clearly demonstrate that TGFβ signaling in retinal neurons and Müller cells contributes in a neuroprotective manner on photoreceptor survival in the adult retina. Moreover, we recently showed that TGFβ2 treatment of in vitro cultures of retinal neurons improved their survival significantly, an effect that could be reversed to that of untreated controls, when SIS3, an inhibitor of SMAD3 phosphorylation, was added (Braunger et al., 2013b). Other groups showed that adeno-associated virus (AAV)-mediated delivery of TGFβ1 rescued degenerating cone photoreceptor cells in mouse models mimicking retinitis pigmentosa (Wang et al., 2020), and our previously published manuscript demonstrated that TGFβ signaling protected inner retinal neurons from ontogenetic cell death during retinal development (Braunger et al., 2013b).

The question remains whether the observed neuroprotective effect was mediated directly (TGFβ signaling in photoreceptors) and/or indirectly (TGFβ signaling in Müller cells and non-photoreceptor retinal neurons). In this context, we recently showed that primary retinal neurons, isolated from newborn pups and treated with TGFβ2, demonstrated significantly higher survival in vitro (Braunger et al., 2013b), indicating that TGFβ signaling regulates the survival of retinal neurons directly. However, TGFβ signaling in Müller cells and/or non-photoreceptor retinal neurons may induce the release of paracrine neuroprotective factors mediating the observed effects on photoreceptors. Therefore, future studies using cell type-specific knockout mouse models of TGFβ signaling are needed to answer this question.

4.5 Conclusions

In this study, we showed that the deletion of TGFβ signaling in retinal neurons and Müller cells affects the retinal transcriptome of adult, healthy mice in only a very minor way, without obvious morphological alterations of the post-developmental retina. In contrast, the concurrent expression of mutant rhodopsin (VPP) (Naash et al., 1993) and deletion of TGFβ signaling resulted in a significantly thinner ONL. The predominant changes in the regulation of gene expression in these mice indicate the dysregulation of cellular homeostasis and the upregulation of pathways involved in neurodegeneration. Moreover, gene ontology analyses found that TGFβ signaling deficiency mediates a shift in the expression of MAPK signaling pathway regulators from pro-survival to pro-apoptosis. Conversely, the stimulation of TGFβ signaling or activation of pro-survival MAPK signaling pathways in retinal neurons or in Müller cells might be promising approaches to attenuate the degeneration of photoreceptors in diseases such as retinitis pigmentosa or age-related macular degeneration.

4.6 Materials and Methods

4.6.1 Mice

All procedures conformed to the tenets of the National Institutes of Health Guidelines on the Care and Use of Animals in Research, the EU Directive, 2010/63/E and institutional guidelines. The mice were on a 129 SV background and kept in a 12 h light/dark cycle. Mice carrying two floxed *Tgfbr2* alleles (*Tgfbr2*$^{fl/fl}$) (Chytil et al., 2002) were crossbred with α-Cre;*Tgfbr2*$^{fl/fl}$ mice (Braunger et al., 2013b; Marquardt et al., 2001) hemizygous for the α-Cre transgene. The α-Cre transgene contains a Cre recombinase under control of the retina-specific α enhancer and minimal promoter of the Pax6 gene (Marquardt et al., 2001). The resulting α-Cre;*Tgfbr2*$^{fl/fl}$ mice (for simplicity referred as *Tgfbr2*$^{\Delta OC}$) had recombined and inactivated Tgfbr2fl alleles in cells that originate from the inner layer of the optic cup (OC), i.e., retinal neurons and Müller cells. Cre-negative littermates carrying floxed *Tgfbr2* alleles (*Tgfbr2*$^{fl/fl}$) still express TGFBR2.

To genetically induce photoreceptor degeneration, the mice were additionally crossbred with hemizygous VPP mice carrying a rhodopsin mutant with point mutations at positions V20G, P27L, and P23H, in addition to wildtype rhodopsin (Naash et al., 1993). The VPP mutation results in a progressive retinal neurodegeneration (Naash et al., 1993). The resulting offspring analyzed in this study were as follows: Control mice (expressing wildtype rhodopsin and carrying *Tgfbr2*$^{fl/fl}$ alleles); *Tgfbr2*$^{\Delta OC}$ mice (expressing wildtype rhodopsin and harboring a Cre-mediated deletion of Tgfbr2 in retinal neurons and Müller cells); *Tgfbr2*$^{fl/fl}$;VPP mice (henceforth termed 'VPP mice'; expressing the VPP rhodopsin mutant protein) and *Tgfbr2*$^{\Delta OC}$;VPP mice (henceforth termed 'double mutant mice'; expressing the VPP transgene in combination with Cre-mediated deletion of Tgfbr2 in retinal neurons and Müller cells). All experiments were performed on mice of both sexes.

4.6.2 Genotyping and Tgfbr2 Deletion

Genotypes were screened by isolating genomic DNA from ear biopsies and tested by PCR analyses as previously described (Bielmeier et al., 2019; Braunger et al., 2013b). Briefly, for VPP genotyping, the following primers were used: 5′-agactgacatggggaggaattcccaga-3′ (sense) and 5′-gagctgctcgaagtgactccgacc-3′ (antisense). The thermal cycle protocol was denaturation at 94 °C for 30 s, annealing at 68 °C for 45 s and elongation at 72 °C for 45 s for 35 cycles. For Tgfbr2 genotyping we used the sense primer 5′-gcaggcatcaggacccagtttgatcc-3` and the antisense primer 5′-agagtgaagccgtggtaggtgagcttg-3′ with the following thermal cycle protocol: denaturation at 95 °C for 30 s, annealing at 61 °C for 30 s and elongation at 72 °C for 45 s for 34 cycles. To genotype for the presence of the Cre recombinase we used the sense primer 5'-atgcttctgtccgtttgccg-3' and the antisense primer 5'-

cctgttttgcacgttcaccg-3' with the thermal cycle protocol denaturation at 95 °C for 30 s, annealing at 60 °C for 30 s and elongation at 72 °C for 30 s for 34 cycles.

4.6.3 BaseScope®/In situ hybridization

In situ hybridization was performed as previously described (Bielmeier et al., 2021). Briefly, the eyes of one-month-old animals were enucleated and fixed for 4 h in 4% PFA. After washing in phosphate buffer (PB, 0.1 M, pH 7.4), the eyes were embedded in paraffin according to standard protocols. For *in situ* hybridization (ACD, Newark, NJ, USA), 6 mm thick paraffin sections were pre-treated with retrieval reagent and protease according to the user manual. BaseScope™ Detection Reagent Kit v2—RED was used to label *TGFβ receptor type 2* (*Tgfbr2*) (ACD catalog number: 845871). The sections were analyzed on an Axio Imager Z1 microscope with the Apotome.2 function (Carl Zeiss, Jena, Germany) using Zeiss Zen software (Carl Zeiss, Jena, Germany).

4.6.4 RNA Sequencing

To perform RNA sequencing, total RNA of pooled retinae (right and left eye) of three-month-old mice was purified using the Rneasy Mini Kit by Qiagen (Venlo, The Netherlands). Library preparation and RNAseq were performed at the service facility 'KFB—Center of Excellence for Fluorescent Bioanalytics' (Regensburg, Germany. www.kfb-regensburg.de, accessed on 01 December 2021). Library preparation and RNAseq were carried out as described in the Illumina TruSeq Stranded mRNA Sample Preparation Guide, the Illumina NextSeq 500 System Guide (Illumina, Inc., San Diego, CA, USA), and the KAPA Library Quantification Kit—Illumina/ABI Prism User Guide (Kapa Biosystems, Inc., Woburn, MA, USA). In brief, 250 ng of total RNA was used for purifying the poly-A-containing mRNA molecules using poly-T oligo-attached magnetic beads. Following purification, the mRNA was fragmented to an average insert size of 200–400 bases using divalent cations under elevated temperature (94 °C for 4 min). Next, the cleaved RNA fragments were reverse transcribed into first strand cDNA using reverse transcriptase and random hexamer primers. Actinomycin D was added to improve strand specificity by preventing spurious DNA-dependent synthesis. Blunt-ended second strand cDNA was synthesized using DNA Polymerase I, Rnase H, and dUTP nucleotides. The incorporation of dUTP, in place of dTTP, quenched the second strand during the later PCR amplification, because the polymerase does not incorporate past this nucleotide. The resulting cDNA fragments were adenylated at the 3′ ends; the indexing adapters were ligated; and, subsequently, specific cDNA libraries were created by PCR enrichment. The libraries were quantified using the KAPA SYBR FAST ABI Prism Library Quantification Kit. Equimolar amounts of each library were sequenced on a NextSeq 500 instrument controlled by the NextSeq Control Software (NCS) v2.2.0, using a 75 Cycles High Output Kit with the single index, paired-end (PE) run parameters. Image analysis and base calling were done with the Real

Time Analysis Software (RTA) v2.4.11. The resulting. Bcl files were converted into. Fastq files with the CASAVA Software v1.8.2.

4.6.5 Bioinformatics

For all samples, at least 30 million reads were analyzed. Fastq files were quality controlled with FastQC v0.11.5. All files passed quality control. The reads were aligned against Ensembl Mus musculus GRCm38 version 94 using STAR aligner v2.5.3a. One sample (R21753) showed poor read alignments of less than 30% and was removed from further analyses. Reads were quantified using salmon v0.8.2. All subsequent analyses were conducted in R v3.5.1. Samples were screened for outliers using PCA and clustering analysis. One sample (R21741) was identified as an outlier and removed from further analyses. Thus, the final sample number was six control, five VPP, four control/VPP and four *Tgfbr2*$^{\Delta OC}$/VPP retinae. Transcriptional dysregulation was computed using tximport v1.10.0 and DESeq2 v1.22.1 with genotype as the variable of interest and sex of the mice as a covariate and using ashr as the fold change shrinkage estimator. The Benjamini–Hochberg procedure was used to correct for multiple comparisons (*p*-adjusted; padj). For correlation network analysis, we used the normalized and variance stabilized counts from the DESeq2 analysis. Batch correction for sex was applied with limma v3.38.3, keeping the genotype as the variable of interest. The normalized, transformed, and batch corrected counts were used to construct a weighted gene correlation network using WGCNA v1.66. Heatmaps and k-mer analysis were carried out using ComplexHeatmap v2.3.2. Visualization was carried out using cytoscape v3.7.2 (http://cytoscape.org, accessed on 01 December 2021) with the Reactome FI app v7.2.1. Ontology analysis was carried out using the Enrichr website (https://maayanlab.cloud/Enrichr/ accessed on 01.12.2021). The scripts are available upon request.

4.6.6 Cell Death Measurement by TdT-Mediated dUTP-Biotin Nick End Labeling (TUNEL)

The number of degenerating photoreceptor cells was determined using TUNEL (DeadEnd Fluorometric TUNEL, Promega, Madison, WI, USA). This method was performed on retinae of one-month-old animals, as described previously (Kugler et al., 2015, 2017). TUNEL labeling was conducted on 4% paraformaldehyde (PFA, in 0.1 M phosphate buffer (PP), pH 7.4) fixed and paraffin embedded eyes according to previously published protocols (Braunger et al., 2015; Braunger et al., 2013a). Labelled sections were visualized by fluorescence microscopy using the Axio Imager Z1 (Carl Zeiss, Jena, Germany). The total number of TUNEL-positive cells was normalized to the area of the ONL [mm^2].

4.6.7 Light Microscopy and Spider Diagram Analyses

Eyes of three-month-old mice were carefully enucleated and fixed for 24 h in Ito's fixative (Karnovsky, 1965). The eyes were marked with a thin, short metal needle at the superior limbus and embedded in Epon (Serva, Heidelberg, Germany). Semithin meridional sections (in nasal-temporal orientation) of 1.0 µm thickness were cut stretching through the optic nerve head (ONH) and the pupil. Sections were stained according to the Richardson's protocol (Richardson et al., 1960) and images taken using an Axio Imager Z1 light/fluorescent microscope (Carl Zeiss, Jena, Germany). The thickness of the outer nuclear layer (ONL) was measured at nine equidistant loci along the circumference of each hemisphere as described in (Boneva et al., 2016; Braunger et al., 2015; Braunger et al., 2013a; Braunger et al., 2013b). The means and corresponding standard errors of the mean (SEM) were calculated for each measure point and the results were plotted as spider diagram.

4.6.8 Statistics

Data are expressed as mean ± SEM. Statistical comparative analyses between the mean variables of two individual test populations were performed using a two-tailed Student's *t*-test in Excel (Microsoft Corporation, Redmond, WA, USA). One-way ANOVA analyses were performed in SPSS (IBM Corporation, Armonk, NY, USA) if more than two individual groups were compared (post-hoc test: Bonferroni). *P* values ≤ 0.05 were considered to be statistically significant.

4.7 Acknowledgments:

We thank Alla Ganscher, Elke Stauber, Angelika Pach, Silvia Babl and Margit Schimmel for great technical assistance. We thank Christoph Möhle and Thomas Stempfl of the Kompetenzzentrum für Bioanalytik, University of Regensburg for the RNA sequencing analysis.

4.8 Supplementary Material

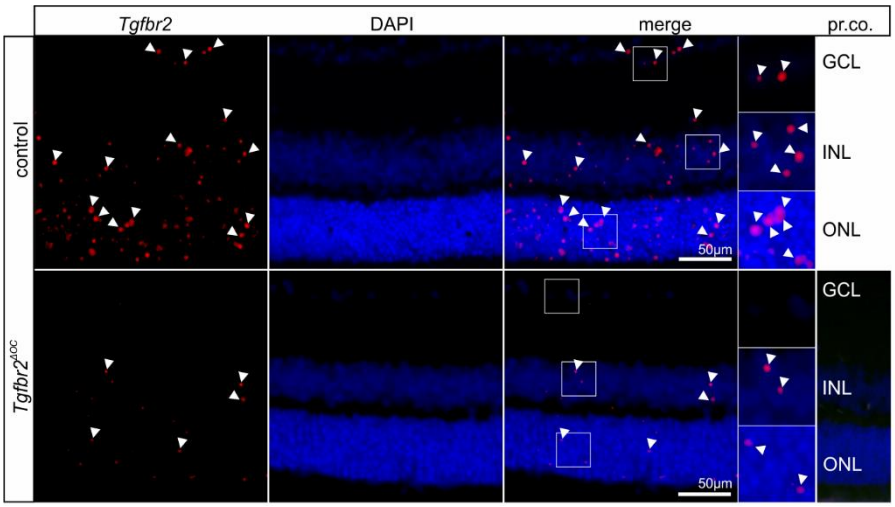

Suppl Fig 7: Tgfbr2 BaseScope

In situ hybridization for Tgfbr2 (red, arrowheads) in retinae of one-month-old animals. Nuclei were DAPI-stained (blue). Manifold Tgfbr2 signals (red, arrowheads) were visible in the retina of the control animal that were remarkably reduced in the Tgfbr2Δoc retina. The boxed areas are shown in high resolution on the right. Tgfbr2 = transforming growth factor β receptor type 2; pr.co. = probe control; GCL = ganglion cell layer; INL = inner nuclear layer; ONL = outer nuclear layer.

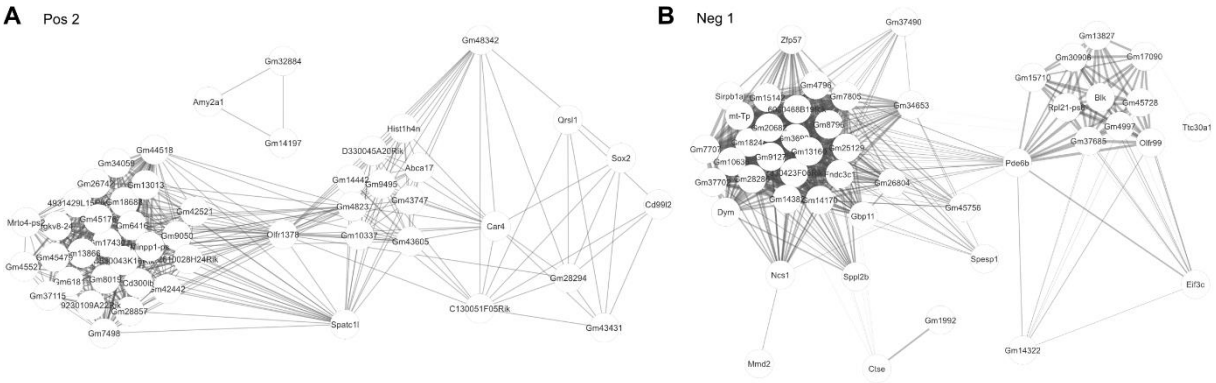

Suppl Fig 8: WGCNA modules of Tgfbr2^{Δoc} retinae.

***(A,B)** Intra-module analysis of the Pos2 (**D**) and Neg1 I modules. The 50 highest connected genes (intramodular connectivity) with the 500 strongest connections are shown. None of the genes were significantly dysregulated in the DESeq2 analysis.*

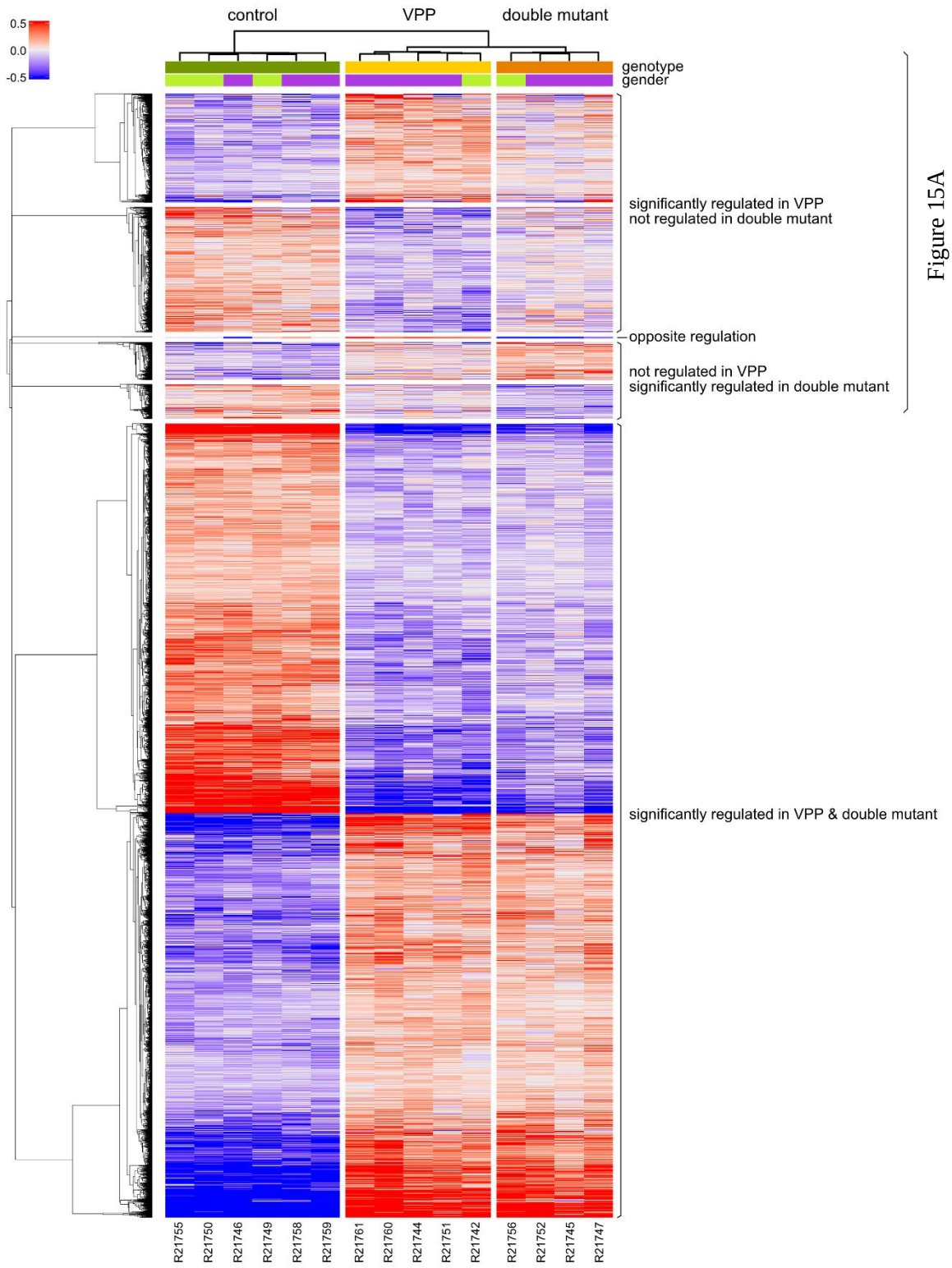

Figure 15A

Suppl Fig 9: Differential regulation of gene expression in the VPP and double *mutant mice.*

Heatmap showing the deviation of expression from the mean of all significantly dysregulated genes in any of the pairwise comparisons: VPP and double mutant, respectively, against control retinae. R21742-R21761 = RNAseq sample number.

4.9 Digital Supplementary Material on CD-R

Suppl Table 4: DESeq2 analysis of Tgfbr2$^{\Delta OC}$ animals compared to controls

Suppl Table 5: WGCNA analysis Tgfbr2$^{\Delta OC}$ animals compared to controls

Suppl Table 6: DESeq2 analysis of double mutants compared to VPPs

4.10 Author Contributions

Conceptualization: A.N. and B.M.B.

Methodology: C.B.B., S.I.S., N.K., S.K.B., A.S., M.V., A.N. and B.M.B.

Software: A.N.

Validation: A.N. and B.M.B.

Formal analysis: C.B.B., S.I.S., S.K.B., A.S., A.N. and B.M.B.

Investigation: C.B.B., S.I.S., S.K.B., A.S., A.N. and B.M.B.

Resources: E.R.T., S.E., J.H. and B.M.B.

Data curation: C.B.B., S.I.S., N.K., S.K.B., A.S., M.V., A.N. and B.M.B.

Writing-original draft preparation: C.B.B., A.N. and B.M.B.

Writing review and editing: C.B.B., S.I.S., N.K., S.K.B., A.S., M.V., J.H., E.R.T., S.E., A.N. and B.M.B.

Visualization: C.B.B., A.N. and B.M.B.

Supervision: E.R.T., S.E. and B.M.B.

Project administration: A.N. and B.M.B.

Funding acquisition: A.N., B.M.B.

Chapter 5

5 General Discussion

To investigate molecular mechanisms involved in Retinitis Pigmentosa (RP), animal models mimicking photoreceptor degeneration are frequently used. By using the light damage paradigm, a well-established model to induce photoreceptor degeneration, we found that (**1**) high light intensities and long exposure times resulted in massive photoreceptor degeneration and dysregulation of retinal reference genes.

Further, we used the VPP transgene as a genetic model mimicking autosomal dominant RP and (**2**) first confirmed the progressive photoreceptor degeneration. Using next generation RNA sequencing (RNAseq) analyses, we found (**3**) an extensive dysregulation of the retinal transcriptome. Subsequent weighted correlation network analysis WGCNA and gene ontology enrichments revealed, amongst others, (**4**) dysregulation of genes involved in TGFβ regulated extracellular matrix organization and cellular homeostasis, (**5**) (ocular) immune system/response and (**6**) dysregulation of several neuroprotective signaling pathways such as TGFβ signaling, G-protein coupled and VEGF in the VPP retinae compared to controls. *In situ* hybridization revealed (**7**) upregulation of representative components (such as *Tgfbr2)* of the identified dysregulated neuroprotective pathways in Müller cells and retinal neurons.

However, depletion of *Tgfbr2* in Müller cells and retinal neurons (**8**) did not affect the healthy adult retina, but (**9**) resulted in an exaggerated neurodegeneration in the case of VPP-induced photoreceptor degeneration. Moreover, RNAseq and subsequent gene ontology and WGCNA analyses of these double mutant retinae, harbouring a conditional deletion of *Tgfbr2* in Müller cells and neurons and VPP-induced photoreceptor degeneration, revealed (**10**) upregulation of pro-apoptotic genes, (**11**) a dysbalance of MAPkinase associated signaling pathways and potentially (**12**) sensitization of photoreceptors to ferroptosis-mediated cell death.

Based on our data, we therefore conclude that neuroinflammation and dysregulation of neuroprotective pathways such as TGFβ signaling in Müller cells and retinal neurons play an essential role in neurodegeneration of ocular diseases such as RP.

5.1 Dysregulation of reference genes after intense light exposure

The light damage paradigm is a commonly used method to induce photoreceptor degeneration and thus enables scientists to investigate the molecular mechanisms promoting neurodegeneration and/or use the model to test therapeutic strategies in animal experiments. In a dose-response study, we investigated the sensitivity of wildtype albino (Balb-C/CD1 genetic background) retinae to different light intensities and exposure times. As expected, high light intensity (10,000 lux) and long exposure time (1h) resulted in an aggravated degeneration of photoreceptors. However, surprisingly, we could also show that an excessive exposure to bright white light resulted in an extensive dysregulation of various retinal reference genes (Bielmeier et al., 2019).

Quantitative PCR (qPCR) is commonly used to evaluate alterations in gene expression levels following light induced photoreceptor degeneration. An essential component of this method is based on the normalization of target genes with endogenous reference genes. Hence, reference genes have to be stable in different experimental settings and therefore have to be chosen very carefully to gain reliable results (Jacob et al., 2013). Therefore, genes involved in basic cellular functions are often used as reference genes as their expression is considered to be stable throughout different experimental conditions. However, the frequently used glycerinaldehyd-3-phosphat-dehydrogenase (*Gapdh*) was found to be very stable during reprogramming processes in induced pluripotent stem cells (Panina et al., 2018), but its expression levels were strongly affected in various other experimental conditions, e.g. in samples from healthy liver tissue, liver cirrhosis and hepatocellular carcinoma or in samples of inguinal white adipose tissue and skeletal muscle (Gong et al., 2016; Kim & Kim, 2003; Mahoney et al., 2004). Accordingly, we could also show a significant downregulation of retinal *Gapdh* following treatment with high light intensities (10,000 lux, 1h). Based on the literature, reference genes such as TATA-binding protein (*Tbp)* (Nakao et al., 2015; Valente et al., 2009) or ubiquitin c (*Ubc*) (Kim & Kim, 2003) are referred as being very stable along different experimental conditions. Yet, again, following exposure to high light intensities (10,000 lux, 1h), we observed their significant downregulation as we did for all the other investigated reference genes. We therefore hypothesize that the exposure of mice in a Balb-C/CD1 background to 10,000 lux for 1h leads to a disturbance of cellular homeostasis. It is conceivable that the resulting massive apoptosis could subsequently also lead to unwanted secondary mediated apoptosis of neighbouring cells. Consequently, the parameters for light damage should be adapted and controlled very carefully for each study as depending on the specific genetic background, genetic or other modulations the stability and expression levels of reference genes after light exposure may vary.

5.2 Retinal degeneration results in apoptosis, neuroinflammation and dysregulation of neuroprotective pathways

RNAseq analyses of VPP retinae revealed an extensive dysregulation of genes compared to control retinae. Amongst other factors, we found upregulated factors associated with apoptosis like caspase 1 (*Casp1*) and bcl2-interacting killer (*Bik*) and scar formation, such as fibrinogen like 2 (*Fgl2*) and *Tgfβ1*. In fact, we identified members of the TGFβ family dysregulated in the VPP animals. One of the well-described features of TGFβ signaling is its contribution to wound healing, tissue fibrosis, and scar formation (Penn et al., 2012; Saika, 2006). Accordingly, previously published data showed that TGFβ contributed to reorganization of the extracellular matrix in primary open-angle glaucoma (Fuchshofer, 2011; Fuchshofer & Tamm, 2009, 2012) and gene ontology enrichments of the RNAseq data from VPP retinae revealed "TGFβ-regulated organization of the extracellular matrix" which may be the result of a healing response after photoreceptor degeneration in VPP retinae.

Neuroinflammation is known to be a common feature in neurodegenerative diseases like Alzheimer's disease, Parkinson's disease, multiple sclerosis or retinal degenerations (Cuenca et al., 2014; Gong et al., 2016; Mullins et al., 2012). Intriguingly, among the 30 most dysregulated genes in the VPPs, we found a substantial number of genes associated with inflammatory or immune response functions. Gene ontology enrichment analyses also indicated upregulation of "cellular responses to cytokine stimuli", suggesting a persistent neuroinflammatory process. These findings are consistent with previously published data describing upregulation of factors such as leukemia inhibitory factor (*Lif*), chemokine (C-C motif) ligand 2 (Cc*l2 = Mcp-1*), chemokine (C-C motif) ligand 28 (*Ccl28*), interleukin-1 (*Il-1*), complement component 1q (*C1q*), and complement factor H (*CFH*) in retinas of genetic mouse models of RP (Bales et al., 2018; Joly et al., 2008; Lohr et al., 2006; Rohrer et al., 2007a; Rohrer et al., 2007b; Samardzija et al., 2006b). Microarray data from the retina of an RP patient carrying two mutations in the *ABCA4* gene showed increased expression of complement system genes (*complement factor B, complement C2*), various cytokines, and cytokine receptors interleukin-6 (*Il-6*), C-X-C motif chemokine ligand 10 and 2 *CXCL10*, *CXCL2*), among others, thus suggesting a neuroinflammatory process in human RP, too (Mullins et al., 2012). Taken together, the results indicate a strong impact of neuroinflammation in retinal degeneration.

After neurotoxic events, neuronal stress signals are released and lead to microglial proliferation, migration, and secretion of specific cytokines and chemokines that can exert neurotoxic or neuroprotective effects (Cuenca et al., 2014; Stoll et al., 2000). We found an accumulation of reactive Ionized calcium-binding adapter molecule 1- (IBA1-) positive cells in the OPL and subneuroretinal space in VPP retinae, which strongly suggests an ongoing neuroinflammatory process. Furthermore, it is conceivable that the reactivity of microglia cells corresponds to a chronic neuroinflammatory

response, and may lead to irreversible neuronal cell death in the VPP model as well (Cuenca et al., 2014; Hanisch & Kettenmann, 2007; Langmann, 2007).

Others and our group (Feng et al., 2017; Rutar et al., 2011b) have shown expression of chemokine (C-C motif) ligand 28 (*Ccl2*) in Müller cells and photoreceptors in the healthy retina and an upregulation of *Ccl2* after retinal damage (Bielmeier et al., 2021; Rutar et al., 2012; Rutar et al., 2011a). Previously published data from Joly and colleagues showed no differences in the retinal morphology of double mutant mice (depleted *Ccl2* and carrying the VPP transgene: VPP; $Ccl2^{-/-}$) compared to VPP transgenic mice on a wildtype background (Joly et al., 2008). Contrary to this findings, Rutar and colleagues could demonstrate that siRNA-mediated silencing of *Ccl2* resulted in significantly lower numbers of apoptotic photoreceptors in rats after light-induced photoreceptor degeneration (Rutar et al., 2012; Rutar et al., 2011a). These results lead to the assumption that *Ccl2* plays a crucial role in neurodegeneration and increased *Ccl2* expression in Müller cells and in the ONL may contribute to the attraction/migration and reactivity of microglial cells in this specific region, but as the data are still conflicting, the central role of CCL2 in this process remains to be elucidated.

We could also identify a substantial number of genes encoding for components of the complement system, which is part of the innate immune system. It has been shown that activation of the complement system can promote microglial/infiltrative macrophage migration (Lohr et al., 2006; Rutar et al., 2011b). In fact, in retinae of human patients suffering from RP and in retinae of mice following genetic or light-induced photoreceptor degeneration several complement factors were upregulated (Hadziahmetovic et al., 2012; Lohr et al., 2006; Rohrer et al., 2007a; Rohrer et al., 2007b; Rutar et al., 2012; Schäfer et al., 2017; Silverman et al., 2019). Rohrer and colleagues have also shown that mice with a deficiency in complement factor D were protected from light-induced photoreceptor degeneration (Rohrer et al., 2007a). Hence, the exact role of the complement system in neurodegeneration still needs to be clarified.

Our group recently showed that endothelin 1 (*Edn1*), endothelin 2 (*Edn2*), endothelin receptor type a (*Ednra*) and endothelin receptor type b (*Ednrb*) were significantly upregulated after various ocular traumata (Schmitt et al., 2019), but in VPP retinas only *Edn2* and *Ednrb* were upregulated. Most likely, this can be explained by the different damage models used that may subsequently result in different activation patterns of downstream signaling pathways (Samardzija et al., 2006b). Recently published data (Boneva et al., 2016; Braunger et al., 2013a; Joly et al., 2008; Rattner & Nathans, 2005; Schmitt et al., 2019) showed, that in response to retinal injury, *Edn2* was expressed by photoreceptors, along with increased expression of *Ednrb* and glial fibrillary acidic protein (*Gfap*), the latter indicating reactivity of Müller cells, and increased expression of *Lif* and fibroblast growth factor 2 (*Fgf2*). The RNAseq data, *in situ* hybridizations, immunofluorescence staining, and qPCR analyses that were performed in this thesis confirmed this observation for VPP retinae. Moreover, we could determine expression of not only *Ednrb* but also of *Tgfbr2* and vascular endothelial growth factor receptor type 2 **(***Vegfr2*) in resting and reactive Müller cells, indicating the close interplay between neuronal and glial cells.

5.3 The role of TGF-β in RP

TGFβ is known to be involved in many cellular processes (Massagué, 2012b) and there is growing evidence that it has a protective impact on neurons (Braunger et al., 2013b; Gabriel et al., 2003; Ma et al., 2008; Park et al., 2008; Walshe et al., 2009). To analyze whether the observed upregulation of Tgfbr2 in retinal neurons and Müller cells following VPP-mediated photoreceptor degeneration might have neuroprotective properties, we studied the impact of TGFβ signaling in Müller cells and retinal neurons. Hence, we used the Cre/*loxP* system to specifically delete the *Tgfbr2* gene in cells originating from the optic cup (α-Cre;*Tgfbr2* = *Tgfbr2*$^{\Delta OC}$) (Marquardt et al., 2001) that will differentiate in Müller cells and retinal neurons. In a previously published work, we could show that *Tgfbr2*$^{\Delta OC}$ had an increased number of degenerating neurons during developmental programmed cell death, especially in the GCL and INL, resulting in mild developmental changes in the adult retina, such as a reduced numbers of retinal ganglion cells or neurons of the INL (Braunger et al., 2013b). However, Cepko and colleagues could show that only a negligible percentage of photoreceptors is affected by programmed cell death during retinal development (Cepko et al., 1996) and accordingly, in morphometric analyses, we observed comparable ONL thickness between control and *Tgfbr2*$^{\Delta OC}$ from two-month-old animals (Braunger et al., 2013b) and three-month-old animals (data in this thesis, Figure 13F). Overall, the depletion of *Tgfbr2* in adult *Tgfbr2*$^{\Delta OC}$ mice had no obvious effect on the retinal morphology nor on the relative mRNA levels or RNAseq data in "healthy" animals, not carrying the VPP transgene. In fact, only 22 dysregulated were found in healthy adult *Tgfbr2*$^{\Delta OC}$ retinae compared to controls, indicating a minor role of TGFβ signaling in retinal neurons and Müller cells in the post-developmental maintenance and homeostasis of the retina.

Intriguingly, crossbreeding *Tgfbr2*$^{\Delta OC}$ with VPP transgene (α-Cre;*Tgfbr2*;VPP = double mutants) animals led to an exacerbated photoreceptor degeneration in double mutant retinae compared to VPP retinae, indicating a neuroprotective effect of TGFβ signaling in retinal neurons and Müller cells. To identify the downstream molecular mechanisms responsible for this aggravated neurodegeneration in double mutants, we performed RNAseq analyses and found more than 600 dysregulated genes in the double mutant retinae which were not affected in VPP retinae. Subsequently performed WGCNA and gene ontology analyses of the RNAseq data revealed members of the Activator-protein (AP1) family significantly upregulated compared to control VPP mice. AP1 is a pluripotent transcription factor and has been shown to be involved in the regulation of cell survival and death (Ameyar et al., 2003; Shaulian & Karin, 2002). Further, we found a significant dysregulation of several Mitogen-activated protein-kinase (MAPK) associated pathways. *Mapk11* was significantly downregulated in VPP retinae but not in double mutants. MAPK11 belongs to the p38 MAPK and is reported to be involved cellular responses, like physical stress (Cuadrado & Nebreda, 2010) and in regulating tumor necrosis factor (TNF) expression in monocytic cells (Mahlknecht et al., 2004).

In addition, *Mapk10* and *Fos* proto-oncogene were significantly upregulated in only double mutant retinae (Figure 15B). MAPK10 modulates neuronal apoptosis (Ying et al., 2006) and FOS interacts with c-JUN to form the transcription factor AP1, that induces the transcription of pro-apoptotic genes (Curran & Morgan, 1995; Zhang et al., 2002). In contrast, *Mapk7* (*Erk7*) was found to be upregulated in the VPP animals, but not in the double mutants. MAPK7 can be activated by nerve growth factor (NGF) or brain derived neurotrophic factor (BDNF) and plays an anti-apoptotic role (Drew et al., 2012) that appears to be absent under TGFβ deficiency. Taken together, the depletion of TGFβ signaling in retinal neurons and Müller seems to lead to a molecular dysbalance in the retina, shifting the effects towards the pro-apoptotic side.

We also identified upregulated HD Domain containing 3 (*Hddc3* = *Mesh1*) levels in *Tgfr2*$^{\Delta OC}$ and double mutant mice, but not in control and VPP mice, indicating an exclusively TGFβ-dependent effect. Upregulated HDDC3 has been reported to sensitize cells to ferroptosis (Ding et al., 2020) and there are further data showing that ferroptosis can lead to neurodegeneration (Qin et al., 2021). Therefore, it is tempting to speculate that the depletion of TGFβ signaling in Müller cells and neurons sensitized photoreceptor cells to ferroptosis-mediated cell death following VPP-mediated photoreceptor degeneration.

6 Summary

Retinitis Pigmentosa (RP) is one of the major causes of blindness in younger patients starting in adolescence, already. To date, there is no therapy that prevents or mitigates this retinal degeneration. Therefore, it is necessary to investigate the downstream molecular mechanisms in detail with the aim to identify future therapeutic approaches.

To this end, animal models have been developed mimicking retinal degeneration and to allow for investigation of causative damaging mechanisms. Amongst these models, the light damage paradigm is a well-established and frequently used damage model. In this thesis, we characterized the impact of different light intensities and exposure times on light-induced photoreceptor degeneration and the expression levels of retinal reference genes. We could show, that the number of degenerating photoreceptor cells increased with light intensity and duration of light exposure. Moreover, following high light intensities, we detected a significant and extensive downregulation in the expression levels of reference genes such as *Gapdh*, *Gnb2l*, *Rpl32*, *Rps9*, *Actb*, *Ubc* and *Tbp* compared to control (no light exposure) animals.

We also studied the VPP mouse line, a model mimicking autosomal dominant RP. TUNEL-labelling at the age of one month, morphometric and relative mRNA analyses at the age of three months confirmed the progressive degeneration of photoreceptors. Moreover, next generation RNAsequencing (RNAseq) analyses revealed more than 9,00 significantly dysregulated genes in VPP retinae and six significantly associated gene modules in the subsequently performed weighted correlation network analysis WGCNA Gene ontology enrichment showed, amongst others, dysregulation of genes involved in TGFβ regulated extracellular matrix organization, the (ocular) immune system/response, and cellular homeostasis. Moreover, we identified dysregulation of several neuroprotective pathways in VPP retinae. Taken together, the predominant effect of VPP-induced photoreceptor degeneration pointed towards induction of neuroinflammation and the upregulation of neuroprotective pathways like TGFβ, G-protein activated, and VEGF signaling. 3D reconstructions of immunostained/*in situ* hybridized sections revealed Müller cells and retinal neurons as the major cellular populations that express representative components of these signaling pathways such as *Tgfbr2, Vegfr2* and *Ednrb*.

Finally, we conditionally deleted *Tgfbr2* in retinal neurons and Müller cells to study, whether the VPP-associated upregulation of *Tgfbr2* in these cell populations might have neuroprotective properties. We therefore crossbred VPP mice and mice with a conditional deletion of *Tgfbr2* in Müller cells and retinal neurons (α-Cre;*Tgfbr2* = $Tgfbr2^{\Delta OC}$). We studied the impact of *Tgfbr2* deletion in "healthy" retinae (not carrying the VPP transgene) and in "diseased" (VPP) retinae. TUNEL-labeling, morphometric analyses and RNAseq analyses showed that the deletion of *Tgfbr2* in Müller cells and retinal neurons in "healthy" animals had no obvious effects on the retinal morphology and affected the retinal transcriptome only

very mildly. However, in diseased, neurodegenerative VPP retinae, *Tgfbr2* deletion in Müller cells and retinal neurons significantly aggravated retinal degeneration in double mutant mice (*Tgfbr2*$^{\Delta OC}$; VPP) compared to VPP mice. RNAseq analyses and subsequently performed gene ontology analysis and weighted correlation network analysis (WGCNA) revealed induction of pro-apoptotic genes and dysregulation of the MAP kinase associated pathways upon VPP-mediated photoreceptor degeneration and *Tgfbr2* deficiency. Moreover, we identified *Hddc3* a factor involved in ferroptosis, as being significantly upregulated in *Tgfbr2* deficient retinae (*Tgfbr2*$^{\Delta OC}$ and *Tgfbr2*$^{\Delta OC}$; VPP) leading to the assumption, that *Tgfbr2* depletion may sensitize photoreceptors to ferroptosis mediated cell death.

In summary, we conclude, that modulation of neuroinflammation, and/or TGFβ signaling in retinal neurons and Müller cells might pose promising therapeutic options to attenuate photoreceptor degeneration in humans.

7 Appendix

7.1 List of Figures

7.2 List of Tables

Digital Supplementary Material on CD-R:

7.3 References

Akhurst, R. J., & Hata, A. (2012). Targeting the TGFß signalling pathway in disease. *Nature Reviews Drug Discovery*, *11*(10), 790–811. https://doi.org/10.1038/nrd3810

Aldewachi, H., Al-Zidan, R. N., Conner, M. T., & Salman, M. M. (2021). High-Throughput Screening Platforms in the Discovery of Novel Drugs for Neurodegenerative Diseases. *Bioengineering (Basel, Switzerland)*, *8*(2). https://doi.org/10.3390/bioengineering8020030

Ambati, J., & Fowler, B. J. (2012). Mechanisms of age-related macular degeneration. *Neuron*, *75*(1), 26–39. https://doi.org/10.1016/j.neuron.2012.06.018

Ameyar, M., Wisniewska, M., & Weitzman, J. B. (2003). A role for AP-1 in apoptosis: the case for and against. *Biochimie*, *85*(8), 747–752. https://doi.org/https://doi.org/10.1016/j.biochi.2003.09.006

Antonetti, D. A., Klein, R., & Gardner, T. W. (2012). Diabetic retinopathy. *The New England Journal of Medicine*, *366*(13), 1227–1239. https://doi.org/10.1056/NEJMra1005073

Bales, K. L., Ianov, L., Kennedy, A. J., Sweatt, J. D., & Gross, A. K. (2018). Autosomal dominant retinitis pigmentosa rhodopsin mutant Q344X drives specific alterations in chromatin complex gene transcription. *Molecular Vision*, *24*, 153–164.

Bäumer, N., Marquardt, T., Stoykova, A., Ashery-Padan, R., Chowdhury, K., & Gruss, P. (2002). Pax6 is required for establishing naso-temporal and dorsal characteristics of the optic vesicle. *Development*, *129*(19), 4535–4545. https://doi.org/10.1242/dev.129.19.4535

Baylor, D. (1996). How photons start vision. *Proceedings of the National Academy of Sciences of the United States of America*, *93*(2), 560–565. https://doi.org/10.1073/pnas.93.2.560

Benedetto, M. M., & Contin, M. A. (2019). Oxidative Stress in Retinal Degeneration Promoted by Constant LED Light . In *Frontiers in Cellular Neuroscience* (Vol. 13). https://www.frontiersin.org/articles/10.3389/fncel.2019.00139

Berson, E. L., Rosner, B., Sandberg, M. A., & Dryja, T. P. (1991). Ocular findings in patients with autosomal dominant retinitis pigmentosa and a rhodopsin gene defect (Pro-23-His). *Archives of Ophthalmology (Chicago, Ill. : 1960)*, *109*(1), 92–101. https://doi.org/10.1001/archopht.1991.01080010094039

Bhutto, I., & Lutty, G. (2012). Understanding age-related macular degeneration (AMD): relationships between the photoreceptor/retinal pigment epithelium/Bruch's membrane/choriocapillaris complex. *Molecular Aspects of Medicine*, *33*(4), 295–317. https://doi.org/10.1016/j.mam.2012.04.005

Bielmeier, C. B., Roth, S., Schmitt, S. I., Boneva, S. K., Schlecht, A., Vallon, M., Tamm, E. R., Ergün, S., Neueder, A., & Braunger, B. M. (2021). Transcriptional Profiling Identifies Upregulation of Neuroprotective Pathways in Retinitis Pigmentosa. *International Journal of Molecular Sciences*, *22*(12). https://doi.org/10.3390/ijms22126307

Bielmeier, C. B., Schmitt, S. I., & Braunger, B. M. (2019). Light Intensity-Dependent Dysregulation of Retinal Reference Genes. *Advances in Experimental Medicine and Biology*, *1185*, 295–299. https://doi.org/10.1007/978-3-030-27378-1_48

Bird, A. C. (1995). Retinal photoreceptor dystrophies LI. Edward Jackson Memorial Lecture. *American Journal of Ophthalmology*, *119*(5), 543–562. https://doi.org/10.1016/s0002-9394(14)70212-0

Boileau, C., Guo, D.-C., Hanna, N., Regalado, E. S., Detaint, D., Gong, L., Varret, M., Prakash, S. K., Li, A. H., d'Indy, H., Braverman, A. C., Grandchamp, B., Kwartler, C. S., Gouya, L., Santos-Cortez, R. L. P., Abifadel, M., Leal, S. M., Muti, C., Shendure, J., … Milewicz, D. M. (2012). TGFB2 mutations cause familial thoracic aortic aneurysms and dissections associated with mild systemic features of Marfan syndrome. *Nature Genetics*, *44*(8), 916–921. https://doi.org/10.1038/ng.2348

Boneva, S. K., Groß, T. R., Schlecht, A., Schmitt, S. I., Sippl, C., Jägle, H., Volz, C., Neueder, A., Tamm, E. R., & Braunger, B. M. (2016). Cre recombinase expression or topical tamoxifen treatment do not affect retinal structure and function, neuronal vulnerability or glial reactivity in the mouse eye. *Neuroscience*, *325*, 188–201. https://doi.org/10.1016/j.neuroscience.2016.03.050

Bowmaker, J. K., & Hunt, D. M. (2006). Evolution of vertebrate visual pigments. *Current Biology*, *16*(13), R484–R489. https://doi.org/10.1016/j.cub.2006.06.016

Bramall, A. N., Wright, A. F., Jacobson, S. G., & McInnes, R. R. (2010). The genomic, biochemical, and cellular responses of the retina in inherited photoreceptor degenerations and prospects for the treatment of these disorders. *Annual Review of Neuroscience*, *33*, 441–472. https://doi.org/10.1146/annurev-neuro-060909-153227

Braunger, B. M., Leimbeck, S. V, Schlecht, A., Volz, C., Jägle, H., & Tamm, E. R. (2015). Deletion of ocular transforming growth factor ß signaling mimics essential characteristics of diabetic retinopathy. *The American Journal of Pathology*, *185*(6), 1749–1768. https://doi.org/10.1016/j.ajpath.2015.02.007

Braunger, B. M., Ohlmann, A., Koch, M., Tanimoto, N., Volz, C., Yang, Y., Bösl, M. R., Cvekl, A., Jägle, H., Seeliger, M. W., & Tamm, E. R. (2013). Constitutive overexpression of Norrin activates Wnt/ß-catenin and endothelin-2 signaling to protect photoreceptors from light damage. *Neurobiology of Disease*, *50*, 1–12. https://doi.org/10.1016/j.nbd.2012.09.008

Braunger, B. M., Pielmeier, S., Demmer, C., Landstorfer, V., Kawall, D., Abramov, N., Leibinger, M., Kleiter, I., Fischer, D., Jägle, H., & Tamm, E. R. (2013). TGF-ß signaling protects retinal neurons from programmed cell death during the development of the mammalian eye. *The Journal of Neuroscience : The Official Journal of the Society for Neuroscience*, *33*(35), 14246–14258. https://doi.org/10.1523/JNEUROSCI.0991-13.2013

Bringmann, A., Pannicke, T., Grosche, J., Francke, M., Wiedemann, P., Skatchkov, S. N., Osborne, N. N., & Reichenbach, A. (2006). Müller cells in the healthy and diseased retina. *Progress in Retinal and Eye Research*, *25*(4), 397–424. https://doi.org/10.1016/j.preteyeres.2006.05.003

Buch, H., Vinding, T., La Cour, M., Appleyard, M., Jensen, G. B., & Nielsen, N. V. (2004). Prevalence and causes of visual impairment and blindness among 9980 Scandinavian adults: the Copenhagen City Eye Study. *Ophthalmology*, *111*(1), 53–61. https://doi.org/10.1016/j.ophtha.2003.05.010

Cepko, C. L., Austin, C. P., Yang, X., Alexiades, M., & Ezzeddine, D. (1996). Cell fate determination in the vertebrate retina. *Proceedings of the National Academy of Sciences of the United States of America*, *93*(2), 589–595. https://doi.org/10.1073/pnas.93.2.589

Chang, G. Q., Hao, Y., & Wong, F. (1993). Apoptosis: final common pathway of photoreceptor death in rd, rds, and rhodopsin mutant mice. *Neuron*, *11*(4), 595–605. https://doi.org/10.1016/0896-6273(93)90072-y

Chen, E. Y., Tan, C. M., Kou, Y., Duan, Q., Wang, Z., Meirelles, G. V., Clark, N. R., & Ma'ayan, A. (2013). Enrichr: interactive and collaborative HTML5 gene list enrichment analysis tool. *BMC Bioinformatics*, *14*(1), 128. https://doi.org/10.1186/1471-2105-14-128

Chen, W.-W., Zhang, X., & Huang, W.-J. (2016). Role of neuroinflammation in neurodegenerative diseases (Review). *Molecular Medicine Reports*, *13*(4), 3391–3396. https://doi.org/10.3892/mmr.2016.4948

Chytil, A., Magnuson, M. A., Wright, C. V. E., & Moses, H. L. (2002). Conditional inactivation of the TGF-ß type II receptor using Cre:Lox. *Genesis*, *32*(2), 73–75. https://doi.org/10.1002/gene.10046

Clayton, S. W., Ban, G. I., Liu, C., & Serra, R. (2020). Canonical and noncanonical TGF-β signaling regulate fibrous tissue differentiation in the axial skeleton. *Scientific Reports*, *10*(1), 21364. https://doi.org/10.1038/s41598-020-78206-4

Conery, A. R., Cao, Y., Thompson, E. A., Townsend, C. M. J., Ko, T. C., & Luo, K. (2004). Akt interacts directly with Smad3 to regulate the sensitivity to TGF-beta induced apoptosis. *Nature Cell Biology*, *6*(4), 366–372. https://doi.org/10.1038/ncb1117

Crooks, J., & Kolb, H. (1992). Localization of GABA, glycine, glutamate and tyrosine hydroxylase in the human retina. *The Journal of Comparative Neurology*, *315*(3), 287–302. https://doi.org/10.1002/cne.903150305

Cuadrado, A., & Nebreda, A. R. (2010). Mechanisms and functions of p38 MAPK signalling. *Biochemical Journal*, *429*(3), 403–417. https://doi.org/10.1042/BJ20100323

Cuenca, N., Fernández-Sánchez, L., Campello, L., Maneu, V., de La Villa, P., Lax, P., & Pinilla, I. (2014). Cellular responses following retinal injuries and therapeutic approaches for neurodegenerative diseases. *Progress in Retinal and Eye Research*, *43*, 17–75. https://doi.org/10.1016/j.preteyeres.2014.07.001

Curran, T., & Morgan, J. I. (1995). Fos: An immediate-early transcription factor in neurons. *Journal of Neurobiology*, *26*(3), 403–412. https://doi.org/https://doi.org/10.1002/neu.480260312

de Jong, P. T. V. M. (2006). Age-related macular degeneration. *The New England Journal of Medicine*, *355*(14), 1474–1485. https://doi.org/10.1056/NEJMra062326

Ding, C.-K. C., Rose, J., Sun, T., Wu, J., Chen, P.-H., Lin, C.-C., Yang, W.-H., Chen, K.-Y., Lee, H., Xu, E., Tian, S., Akinwuntan, J., Zhao, J., Guan, Z., Zhou, P., & Chi, J.-T. (2020). MESH1 is a cytosolic NADPH phosphatase that regulates ferroptosis. *Nature Metabolism*, *2*(3), 270–277. https://doi.org/10.1038/s42255-020-0181-1

Dobin, A., Davis, C. A., Schlesinger, F., Drenkow, J., Zaleski, C., Jha, S., Batut, P., Chaisson, M., & Gingeras, T. R. (2013). STAR: ultrafast universal RNA-seq aligner. *Bioinformatics (Oxford, England)*, *29*(1), 15–21. https://doi.org/10.1093/bioinformatics/bts635

Drew, B. A., Burow, M. E., & Beckman, B. S. (2012). MEK5/ERK5 pathway: The first fifteen years. *Biochimica et Biophysica Acta (BBA) - Reviews on Cancer*, *1825*(1), 37–48. https://doi.org/https://doi.org/10.1016/j.bbcan.2011.10.002

Farrar, G. J., Kenna, P. F., & Humphries, P. (2002). On the genetics of retinitis pigmentosa and on mutation-independent approaches to therapeutic intervention. *The EMBO Journal*, *21*(5), 857–864. https://doi.org/10.1093/emboj/21.5.857

Feng, C., Wang, X., Liu, T., Zhang, M., Xu, G., & Ni, Y. (2017). Expression of CCL2 and its receptor in activation and migration of microglia and monocytes induced by photoreceptor apoptosis. *Molecular Vision*, *23*, 765–777.

Fuchshofer, R. (2011). The pathogenic role of transforming growth factor-ß2 in glaucomatous damage to the optic nerve head. *Experimental Eye Research*, *93*(2), 165–169. https://doi.org/10.1016/j.exer.2010.07.014

Fuchshofer, R., & Tamm, E. R. (2009). Modulation of extracellular matrix turnover in the trabecular meshwork. *Experimental Eye Research*, *88*(4), 683–688. https://doi.org/10.1016/j.exer.2009.01.005

Fuchshofer, R., & Tamm, E. R. (2012). The role of TGF-ß in the pathogenesis of primary open-angle glaucoma. *Cell and Tissue Research*, *347*(1), 279–290. https://doi.org/10.1007/s00441-011-1274-7

Gabriel, C., Ali, C., Lesné, S., Fernández-Monreal, M., Docagne, F., Plawinski, L., MacKenzie, E. T., Buisson, A., & Vivien, D. (2003). Transforming growth factor α-induced expression of type-1 plasminogen activator inhibitor in astrocytes rescues neurons from excitotoxicity. *The FASEB Journal*, *17*(2), 277–279. https://doi.org/https://doi.org/10.1096/fj.02-0403fje

Garcia, T. B., Hollborn, M., & Bringmann, A. (2017). Expression and signaling of NGF in the healthy and injured retina. *Cytokine & Growth Factor Reviews*, *34*, 43–57. https://doi.org/https://doi.org/10.1016/j.cytogfr.2016.11.005

Giaume, C., Kirchhoff, F., Matute, C., Reichenbach, A., & Verkhratsky, A. (2007). Glia: the fulcrum of brain diseases. *Cell Death {\&} Differentiation*, *14*(7), 1324–1335. https://doi.org/10.1038/sj.cdd.4402144

Gibbs, D., Azarian, S. M., Lillo, C., Kitamoto, J., Klomp, A. E., Steel, K. P., Libby, R. T., & Williams, D. S. (2004). Role of myosin VIIa and Rab27a in the motility and localization of RPE melanosomes. *Journal of Cell Science*, *117*(26), 6473–6483. https://doi.org/10.1242/jcs.01580

Ginzinger, D. G. (2002). Gene quantification using real-time quantitative PCR: an emerging technology hits the mainstream. *Experimental Hematology*, *30*(6), 503–512. https://doi.org/10.1016/s0301-472x(02)00806-8

Gong, H., Sun, L., Chen, B., Han, Y., Pang, J., Wu, W., Qi, R., & Zhang, T.-M. (2016). Evaluation of candidate reference genes for RT-qPCR studies in three metabolism related tissues of mice after caloric restriction. *Scientific Reports*, *6*, 38513. https://doi.org/10.1038/srep38513

Goumans, M.-J., Liu, Z., & ten Dijke, P. (2009). TGF-ß signaling in vascular biology and dysfunction. *Cell Research*, *19*(1), 116–127. https://doi.org/10.1038/cr.2008.326

Goumans, M. J., & Mummery, C. (2000). Functional analysis of the TGFbeta receptor/Smad pathway through gene ablation in mice. *The International Journal of Developmental Biology*, *44*(3), 253–265.

Grimm, C., & Remé, C. E. (2013). Light damage as a model of retinal degeneration. *Methods in Molecular Biology (Clifton, N.J.)*, *935*, 87–97. https://doi.org/10.1007/978-1-62703-080-9_6

Gu, Z., Eils, R., & Schlesner, M. (2016). Complex heatmaps reveal patterns and correlations in multidimensional genomic data. *Bioinformatics*, *32*(18), 2847–2849. https://doi.org/10.1093/bioinformatics/btw313

Hadziahmetovic, M., Kumar, U., Song, Y., Grieco, S., Song, D., Li, Y., Tobias, J. W., & Dunaief, J. L. (2012). Microarray analysis of murine retinal light damage reveals changes in iron regulatory, complement, and antioxidant genes in the neurosensory retina and isolated RPE. *Investigative Ophthalmology {\&} Visual Science*, *53*(9), 5231–5241. https://doi.org/10.1167/iovs.12-10204

Hanisch, U.-K., & Kettenmann, H. (2007). Microglia: active sensor and versatile effector cells in the normal and pathologic brain. *Nature Neuroscience*, *10*(11), 1387–1394. https://doi.org/10.1038/nn1997

Hartong, D. T., Berson, E. L., & Dryja, T. P. (2006). Retinitis pigmentosa. *Lancet (London, England)*, *368*(9549), 1795–1809. https://doi.org/10.1016/S0140-6736(06)69740-7

Huang, T., Schor, S. L., & Hinck, A. P. (2014). Biological activity differences between TGF-β1 and TGF-β3 correlate with differences in the rigidity and arrangement of their component monomers. *Biochemistry*, *53*(36), 5737–5749. https://doi.org/10.1021/bi500647d

Jacob, F., Guertler, R., Naim, S., Nixdorf, S., Fedier, A., Hacker, N. F., & Heinzelmann-Schwarz, V. (2013). Careful selection of reference genes is required for reliable performance of RT-qPCR in human normal and cancer cell lines. *PloS One*, *8*(3), e59180. https://doi.org/10.1371/journal.pone.0059180

Joly, S., Lange, C., Thiersch, M., Samardzija, M., & Grimm, C. (2008). Leukemia Inhibitory Factor Extends the Lifespan of Injured Photoreceptors In Vivo. *The Journal of Neuroscience*, *28*(51), 13765. https://doi.org/10.1523/JNEUROSCI.5114-08.2008

Karnovsky, M. (1965). J. 1965. A formaldehydeglutaraldehyde fixative of high osmolarity for use in electron microscopy. *J. Cell Biol*, *27*(2 Pt 2), 137–138.

Kellner, U., Tillack, H., & Renner, A. B. (2004). Hereditary retinochoroidal dystrophies. Part 1: Pathogenesis, diagnosis, therapy and patient counselling. *Der Ophthalmologe : Zeitschrift Der Deutschen Ophthalmologischen Gesellschaft*, *101*(3), 307–319; quiz 320. https://doi.org/10.1007/s00347-003-0944-6

Kim, S., & Kim, T. (2003). Selection of optimal internal controls for gene expression profiling of liver disease. *BioTechniques*, *35*(3), 456-458,460. https://doi.org/10.2144/03353bm03

Kitchen, P., Salman, M. M., Halsey, A. M., Clarke-Bland, C., MacDonald, J. A., Ishida, H., Vogel, H. J., Almutiri, S., Logan, A., Kreida, S., Al-Jubair, T., Winkel Missel, J., Gourdon, P., Törnroth-Horsefield, S., Conner, M. T., Ahmed, Z., Conner, A. C., & Bill, R. M. (2020). Targeting Aquaporin-4 Subcellular Localization to Treat Central Nervous System Edema. *Cell*, *181*(4), 784-799.e19. https://doi.org/10.1016/j.cell.2020.03.037

Kleinberger, G., Yamanishi, Y., Suárez-Calvet, M., Czirr, E., Lohmann, E., Cuyvers, E., Struyfs, H., Pettkus, N., Wenninger-Weinzierl, A., Mazaheri, F., Tahirovic, S., Lleó, A., Alcolea, D., Fortea, J., Willem, M., Lammich, S., Molinuevo, J. L., Sánchez-Valle, R., Antonell, A., … Haass, C. (2014). TREM2 mutations implicated in neurodegeneration impair cell surface transport and phagocytosis. *Science Translational Medicine*, *6*(243), 243ra86. https://doi.org/10.1126/scitranslmed.3009093

Kolb, H. (1995). Simple Anatomy of the Retina. In H. Kolb, E. Fernandez, & R. Nelson (Eds.), *Webvision: The Organization of the Retina and Visual System*.

Kolb, H., Fernandez, E., & Nelson, R. (Eds.). (1995). *Webvision: The Organization of the Retina and Visual System*.

Kozera, B., & Rapacz, M. (2013). Reference genes in real-time PCR. *Journal of Applied Genetics*, *54*(4), 391–406. https://doi.org/10.1007/s13353-013-0173-x

Kremer, H., van Wijk, E., Märker, T., Wolfrum, U., & Roepman, R. (2006). Usher syndrome: molecular links of pathogenesis, proteins and pathways. *Human Molecular Genetics*, *15*(suppl_2), R262–R270. https://doi.org/10.1093/hmg/ddl205

Krieglstein, K., & Unsicker, K. (1996). Distinct modulatory actions of TGF-β and LIF on neurotrophin-mediated survival of developing sensory neurons. *Neurochemical Research*, *21*(7), 843–850. https://doi.org/10.1007/BF02532308

Kugler, M., Schlecht, A., Fuchshofer, R., Kleiter, I., Aigner, L., Tamm, E. R., & Braunger, B. M. (2015). Heterozygous modulation of TGF-β signaling does not influence Müller glia cell reactivity or proliferation following NMDA-induced damage. *Histochemistry and Cell Biology*, *144*(5), 443–455. https://doi.org/10.1007/s00418-015-1354-y

Kugler, M., Schlecht, A., Fuchshofer, R., Schmitt, S. I., Kleiter, I., Aigner, L., Tamm, E. R., & Braunger, B. M. (2017). SMAD7 deficiency stimulates Müller progenitor cell proliferation during the development of the mammalian retina. *Histochemistry and Cell Biology*, *148*(1), 21–32. https://doi.org/10.1007/s00418-017-1549-5

Kühn, R., & M. Torres, R. (2002). *Cre/loxP Recombination System and Gene Targeting BT - Transgenesis Techniques: Principles and Protocols* (A. R. Clarke (Ed.); pp. 175–204). Springer New York. https://doi.org/10.1385/1-59259-178-7:175

Kuleshov, M. V, Jones, M. R., Rouillard, A. D., Fernandez, N. F., Duan, Q., Wang, Z., Koplev, S., Jenkins, S. L., Jagodnik, K. M., Lachmann, A., McDermott, M. G., Monteiro, C. D., Gundersen, G. W., & Ma'ayan, A. (2016). Enrichr: a comprehensive gene set enrichment analysis web server 2016 update. *Nucleic Acids Research*, *44*(W1), W90–W97. https://doi.org/10.1093/nar/gkw377

Langfelder, P., & Horvath, S. (2008). WGCNA: an R package for weighted correlation network analysis. *BMC Bioinformatics*, *9*(1), 559. https://doi.org/10.1186/1471-2105-9-559

Langfelder, P., Mischel, P. S., & Horvath, S. (2013). When Is Hub Gene Selection Better than Standard Meta-Analysis? *PLOS ONE*, *8*(4), e61505. https://doi.org/10.1371/journal.pone.0061505

Langmann, T. (2007). Microglia activation in retinal degeneration. *Journal of Leukocyte Biology*, *81*(6), 1345–1351. https://doi.org/10.1189/jlb.0207114

LaVail, M. M., Gorrin, G. M., Repaci, M. A., Thomas, L. A., & Ginsberg, H. M. (1987). Genetic regulation of light damage to photoreceptors. *Investigative Ophthalmology {\&} Visual Science*, *28*(7), 1043–1048.

Lévy, G., Levi-Acobas, F., Blanchard, S., Gerber, S., Larget-Piet, D., Chenal, V., Liu, X. Z., Newton, V., Steel, K. P., Brown, S. D., Munnich, A., Kaplan, J., Petit, C., & Weil, D. (1997). Myosin VIIA gene: heterogeneity of the mutations responsible for Usher syndrome type IB. *Human Molecular Genetics*, *6*(1), 111–116. https://doi.org/10.1093/hmg/6.1.111

Lewis, G. P., Erickson, P. A., Kaska, D. D., & Fisher, S. K. (1988). An immunocytochemical comparison of Müller cells and astrocytes in the cat retina. *Experimental Eye Research*, *47*(6), 839–853. https://doi.org/10.1016/0014-4835(88)90067-X

Livak, K. J., & Schmittgen, T. D. (2001). Analysis of relative gene expression data using real-time quantitative PCR and the 2(-Delta Delta C(T)) Method. *Methods (San Diego, Calif.)*, *25*(4), 402–408. https://doi.org/10.1006/meth.2001.1262

Lohr, H. R., Kuntchithapautham, K., Sharma, A. K., & Rohrer, B. (2006). Multiple, parallel cellular suicide mechanisms participate in photoreceptor cell death. *Experimental Eye Research*, *83*(2), 380–389. https://doi.org/10.1016/j.exer.2006.01.014

Love, M. I., Huber, W., & Anders, S. (2014). Moderated estimation of fold change and dispersion for RNA-seq data with DESeq2. *Genome Biology*, *15*(12), 550. https://doi.org/10.1186/s13059-014-0550-8

Ma, M., Ma, Y., Yi, X., Guo, R., Zhu, W., Fan, X., Xu, G., Frey, W. H. 2nd, & Liu, X. (2008). Intranasal delivery of transforming growth factor-beta1 in mice after stroke reduces infarct volume and increases neurogenesis in the subventricular zone. *BMC Neuroscience*, *9*, 117. https://doi.org/10.1186/1471-2202-9-117

Ma, W., Silverman, S. M., Zhao, L., Villasmil, R., Campos, M. M., Amaral, J., & Wong, W. T. (2019). Absence of TGFβ signaling in retinal microglia induces retinal degeneration and exacerbates choroidal neovascularization. *ELife*, *8*, e42049. https://doi.org/10.7554/eLife.42049

Mahlknecht, U., Will, J., Varin, A., Hoelzer, D., & Herbein, G. (2004). Histone Deacetylase 3, a Class I Histone Deacetylase, Suppresses MAPK11-Mediated Activating Transcription Factor-2 Activation and Represses TNF Gene Expression. *The Journal of Immunology*, *173*(6), 3979 LP – 3990. https://doi.org/10.4049/jimmunol.173.6.3979

Mahoney, D. J., Carey, K., Fu, M.-H., Snow, R., Cameron-Smith, D., Parise, G., & Tarnopolsky, M. A. (2004). Real-time RT-PCR analysis of housekeeping genes in human skeletal muscle following acute exercise. *Physiological Genomics*, *18*(2), 226–231. https://doi.org/10.1152/physiolgenomics.00067.2004

Marquardt, T., Ashery-Padan, R., Andrejewski, N., Scardigli, R., Guillemot, F., & Gruss, P. (2001). Pax6 Is Required for the Multipotent State of Retinal Progenitor Cells. *Cell*, *105*(1), 43–55. https://doi.org/10.1016/S0092-8674(01)00295-1

Massagué, J. (2000). How cells read TGF-β signals. *Nature Reviews Molecular Cell Biology*, *1*(3), 169–178. https://doi.org/10.1038/35043051

Massagué, J. (2004). G1 cell-cycle control and cancer. *Nature*, *432*(7015), 298–306. https://doi.org/10.1038/nature03094

Massagué, J. (2012a). TGFß signalling in context. *Nature Reviews. Molecular Cell Biology*, *13*(10), 616–630. https://doi.org/10.1038/nrm3434

Massagué, J. (2012b). TGFβ signalling in context. *Nature Reviews. Molecular Cell Biology*, *13*(10), 616–630. https://doi.org/10.1038/nrm3434

Moffitt, J. R., Bambah-Mukku, D., Eichhorn, S. W., Vaughn, E., Shekhar, K., Perez, J. D., Rubinstein, N. D., Hao, J., Regev, A., Dulac, C., & Zhuang, X. (2018). Molecular, spatial, and functional single-cell profiling of the hypothalamic preoptic region. *Science*, *362*(6416), eaau5324. https://doi.org/10.1126/science.aau5324

Moffitt, J. R., Hao, J., Wang, G., Chen, K. H., Babcock, H. P., & Zhuang, X. (2016). High-throughput single-cell gene-expression profiling with multiplexed error-robust fluorescence in situ hybridization. *Proceedings of the National Academy of Sciences*, *113*(39), 11046–11051. https://doi.org/10.1073/pnas.1612826113

Mullins, R. F., Kuehn, M. H., Radu, R. A., Enriquez, G. S., East, J. S., Schindler, E. I., Travis, G. H., & Stone, E. M. (2012). Autosomal recessive retinitis pigmentosa due to ABCA4 mutations: clinical, pathologic, and molecular characterization. *Investigative Ophthalmology {\&} Visual Science*, *53*(4), 1883–1894. https://doi.org/10.1167/iovs.12-9477

Naash, M. I., Hollyfield, J. G., al-Ubaidi, M. R., & Baehr, W. (1993). Simulation of human autosomal dominant retinitis pigmentosa in transgenic mice expressing a mutated murine opsin gene. *Proceedings of the National Academy of Sciences*, *90*(12), 5499–5503. https://doi.org/10.1073/pnas.90.12.5499

Nagy, A. (2000). Cre recombinase: the universal reagent for genome tailoring. *Genesis (New York, N.Y. : 2000)*, *26*(2), 99–109.

Nakamura, M., Kuse, Y., Tsuruma, K., Shimazawa, M., & Hara, H. (2017). The Involvement of the Oxidative Stress in Murine Blue LED Light-Induced Retinal Damage Model. *Biological and Pharmaceutical Bulletin*, *40*(8), 1219–1225. https://doi.org/10.1248/bpb.b16-01008

Nakao, R., Yamamoto, S., Yasumoto, Y., Kadota, K., & Oishi, K. (2015). Impact of denervation-induced muscle atrophy on housekeeping gene expression in mice. *Muscle {\&} Nerve*, *51*(2), 276–281. https://doi.org/10.1002/mus.24310

Organisciak, D. T., & Vaughan, D. K. (2010). Retinal light damage: mechanisms and protection. *Progress in Retinal and Eye Research*, *29*(2), 113–134. https://doi.org/10.1016/j.preteyeres.2009.11.004

Panina, Y., Germond, A., Masui, S., & Watanabe, T. M. (2018). Validation of Common Housekeeping Genes as Reference for qPCR Gene Expression Analysis During iPS Reprogramming Process. *Scientific Reports*, *8*(1), 8716. https://doi.org/10.1038/s41598-018-26707-8

Park, S. M., Jung, J. S., Jang, M. S., Kang, K. S., & Kang, S. K. (2008). Transforming growth factor-β1 regulates the fate of cultured spinal cord-derived neural progenitor cells. *Cell Proliferation*, *41*(2), 248–264. https://doi.org/https://doi.org/10.1111/j.1365-2184.2008.00514.x

Patro, R., Duggal, G., Love, M. I., Irizarry, R. A., & Kingsford, C. (2017). Salmon provides fast and bias-aware quantification of transcript expression. *Nature Methods*, *14*(4), 417–419. https://doi.org/10.1038/nmeth.4197

Peng, D., Fu, M., Wang, M., Wei, Y., & Wei, X. (2022). Targeting TGF-β signal transduction for fibrosis and cancer therapy. *Molecular Cancer*, *21*(1), 104. https://doi.org/10.1186/s12943-022-01569-x

Penn, J. W., Grobbelaar, A. O., & Rolfe, K. J. (2012). The role of the TGF-ß family in wound healing, burns and scarring: a review. *International Journal of Burns and Trauma*, *2*(1), 18–28.

Portera-Cailliau, C., Sung, C. H., Nathans, J., & Adler, R. (1994). Apoptotic photoreceptor cell death in mouse models of retinitis pigmentosa. *Proceedings of the National Academy of Sciences of the United States of America*, *91*(3), 974–978. https://doi.org/10.1073/pnas.91.3.974

Purves, D., George J, A., David, F., Lawrence C, K., Anthony-Samuel, L., James O, M., & S Mark, W. (2001). Anatomical Distribution of Rods and Cones. In *Neuroscience, 2nd edition*. Sunderland (MA): Sinauer Associates. https://www.ncbi.nlm.nih.gov/books/NBK10848/

Qin, D., Wang, J., Le, A., Wang, T. J., Chen, X., & Wang, J. (2021). Traumatic Brain Injury: Ultrastructural Features in Neuronal Ferroptosis, Glial Cell Activation and Polarization, and Blood–Brain Barrier Breakdown. *Cells*, *10*(5). https://doi.org/10.3390/cells10051009

Rapp, L. M. and Williams, T. P. (1980). A Parametric Study of Retinal Light Damage in Albino and Pigmented Rats. In B. N. Williams, Theodore P. and Baker (Ed.), *The Effects of Constant Light on Visual Processes* (pp. 135–159). Springer US. https://doi.org/10.1007/978-1-4684-7257-8{\textunderscore }6

Rattner, A., & Nathans, J. (2005). The Genomic Response to Retinal Disease and Injury: Evidence for Endothelin Signaling from Photoreceptors to Glia. *The Journal of Neuroscience*, *25*(18), 4540. https://doi.org/10.1523/JNEUROSCI.0492-05.2005

Richardson, K. C., Jarett, L., & Finke, E. H. (1960). Embedding in Epoxy Resins for Ultrathin Sectioning in Electron Microscopy. *Stain Technology*, *35*(6), 313–323. https://doi.org/10.3109/10520296009114754

Ritchie, M. E., Phipson, B., Di Wu, Hu, Y., Law, C. W., Shi, W., & Smyth, G. K. (2015). limma powers differential expression analyses for RNA-sequencing and microarray studies. *Nucleic Acids Research*, *43*(7), e47–e47. https://doi.org/10.1093/nar/gkv007

Rohrer, B., Demos, C., Frigg, R., & Grimm, C. (2007). Classical complement activation and acquired immune response pathways are not essential for retinal degeneration in the rd1 mouse. *Experimental Eye Research*, *84*(1), 82–91. https://doi.org/10.1016/j.exer.2006.08.017

Rohrer, B., Guo, Y., Kunchithapautham, K., & Gilkeson, G. S. (2007). Eliminating complement factor D reduces photoreceptor susceptibility to light-induced damage. *Investigative Ophthalmology {\&} Visual Science*, *48*(11), 5282–5289. https://doi.org/10.1167/iovs.07-0282

Rutar, M., Natoli, R., Kozulin, P., Valter, K., Gatenby, P., & Provis, J. M. (2011b). Analysis of complement expression in light-induced retinal degeneration: synthesis and deposition of C3 by microglia/macrophages is associated with focal photoreceptor degeneration. *Investigative Ophthalmology {\&} Visual Science*, *52*(8), 5347–5358. https://doi.org/10.1167/iovs.10-7119

Rutar, M., Natoli, R., & Provis, J. M. (2012). Small interfering RNA-mediated suppression of Ccl2 in Müller cells attenuates microglial recruitment and photoreceptor death following retinal degeneration. *Journal of Neuroinflammation*, *9*, 221. https://doi.org/10.1186/1742-2094-9-221

Rutar, M., Natoli, R., Valter, K., & Provis, J. M. (2011a). Early Focal Expression of the Chemokine Ccl2 by Müller Cells during Exposure to Damage-Inducing Bright Continuous Light. *Investigative Ophthalmology {\&} Visual Science*, *52*(5), 2379–2388. https://doi.org/10.1167/iovs.10-6010

Ruzickova, S., & Stanek, D. (2017). Mutations in spliceosomal proteins and retina degeneration. *RNA Biology*, *14*(5), 544–552. https://doi.org/10.1080/15476286.2016.1191735

Saika, S. (2006). TGFbeta pathobiology in the eye. *Laboratory Investigation; a Journal of Technical Methods and Pathology*, *86*(2), 106–115. https://doi.org/10.1038/labinvest.3700375

Saint-Geniez, M., Maharaj, A. S. R., Walshe, T. E., Tucker, B. A., Sekiyama, E., Kurihara, T., Darland, D. C., Young, M. J., & D'Amore, P. A. (2008). Endogenous VEGF Is Required for Visual Function: Evidence for a Survival Role on Müller Cells and Photoreceptors. *PLOS ONE*, *3*(11), e3554. https://doi.org/10.1371/journal.pone.0003554

Salman, M. M., Al-Obaidi, Z., Kitchen, P., Loreto, A., Bill, R. M., & Wade-Martins, R. (2021). Advances in Applying Computer-Aided Drug Design for Neurodegenerative Diseases. *International Journal of Molecular Sciences*, *22*(9). https://doi.org/10.3390/ijms22094688

Samardzija, M., Wenzel, A., Aufenberg, S., Thiersch, M., Remé, C., & Grimm, C. (2006a). Differential role of Jak-STAT signaling in retinal degenerations. *FASEB Journal : Official Publication of the Federation of American Societies for Experimental Biology*, *20*(13), 2411–2413. https://doi.org/10.1096/fj.06-5895fje

Samardzija, M., Wenzel, A., Thiersch, M., Frigg, R., Remé, C., & Grimm, C. (2006b). Caspase-1 ablation protects photoreceptors in a model of autosomal dominant retinitis pigmentosa. *Investigative Ophthalmology {\&} Visual Science*, *47*(12), 5181–5190. https://doi.org/10.1167/iovs.06-0556

Schäfer, N., Grosche, A., Schmitt, S. I., Braunger, B. M., & Pauly, D. (2017). Complement Components Showed a Time-Dependent Local Expression Pattern in Constant and Acute White Light-Induced Photoreceptor Damage. *Frontiers in Molecular Neuroscience*, *10*, 197. https://doi.org/10.3389/fnmol.2017.00197

Schlecht, A., Leimbeck, S. V, Jägle, H., Feuchtinger, A., Tamm, E. R., & Braunger, B. M. (2017). Deletion of Endothelial Transforming Growth Factor-ß Signaling Leads to Choroidal Neovascularization. *The American Journal of Pathology*, *187*(11), 2570–2589. https://doi.org/10.1016/j.ajpath.2017.06.018

Schlecht, A., Vallon, M., Wagner, N., Ergün, S., & Braunger, B. M. (2021). TGFβ-Neurotrophin Interactions in Heart, Retina, and Brain. *Biomolecules*, *11*(9). https://doi.org/10.3390/biom11091360

Schmitt, S. I., Bielmeier, C. B., & Braunger, B. M. (2019). New Insights into Endothelin Signaling and Its Diverse Roles in the Retina. *Advances in Experimental Medicine and Biology*, *1185*, 519–523. https://doi.org/10.1007/978-3-030-27378-1{\textunderscore }85

Shaulian, E., & Karin, M. (2002). AP-1 as a regulator of cell life and death. *Nature Cell Biology*, *4*(5), E131-6. https://doi.org/10.1038/ncb0502-e131

Shi, Y., & Massagué, J. (2003). Mechanisms of TGF-beta signaling from cell membrane to the nucleus. *Cell*, *113*(6), 685–700. https://doi.org/10.1016/s0092-8674(03)00432-x

Shull, M. M., Ormsby, I., Kier, A. B., Pawlowski, S., Diebold, R. J., Yin, M., Allen, R., Sidman, C., Proetzel, G., & Calvin, D. (1992). Targeted disruption of the mouse transforming growth factor-beta 1 gene results in multifocal inflammatory disease. *Nature*, *359*(6397), 693–699. https://doi.org/10.1038/359693a0

Silverman, S. M., Ma, W., Wang, X., Zhao, L., & Wong, W. T. (2019). C3- and CR3-dependent microglial clearance protects photoreceptors in retinitis pigmentosa. *The Journal of Experimental Medicine*, *216*(8), 1925–1943. https://doi.org/10.1084/jem.20190009

Sofroniew, M. V, & Vinters, H. V. (2010). Astrocytes: biology and pathology. *Acta Neuropathologica*, *119*(1), 7–35. https://doi.org/10.1007/s00401-009-0619-8

Sometani, A., Kataoka, H., Nitta, A., Fukumitsu, H., Nomoto, H., & Furukawa, S. (2001). Transforming growth factor-β1 enhances expression of brain-derived neurotrophic factor and its receptor, TrkB, in neurons cultured from rat cerebral cortex. *Journal of Neuroscience Research*, *66*(3), 369–376. https://doi.org/https://doi.org/10.1002/jnr.1229

Soneson, C and Love, MI and Robinson, MD. (2015). Differential analyses for RNA-seq: transcript-level estimates improve gene-level inferences [version 1; peer review: 2 approved]. *F1000Research*, *4*(1521). https://doi.org/10.12688/f1000research.7563.1

Stephens, M. (2017). False discovery rates: a new deal. *Biostatistics*, *18*(2), 275–294. https://doi.org/10.1093/biostatistics/kxw041

Sternberg, N., & Hamilton, D. (1981). Bacteriophage P1 site-specific recombination. I. Recombination between loxP sites. *Journal of Molecular Biology*, *150*(4), 467–486. https://doi.org/10.1016/0022-2836(81)90375-2

Stoll, G., Jander, S., & Schroeter, M. (2000). Cytokines in CNS disorders: neurotoxicity versus neuroprotection. In K. Jellinger, R. Schmidt, & M. Windisch (Eds.), *Advances in Dementia Research* (pp. 81–89). Springer Vienna.

Sun, D., Lee, G., Lee, J. H., Kim, H.-Y., Rhee, H.-W., Park, S.-Y., Kim, K.-J., Kim, Y., Kim, B. Y., Hong, J.-I., Park, C., Choy, H. E., Kim, J. H., Jeon, Y. H., & Chung, J. (2010). A metazoan ortholog of SpoT hydrolyzes ppGpp and functions in starvation responses. *Nature Structural & Molecular Biology*, *17*(10), 1188–1194. https://doi.org/10.1038/nsmb.1906

Sung, C. H., Davenport, C. M., Hennessey, J. C., Maumenee, I. H., Jacobson, S. G., Heckenlively, J. R., Nowakowski, R., Fishman, G., Gouras, P., & Nathans, J. (1991). Rhodopsin mutations in autosomal dominant retinitis pigmentosa. *Proceedings of the National Academy of Sciences of the United States of America*, *88*(15), 6481–6485. https://doi.org/10.1073/pnas.88.15.6481

Sylvain, N. J., Salman, M. M., Pushie, M. J., Hou, H., Meher, V., Herlo, R., Peeling, L., & Kelly, M. E. (2021). The effects of trifluoperazine on brain edema, aquaporin-4 expression and metabolic markers during the acute phase of stroke using photothrombotic mouse model. *Biochimica et Biophysica Acta (BBA) - Biomembranes*, *1863*(5), 183573. https://doi.org/10.1016/j.bbamem.2021.183573

Taya, Y., O'Kane, S., & Ferguson, M. W. (1999). Pathogenesis of cleft palate in TGF-beta3 knockout mice. *Development*, *126*(17), 3869–3879. https://doi.org/10.1242/dev.126.17.3869

Tesseur, I., Nguyen, A., Chang, B., Li, L., Woodling, N. S., Wyss-Coray, T., & Luo, J. (2017). Deficiency in Neuronal TGF-ß Signaling Leads to Nigrostriatal Degeneration and Activation of TGF-ß Signaling Protects against MPTP Neurotoxicity in Mice. *The Journal of Neuroscience : The Official Journal of the Society for Neuroscience*, *37*(17), 4584–4592. https://doi.org/10.1523/JNEUROSCI.2952-16.2017

Thomas, J. L., & Thummel, R. (2013). A novel light damage paradigm for use in retinal regeneration studies in adult zebrafish. *Journal of Visualized Experiments : JoVE*, *80*, e51017. https://doi.org/10.3791/51017

Tian, Y., James, S., Zuo, J., Fritzsch, B., & Beisel, K. W. (2006). Conditional and inducible gene recombineering in the mouse inner ear. *Brain Research*, *1091*(1), 243–254. https://doi.org/10.1016/j.brainres.2006.01.040

Valente, V., Teixeira, S. A., Neder, L., Okamoto, O. K., Oba-Shinjo, S. M., Marie, S. K. N., Scrideli, C. A., Paçó-Larson, M. L., & Carlotti JR, C. G. (2009). Selection of suitable housekeeping genes for expression analysis in glioblastoma using quantitative RT-PCR. *BMC Molecular Biology*, *10*, 17. https://doi.org/10.1186/1471-2199-10-17

Walshe, T. E., Leach, L. L., & D'Amore, P. A. (2011). TGF-β signaling is required for maintenance of retinal ganglion cell differentiation and survival. *Neuroscience*, *189*, 123–131. https://doi.org/https://doi.org/10.1016/j.neuroscience.2011.05.020

Walshe, T. E., Saint-Geniez, M., Maharaj, A. S. R., Sekiyama, E., Maldonado, A. E., & D'Amore, P. A. (2009). TGF-beta is required for vascular barrier function, endothelial survival and homeostasis of the adult microvasculature. *PloS One*, *4*(4), e5149. https://doi.org/10.1371/journal.pone.0005149

Wang, S. K., Xue, Y., & Cepko, C. L. (2020). Microglia modulation by TGF-ß1 protects cones in mouse models of retinal degeneration. *The Journal of Clinical Investigation*, *130*(8), 4360–4369. https://doi.org/10.1172/JCI136160

Wenzel, A., Grimm, C., Samardzija, M., & Remé, C. E. (2003). The genetic modifier Rpe65Leu(450): effect on light damage susceptibility in c-Fos-deficient mice. *Investigative Ophthalmology {\&} Visual Science*, *44*(6), 2798–2802. https://doi.org/10.1167/iovs.02-1134

Wu, G., Feng, X., & Stein, L. (2010). A human functional protein interaction network and its application to cancer data analysis. *Genome Biology*, *11*(5), R53. https://doi.org/10.1186/gb-2010-11-5-r53

Xu, P., Liu, J., & Derynck, R. (2012). Post-translational regulation of TGF-β receptor and Smad signaling. *FEBS Letters*, *586*(14), 1871–1884. https://doi.org/10.1016/j.febslet.2012.05.010

Yan, X., Liu, Z., & Chen, Y. (2009). Regulation of TGF-beta signaling by Smad7. *Acta Biochimica et Biophysica Sinica*, *41*(4), 263–272. https://doi.org/10.1093/abbs/gmp018

Ying, J., Li, H., Cui, Y., Wong, A. H. Y., Langford, C., & Tao, Q. (2006). Epigenetic disruption of two proapoptotic genes MAPK10/JNK3 and PTPN13/FAP-1 in multiple lymphomas and carcinomas through hypermethylation of a common bidirectional promoter. *Leukemia*, *20*(6), 1173–1175. https://doi.org/10.1038/sj.leu.2404193

Yusifov, E. Y., Kerimova, A. A., Atalay, M., & Kerimov, T. M. (2000). Light exposure induces antioxidant enzyme activities in eye tissues of frogs. *Pathophysiology*, *7*(3), 203–207. https://doi.org/https://doi.org/10.1016/S0928-4680(00)00051-1

Zhang, J., Zhang, D., McQuade, J. S., Behbehani, M., Tsien, J. Z., & Xu, M. (2002). c-fos regulates neuronal excitability and survival. *Nature Genetics*, *30*(4), 416–420. https://doi.org/10.1038/ng859

Zhang, Y. E. (2009). Non-Smad pathways in TGF-beta signaling. *Cell Research*, *19*(1), 128–139. https://doi.org/10.1038/cr.2008.328

7.4 Abbreviations

α	alpha
AAV	Adeno-associated virus
Actb	Actin-beta
AMD	Age related macular degeneration
AP1	Activator protein 1
β	beta
Bdnf	Brain derived neuroprotective factor
Bik	Bcl2-interacting killer
BMP	Bone morphogenetic Protein
C1q	Complement component 1q
C3	Complement component 3
Casp1	Caspase 1
Ccl2	Chemokine (C-C motif) ligand 2
Ccl5	Chemokine (C-C motif) ligand 5
Ccl28	Chemokine (C-C motif) ligand 28
Cd29	Integrin beta1
Cd3g	T-cell receptor T3 gamma chain
cGMP	Cyclic guanosine monophosphate
Cfh	Complement factor H
Cfi	Complement component factor i
c-Jun	Transcription factor Jun
CNS	Central nervous system
Cralbp	Cellular retinaldehyde-binding protein
Cr3	Complement receptor 3
Cxcl2	C-X-C motif chemokine ligand 2
Cxcl10	C-X-C motif chemokine ligand 10
Cxcl13	C-X-C motif chemokine ligand 13
Δ	Delta
DAPI	4`, 6-diamidino-2-phenylindole
DNA	Deoxyribonucleotide
Edn1	Endothelin 1
Edn2	Endothelin 2
Ednra	Endothelin receptor type a
Ednrb	Endothelin receptor type b
EMT	Epithelial-mesenchymal transition

Erk7	Extracellular-signal regulated kinase 7
Et al.	And others
Fgf2	Fibroblast growth factor 2
Fgl2	Fibrinogen-like 2
Fos	Fos proto-oncogene
Gapdh	Glycerinaldehyd-3-phosphat-dehydrogenase
GC	Guanylate cyclase
GCL	Ganglion cell layer
Gfap	Glial fibrillary acidic protein
Glb1l3	Galactosidase beta 1 like 3
Glul	Glutamine synthetase
GMP	Guanosine monophosphate
Gnb2l	Guanine nucleotide binding protein subunit beta 2 like 1
GS	Glutamine synthetase
GTP	Guanosine triphosphate
GTPase	Guanosine triphosphatase
h	Hour
Hdc	Histidine decarboxylse
Hddc3	HD Domain containing 3
Iba1	Ionized calcium-binding adapter molecule 1
Il-1	Interleukin-1
Il-6	Interleukin-6
INL	Inner nuclear layer
IPL	Inner plexiform layer
Itgb1	Integrin beta-1
Jnk3	c-Jun N-terminal kinase3
Kdr	Kinase insert domain receptor
Lif	Leukemia inhibitory factor
Lcn2	Lipocalin 2
LWS	Long-wave sensitive
MAP	Mitogen-activated protein
MAPK	Mitogen-activated protein kinase
Mcp-1	Monocyte chemotactic protein 1
Mesh1	HD Domain containing 3
min	Minutes
Mrpl48ps	Mitochondrial ribosomal protein L48 pseudogene
mRNA	Messenger ribonucleic acid

mTOR	Mechanistic target of rapamycin
Myo7a	Myosin VIIA
Ngf	Neurotrophins nerve growth factor
OC	Optic nerve
ONH	Optic nerve head
ONL	Outer nuclear layer
OPL	Outer plexiform layer
OS	Ora serrata
PB	Phosphate buffer
PCR	Polymerase-chain-reaction
PDE	Phosphodiesterase
PI3K	phosphatidylinositol-3-kinase
Prss56	Serine protease 56
PFA	Paraformaldehyde
pr. Co.	Probe control
R	Rhodopsin
Ras	Rat sarcoma virus
Raf	Rapidly growing fibrosarcoma
Rh1	Rhodopsin-like 1
Rh2	Rhodopsin-like 2
Rho	Ras homologue
Rhox4c	Reproductive homeobox 4C
Rlbp1	Retinaldehyde-binding protein 1
RNAseq	Next generation RNA sequencing
RP	Retinitis pigmentosa
RPE	Retinal pigment epithelium
Rpl32	60S ribosomal protein L32
Rps9	ribosomal protein 9
R6K	Ribosomal protein S6 kinase
s	Seconds
SEM	Standard error of the means
Serpina3n	Serine protease inhibitor A3N
Smad	Mothers against decapentaplegic homolog
SWS1	Short-wave sensitive 1
SWS2	Short-wave sensitive 2
T	Transducin
Tak1	Transforming growth factor beta-activated kinase 1

Tbp	TATA-binding protein
Tg	Transgene
Tgf	Transforming growth factor
Tgfbr1	Transforming growth factor receptor type 1
Tgfbr2	Transforming growth factor receptor type 2
Tnf	Tumor necrosis factor
Traf6	TNF receptor associated factor 6
Trem2	Triggering receptor expressed on Myeloid cells 2
Ubc	Ubiquitin C
VEGF	Vascular endothelial growth factor
Vegfr1	Vascular endothelial growth factor receptor type 1
Vegfr2	Vascular endothelial growth factor receptor type 2
WGCNA	Weighted gene correlation network analysis

7.5 Danksagung

Zuallererst möchte ich mich sehr bei Herrn Prof. Dr. Ernst Tamm bedanken, dass Sie mir an Ihrem Lehrstuhl die Möglichkeit gegeben haben meine Dissertation durchzuführen. Es war eine sehr schöne Zeit, in der ich sehr viel gelernt habe und an die ich sehr gerne zurückdenke.

Des Weiteren möchte ich mich sehr bei Herrn Prof. Dr. Süleyman Ergün bedanken, dass ich nach dem Umzug nach Würzburg meine Doktorarbeit in Ihrem Lehrstuhl weiterführen durfte und dort so freundlich von allen empfangen wurde.

Mein ganz besonderer Dank gilt Frau Prof. Dr. Dr. Barbara Braunger, dass du mich so großartig durch diese Arbeit geleitet hast. Ich habe in den letzten Jahren sehr viel von dir lernen dürfen. Sowohl fachlich als auch persönlich hast du mir immer weitergeholfen und selbst Umzüge und Schwangerschaften konnten wir meistern. Vielen Dank, dass ich jederzeit zu dir kommen konnte und wir gemeinsam immer einen Weg gefunden haben.

Vielen Dank auch an Frau Prof. Dr. Charlotte Wagner, dass Sie sich bereit erklärt haben, das Erstgutachten meiner Dissertation zu übernehmen. In diesem Zuge will ich mich auch bei Frau Prof. Dr. Veronika Egger sowohl für die Mentorenschaft als auch die Bereitschaft als Drittprüfer bedanken.

Ich will mich auch sehr bei Herrn Dr. Andreas Neueder bedanken, dass er mit seinem Wissen und seinen statistischen Auswertungen den riesigen Datenbergen des RNAseq einen Sinn gegeben hat und mich damit vertraut gemacht hat.

Ganz herzlich will ich mich bei den Technischen Angestellten in Regensburg Elke Stauber, Margit Schimmel, Angelika Pach und Silvia Babl bedanken, die mir im Labor und in der „Histo“ jederzeit mit Rat und Tat weitergeholfen haben. Auch will ich mich herzlich bei der Technischen Angestellten in Würzburg Alla Ganscha bedanken, die mich tatkräftig unterstützt hat und viele Stunden mit mir genotypisiert hat. Die Kaffepausen und interessanten Gesprächen mit euch vermisse ich sehr.

Vielen Dank auch an die vielen Mitstreiter, die mich sowohl in Regensburg als auch in Würzburg durch diese Arbeit begleitet und mir diese schöne Zeit verschafft haben. Gerne denke ich an viele schöne und lustige Momente zurück und an die ein oder andere geköpfte Flasche Sekt. Ein großer Dank gilt dabei vor allen Sabrina Schmitt, der ich diese schöne Zeit erst zu verdanken habe, da sie mich so wunderbar angeleitet hat und mich bis heute immer unterstützt hat. Ein herzliches Danke gilt auch Andrea Dillinger, Franzi Fröml, Anja Schlecht und Silke Seibold, ohne euch wäre diese Zeit nur halb so schön gewesen.

Ganz besonders möchte ich mich noch bei meinem Mann Andreas bedanken, der mich all die Zeit ermutigt und unterstützt hat, egal wie stressig es auch wurde. Ein großer Dank gilt auch unseren Familien, durch die mein Studium und gerade durch die vielen Betreuungsstunden von Markus die Fertigstellung meiner Arbeit letztendlich ermöglicht wurde.

7.6 Eidesstattliche Erklärung

Ich erkläre hiermit an Eides statt, dass ich die vorliegende Arbeit “Transforming growth factor β signaling - a regulator of photoreceptor degeneration in Retinitis Pigmentosa“ ohne unzulässige Hilfe Dritter und ohne Benutzung anderer als der angegebenen Hilfsmittel angefertigt habe. Die aus anderen Quellen direkt oder indirekt übernommen Daten und Konzepte sind unter Angabe des Literaturzitats gekennzeichnet.

Weitere Personen waren an der inhaltlich-materiellen Herstellung der vorliegenden Arbeit nicht beteiligt. Insbesondere habe ich hierfür nicht die entgeltliche Hilfe eines Promotionsberaters oder anderer Personen in Anspruch genommen. Niemand hat von mir weder unmittelbar noch mittelbar geldwerte Leistungen für Arbeiten erhalten, die im Zusammenhang mit dem Inhalt der vorgelegten Dissertation stehen.

Die Arbeit wurde bisher weder im In- noch im Ausland in gleicher oder ähnlicher Form einer Prüfungsbehörde vorgelegt

Ich versichere an Eides Statt, dass ich nach bestem Gewissen die reine Wahrheit gesagt und nichts verschwiegen habe.

Vor Aufnahme der obigen Versicherung an Eides statt wurde ich über die Bedeutung der eidesstattlichen Versicherung und die strafrechtlichen Folgen einer unrichtigen oder unvollständigen eidesstattlichen Versicherung belehrt

Regensburg, den 12.01.2023

……..